EVALUATING CORROSIVE SITE PERFORMANCE AND POLICY WITH CONCRETE ADMIXTURES

by

Keith Alexander Violette

A thesis submitted to the faculty of
The University of North Carolina at Charlotte
in partial fulfillment of the requirements
for the degree of Master of Science in
Civil Engineering

Charlotte

2020

Approved by:

_____
Dr. Brett Tempest

_____
Dr. Tara Cavalline

_____
Dr. Matthew Whelan

ABSTRACT

KEITH ALEXANDER VIOLETTE. Evaluating Corrosive Site Performance and Policy with Concrete Admixtures. (Under the direction of DR. BRETT Q. TEMPEST)

The coastline of North Carolina (NC) is home to a large number of state-owned concrete structures such as bridges that can be adversely affected by the aggressive, chloride-rich environments in which they are constructed. To delay the corrosion-related deterioration of structural concrete in these environments, the North Carolina Department of Transportation (NCDOT) Structures Management Unit (SMU) created a Design Manual in 2003 that includes multiple corrosion prevention specifications such as the creation of corrosive boundaries, increased concrete cover, epoxy coated steel, and the addition of pozzolans and corrosion inhibitors. As of 2018, there have been more than 200 structures newly constructed or replaced within these zones.

The specifications presented within the Design Manual vary based on which corrosive boundary the structure is constructed within (highly corrosive zone or corrosive zone). The highly corrosive zone is the easternmost region and considered the most chloride-rich environment. The corrosive zone is located immediately to the west and is considered the second most chloride-rich environment. Structures constructed within the highly corrosive zone are required to apply the NCDOT corrosion prevention specifications to all elements while structures constructed within the corrosive zone are required to apply the NCDOT corrosion prevention specifications only to elements located within 15 feet of the mean high tide line.

The primary objective of this research was to determine the effectiveness of the NCDOT corrosion policy as currently written. To achieve this, the project was divided

into three investigations which included a field study of eight structures constructed under the policy, analysis of potentially corrosion-related damages using NCDOT maintenance records, and the creation of deterioration models using National Bridge Inventory (NBI) condition rating data. These investigations aimed to answer whether the corrosive zone boundary lines are in the most effective location, whether the corrosion prevention methods are working to extend the service lives of structures located in chloride-rich environments, and whether structures constructed using these specifications are outperforming structures constructed before the policy was created.

Given the research and results collected across the three investigations, it was concluded that the corrosion policy as currently written is conservative and it seems under certain circumstances (such as locations further from the coast, elements high above brackish water, and unsubmerged elements), the policy is likely overly conservative. Additionally, as there were multiple investigations from different sources (field investigation, NCDOT database, and NBI database) suggesting the same result, the following was concluded: the current location of the corrosive boundary lines and specifications for each zone are adequate to delay the onset of corrosion. From this, it was recommended that no changes be made to the current location of the corrosive boundary lines or to the current specifications.

Future work intended to further investigate the efficacy of the NCDOT corrosion policy is recommended within. The work suggested is based on hypotheses that were unable to be definitively concluded upon based on the work performed in this thesis and could lead to refinement and enhancement of the policy or further confirm its adequacy as currently written.

ACKNOWLEDGEMENTS

The completion of this thesis was made possible with the assistance and guidance of multiple people. As such, I would like to acknowledge the contributions of all who were involved in helping me achieve this monumental task. First, I would like to thank my advisor, Dr. Brett Tempest, P.E., for providing me with this opportunity and guiding me through every step of the way. His feedback helped shape my thesis into the final product it is today. I would like to thank Dr. Tara Cavalline, P.E., for providing guidance and feedback during weekly research meetings and for reviewing my writing throughout the entire project. I would like to thank Dr. Matthew Whelan, P.E., for serving on my committee.

While the assistance from my advisor and committee was invaluable, this entire project would not have been made possible if not for the NCDOT for financial assistance and the members of the Research Project 2019-22 steering committee for ensuring that the research conducted would provide meaningful insight into the current policies protecting North Carolina's coastal infrastructure.

I would like to thank those involved in the multiple field visits to the coast. This includes Dr. Tempest, Dr. Cavalline, Ross Newsome, and Alex Dilworth. The early mornings, hours spent travelling in the car, and hours spent performing tests from a small boat were all essential to completing this research.

Finally, I would like to thank my family for the unconditional support they provide me in all pursuits.

TABLE OF CONTENTS

LIST OF TABLES

LIST OF FIGURES

LIST OF ABBREVIATIONS

AASHTO	American Association of State Highway and Transportation Officials
AC	Alternating Current
ADT	Average Daily Traffic
ASTM	American Society for Testing and Materials
C	Corrosive
°C	Degrees Celsius
CEPRA	Connectionless Electrical Pulse Response Analysis
CIP	Cast-in-Place
Cl	Chloride
cm	Centimeters
CR	Condition Rating
DC	Direct Current
DelDOT	Delaware Department of Transportation
DOT	Department of Transportation
EIS	Electrochemical Impedance Spectroscopy
°F	Degrees Fahrenheit
FDOT	Florida Department of Transportation
GDOT	Georgia Department of Transportation
HC	Highly Corrosive
in	Inch
kohm-cm	Kiloohm-Centimeter
LP	Low Permeability

MHHW	Mean Higher High Water
MLLW	Mean Lower Low Water
NBI	National Bridge Inventory
NC	North Carolina
NCDOT	North Carolina Department of Transportation
NDT	Non-Destructive Testing
NJDOT	New Jersey Department of Transportation
ppm	Parts-Per-Million
SCDOT	South Carolina Department of Transportation
SMU	Structures Management Unit
SN	Structure Number
std.err	Standard Error
std.dev	Standard Deviation
UNC	University of North Carolina
UNCC	University of North Carolina at Charlotte
US	United States
V	Volts
w/c	Water-to-Cement
μm/year	Micrometers per Year

CHAPTER 1: INTRODUCTION

1.1 Background

The coastline of North Carolina is home to a large number of state-owned bridges that can be adversely affected by the ingress of chlorides. There are multiple sources of chlorides in these coastal environments, with major contributors being seawater and deicing agents (Li 2016). Some of the common methods of chloride ingress originating from seawater include direct contact (submerged elements), intermittent contact (elements within the splash zone but not always submerged), atmospheric deposition, and through deicing application. Deicing agents are deposited on the driving surface of roads and bridges when there is a potential for freezing weather that may create unsafe driving conditions. Commonly used deicing agents include chlorides which, once mixed with melting ice on the deck surface of a bridge, can create a chloride solution that can then enter the concrete. The scope of this thesis is focused on the seawater induced corrosion of reinforcing steel, therefore, deicing agent induced corrosion will not be discussed in detail. The ingress of chlorides in structural concrete can result in the corrosion and deterioration of the reinforcing steel. As the reinforcing steel corrodes, it undergoes a significant increase in volume leading to cracking of the surrounding concrete. This can lead to significantly shortened service lives and high maintenance costs.

1.1.1 Corrosive Sites

To delay the deterioration of structural concrete in areas of increased chloride concentrations, the North Carolina Department of Transportation (NCDOT) Structures Management Unit (SMU) created a Design Manual that includes multiple requirements and specifications related to the prevention of corrosion related damage. The SMU Design Manual divides the coast into two regions, each requiring additional treatments to deter and/or slow the ingress of chlorides (NCDOT 2018). Structures lying east of these lines and meeting additional criteria are identified as corrosive sites. The dividing lines are shown below in Figure 1.1.

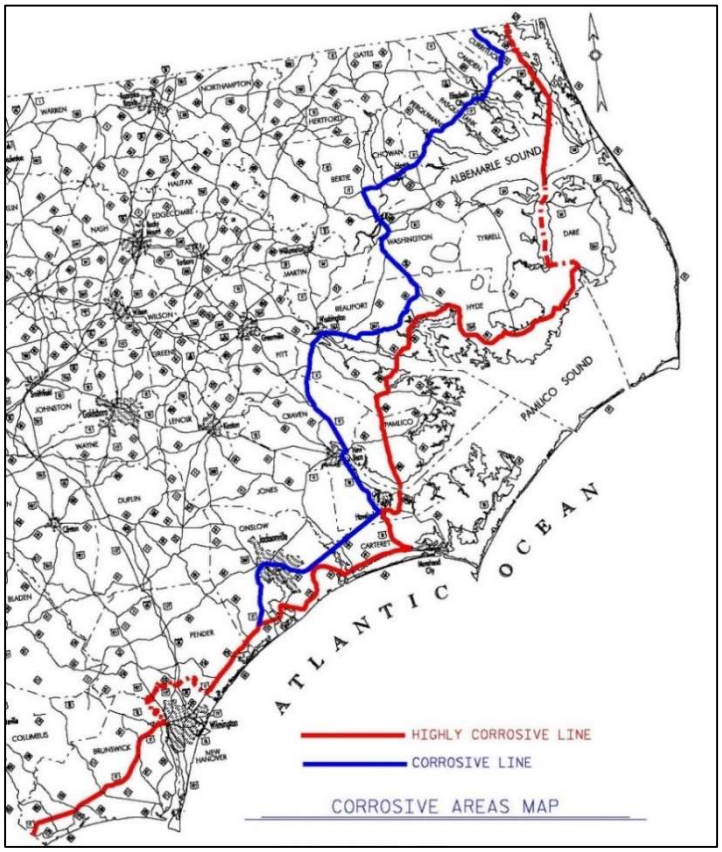

Figure 1.1. Map of Corrosive Sites Dividing Lines. (Originally from NCDOT SMU Design Manual, Figure 12-29 (NCDOT 2018))

There are qualifications that a bridge must meet to be classified as a corrosive sites structure and require special treatment. While these are not the only structures that the NCDOT requires special treatment be applied to, the structures of focus for this thesis are those classified specifically as a corrosive sites structure. To qualify as being a corrosive site, a structure must be a stream crossing that is located east of either corrosive line as previously defined.

All structures falling east of the highly corrosive line (red) are to follow all corrosive sites requirements and apply them to all bridge elements. Bridges falling east of the corrosive line (blue) and west of the highly corrosive line (red) are to apply all corrosive sites requirements only to those bridge elements located within 15 feet of the mean high tide.

In the Design Manual, there are separate specifications related to structures located within North Carolina (NC) Divisions 5, 7, or 9 through 14 (see Figure 1.2 below). The reasoning for this is that these divisions are located on the western side of the state where the corrosion protection is focused on deicing agents being applied to the decks, therefore a different set of prevention strategies are specified. These bridges will not be analyzed as they do not fall within the scope of this thesis.

Figure 1.2. Map of NC Divisions (https://connect.ncdot.gov/).

1.1.2 NCDOT Corrosion Prevention Measures

The NCDOT SMU Design Manual provides guidelines for treating structures located within either of the corrosive site boundaries previously mentioned. This section will briefly describe each corrosion prevention measure detailed in the Design Manual. The manual is organized in such a way that there are very few corrosion prevention measures found in each section, however, the user is frequently referenced to Section 12-12. While most measures were found in this section of the manual, there were protective measures found in earlier sections. The following paragraphs are organized in a similar manner, with the protective measures found within the manual described first, followed by the protective measures found within Section 12-12.

Section 12-5 of the SMU Design Manual explains requirements related to when epoxy coated reinforcing steel is required. At corrosive sites, all cast-in-place (CIP) concrete elements shall have epoxy coated reinforcing steel, bar supports, and incidental steel. Additionally, all precast and CIP culverts falling east of the corrosive line shall have epoxy coated reinforcing steel and bar supports.

Section 12-12 (“Corrosion Protection”) of the SMU Design Manual describes the different measures that may be used as corrosion protection. A least one of the following measures is suggested for use:

- Increased clear cover for reinforcing steel
- Epoxy coated reinforcing steel
- Addition of calcium nitrite corrosion inhibitor
- Addition of silica fume
- Addition of fly ash or granulated blast furnace slag

- Specification of Class AA concrete in substructure elements
- Limiting the use of uncoated structural steel

The selection of a measure and the degree of protection required varies depending on the location of the bridge. The factors that influence the selection of a certain measure over another are whether the bridge falls east of the corrosive line or east of the highly corrosive line, and if the bridge falls within certain state divisions that experience significant levels of deicing agents. The SMU references the use of the flowchart shown in Figure 1.3 on the following page (Figure 12-30 in NCDOT SMU Design Manual) to determine the extent of corrosion protection required.

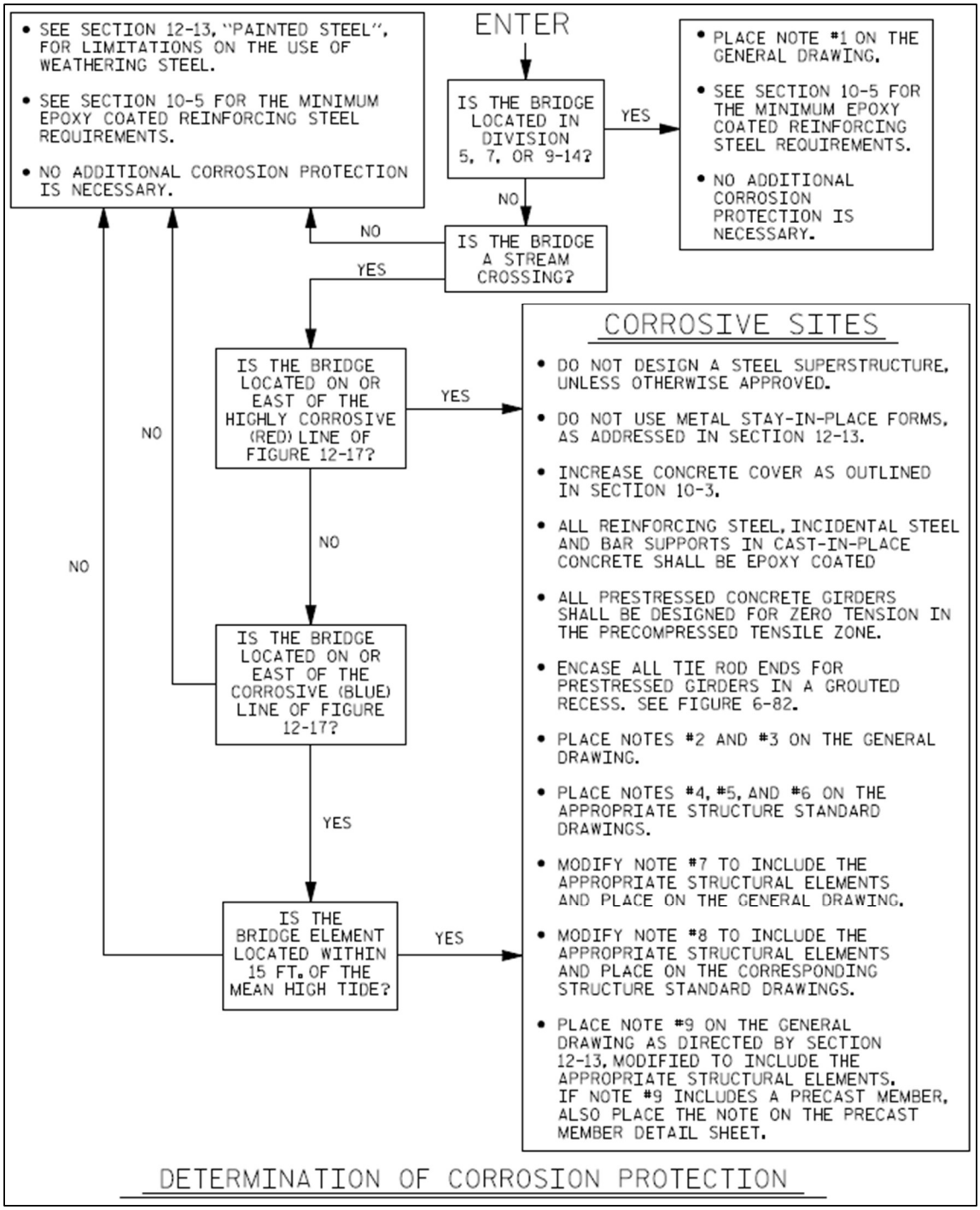

Figure 1.3. Flowchart to Determine Level of Corrosion Protection Required. (Originally from NCDOT SMU Design Manual, Figure 12-30 (NCDOT 2018))

1.2 Objectives and Scope

The current NCDOT policies intended to delay the onset of corrosion in aggressive coastal environments were established in 2003. As of 2018, there have been more than 200 bridges either newly constructed or replaced within the corrosive boundary lines. The primary objective of this project was to study these structures to determine the effectiveness of the current corrosion policies being used by the NCDOT. To achieve this primary objective, the project was divided into smaller objectives and completed with the help of a fellow UNC Charlotte (UNCC) graduate student, Ross Newsome (Newsome 2020). The objectives that are specific to this thesis include the following:

- Field Investigation
    - Analysis of visual inspection, corrosion rate data, and surface resistivity data acquired over the course of multiple field visits to the North Carolina coast.
- Defect Mapping Investigation
    - Location-based analysis of potential corrosion-related damages from inspection and maintenance records completed by the NCDOT in 2016.
- Deterioration Modeling Investigation
    - Analysis of deterioration models created using National Bridge Inventory (NBI) condition rating data dating from 1993 to 2012.

1.2.1 Field Investigation

To obtain a clear picture of how these structures were performing, a representative subset of structures constructed under the current corrosion policy were selected and field inspections were performed to determine the current state of corrosion related deterioration. The structures selected were within the age range of 10 to 15 years old to ensure that they have had a significant amount of time to be exposed to conditions that cause weathering and potentially show early signs of corrosion. The investigation included corrosion rate and surface resistivity readings at multiple locations on each structure, along with a visual inspection. This investigation is intended to provide information to determine the current state of corrosion of typical structures near the North Carolina coastline.

1.2.2 Defect Mapping Investigation

An analysis of NCDOT maintenance records for structures located in the corrosive boundaries was performed to determine if structures constructed after the policy was enacted are performing better (i.e. longer maintenance-free service lives, delayed onset of corrosion, etc.) than structures constructed before the policy. The maintenance records were filtered to contain only defects that were potentially caused by corrosion of the embedded steel. In addition to determining whether structures are performing better following the enactment of the corrosion policy, this study was also intended to aid in determining whether the corrosive boundary lines are drawn in the correct location.

1.2.3 Deterioration Modeling Investigation

Condition rating data sourced from the NBI database for structures located near the North Carolina coastline were used to create deterioration models. These models show the average time taken for a structure to deteriorate from condition rating 9 to condition rating 6 or 5 (not all structures reached condition rating 5 before receiving maintenance which increased the condition rating). Additionally, a statistical analysis of this same dataset was performed using Minitab to determine whether the differences shown on the deterioration models were statistically significant. This study was intended to determine whether structures constructed after the corrosion policy were performing better than those constructed before and to determine if structures constructed within the corrosive boundaries are performing equally to those constructed outside of the corrosive boundaries (i.e. west of the corrosive boundary line). This study also aided in determining whether the boundary lines are drawn in the correct location.

1.2.4 Scope of Structures Included

Due to the primary focus of this research being on the performance of structures constructed under the current NCDOT corrosion policy, the only structures that were included in the previously described analyses were those located within one of the two corrosive zones, as previously defined in Figure 1.1, and a subset of structures located just west of the outermost corrosive boundary line. These structures were included to aid in determining if the corrosive boundary lines are located in the correct location.

CHAPTER 2: LITERATURE REVIEW

2.1 Overview of Corrosion

Corrosion in steel is an electrochemical process in which iron (Fe) is removed from the steel and dissolves into the surrounding pore solution. Once dissolved in the solution, the iron then appears as ferrous ions (Fe^{+}). These ferrous ions then typically react with hydroxide ions (OH^{-}) and dissolved oxygen molecules (O_2) to form one of the many varieties of rust (ACI 2019).

2.1.1 Initiation

When the concentration of chlorides at the depth of the reinforcing steel reaches a certain threshold level, which varies due to the differing concrete and steel configurations and properties, corrosion processes are likely to begin. This corrosion threshold concentration, also referred to as the critical chloride content, can vary greatly and is dependent on many factors such as the interface between steel and concrete, the chemistry of the pore solution, and the amount of oxygen that can make its way to the steel (Bertolini et al. 2013). There are two main sources of chloride-containing fluids coming into contact with bridge elements: deicing materials and seawater, which may be introduced by direct contact through submersion or indirect contact through splashing or by deicing operations. The scope of this project is focused on structural deterioration due to chloride ingress from seawater, therefore there is no discussion of deterioration due to deicing operations.

2.1.2 Mechanism

The process of corrosion occurs along the length of the reinforcing steel from an anodic site to a cathodic site. The process begins at the anode by the dissolving of iron in the pore solution, along with the loss of electrons (ACI 2019), as described by the following anodic reaction:

$$\mathrm{Fe} \rightarrow \mathrm{Fe}^{2+} + 2\mathrm{e}^{-} \qquad (2.1)$$

These electrons then flow through the reinforcement to the cathode, combining with the available water and oxygen which flows through the pores of the concrete. This combination leads to the creation of hydroxides (ACI 2019) as shown in the following cathodic reaction:

$$4\mathrm{e}^{-} + 2\mathrm{H_2O} + \mathrm{O_2} \rightarrow 4\mathrm{OH}^{-} \qquad (2.2)$$

The creation of an anodic and cathodic site are the beginning reactions in the formation of a rust by-product, with the actual formation of rust requiring several additional reactions. As there are many different ways to express the formation of rust, only one was demonstrated here. The following series of reactions display how iron and hydroxide ions (OH^{-}) formed at the cathode (Equation 2.2) combine to create ferrous hydroxide. The ferrous hydroxide combines with available oxygen and water to create ferric hydroxide, which then dissolves into hydrated ferric oxide rust (Zhao and Jin 2016). These reactions are shown below.

$$Fe + 2OH^{-} \rightarrow Fe(OH)_2 \qquad \text{Ferrous hydroxide} \qquad (2.3)$$

$$4Fe(OH)_2 + O_2 + 2H_2O \rightarrow 4Fe(OH)_3 \qquad \text{Ferric hydroxide} \qquad (2.4)$$

$$Fe(OH)_3 \rightarrow Fe_2O_3 \cdot H_2O + H_2O \qquad \text{Hydrated ferric oxide rust} \qquad (2.5)$$

2.1.3 Factors Affecting Corrosion Rate

As described above, the creation of an anodic and cathodic process leads to the accumulation of positive and negative charges. Hydroxide ions diffuse in the direction of the anode where they combine with the available ferrous ions. This combination, when the anodic and cathodic processes take the form of a corrosion cell with no additional electrons, causes electrical neutralization. If no source of electrons is present, then the oxidation rate at the anode must be equal to the reduction rate at the cathode. Therefore, the corrosion rate is reflected by the rate of electron flow (Zhao and Jin 2016).

The rate at which corrosion occurs is influenced by many different factors such as concrete, steel, and environmental properties. One factor that can hinder the rate of corrosion is the availability of dissolved oxygen in the cathodic regions (Zhao and Jin 2016). As oxygen is consumed in the cathodic reaction as shown in Equation 2.2, the lack of a continuous supply of oxygen can significantly reduce the rate of corrosion. One way that oxygen is limited is with increased concrete cover.

Another factor that has a significant impact on the rate of corrosion is passivation. Passivation occurs when a thin, passive layer of insoluble metal oxide or hydroxide forms on the surface of the steel. This layer forms when the steel is exposed to an alkaline condition with a pH greater than 11.5 in an environment containing dissolved oxygen. Under these conditions, the steel can react with the oxygen to form the passive layer. With a passive layer surrounding the steel and given the same conditions required to create the passive layer, the rate of corrosion is effectively reduced to a negligible amount (ACI 2019). Even under continuous environmental exposure to alkaline conditions, the passive layer can be broken down by the ingress of chlorides, as discussed in Section 2.2.

2.2 Methods of Chloride Ingress

The four main mechanisms that allow the transport of chlorides into the concrete matrix include diffusion, capillary suction, permeation, and migration (Bertolini et al. 2013). Each mechanism is discussed generally below, as well as their relation to chloride ingress in reinforced concrete bridges. Additionally, the effects of cracking with relation to chloride ingress will also be discussed.

2.2.1 Diffusion

Diffusion is a process in which chemicals are transported into concrete due to a concentration gradient (Li 2016). This occurs when there is a higher concentration of a certain element on the surface than there is internally, and the gradient drives the element to travel in the direction of lower concentration. Diffusion is quantified using the diffusion coefficient, which has been characterized as one of the key parameters that controls the rate of chloride ingress into concrete (Andrade 2002). The rate of diffusion is affected by many factors, including the water-to-cement (w/c) ratio, cement type, temperature, and the age of the concrete (ACI 2001). Either due to direct contact with seawater or to splashing, a high concentration of salts can develop on the surface of multiple bridge elements. This leads to the development of a concentration gradient that promotes the flow of salts into the concrete matrix. Additionally, this process can occur due to the application of deicing agents.

2.2.2 Capillary Suction

When water comes into contact with a dry bridge deck, the water is rapidly absorbed into the pores of the concrete due to a process called capillary action. Bertolini et al. (2013) explains that this process depends on the surface tension, viscosity, density

of the liquid, angle of contact between the liquid and pore walls, and the radius of the pores. Additionally, it is stated that the contact angle is small in concrete due to the molecular attraction between the liquid and the substrate (i.e. pore water and cement paste) (Bertolini et al. 2013). The test commonly performed as a way to measure the capillary action in concrete is called a sorptivity test, which is governed by ASTM (American Society for Testing and Materials) C1585 (ASTM 2013). Sorptivity, or the water absorption rate, is an effective way to describe the transport capacity of a concrete surface (Li 2016).

2.2.3 Permeation

Permeation is the mechanism that causes the transport of chlorides due to a pressure difference within the concrete (Bertolini et al. 2013). This method is similar to that of diffusion and can work to help or hinder the speed of diffusion. When water is sitting on the surface of a bridge deck, this becomes a region of high pressure. Unless there is a waterproof membrane on the surface, this water will naturally travel in the direction of high to low pressure. The area of low pressure would be within the pore structure of the concrete, which is what allows the transport of chlorides from the surface of the concrete to the surface of the reinforcing steel.

2.2.4 Migration

Migration is defined by the transport of ions in pore solution due to the effects of an electric field. The rate at which migration occurs is directly proportional to the strength of the electric field, charge, and ion size. Additionally, temperature has a noticeable effect on migration due to the effects of current flow and electrical resistivity (Bertolini et al. 2013).

2.2.5 Cracking

As rust is a solid by-product of corrosion, a volumetric increase occurs between the interface of the steel and concrete. This induces stresses in the concrete cover leading to cracking and spalling. When the concrete cover is cracked, this can increase the rate at which chlorides may reach the reinforcing steel leading to an increase in the chloride loading.

2.2.6 Rate of Ingress

While each mechanism can work alone, they often work simultaneously or in sequence with one another. Under different circumstances, a particular method is more likely to be the dominant transport mechanism. When the pores of the concrete are relatively dry, capillary suction is likely to be the driving mechanism, however, when the pores are relatively saturated, diffusion is likely to be the driving mechanism (Basheer et al. 2001).

2.3 Corrosion Mitigation Methods

Corrosion mitigation methods typically revolve around the protection of the reinforcing steel, as that is where the corrosive damage will begin. The first step in determining an appropriate mitigation method is to determine which bridges are most susceptible to corrosive damage during their projected service life. This is different for each state and is discussed in the following paragraph. The methods covered in this section include minimum concrete cover requirements, reinforcing steel coatings, material selection, and common admixtures.

States with a coastal border have different methods of defining what bridges are required to receive additional treatments or design restrictions. It seems that the states

with the largest coastlines (California, Florida, etc.) have more specifically defined locations that require special treatments than states with smaller coastlines (Alabama, Mississippi, etc.). Some of the common ways to define a corrosive environment include a threshold content of chlorides measured in the water (California, Florida), distance from the nearest coastline (Florida, North Carolina), marine water crossings (Louisiana, Maine), and defining specific counties as coastal counties (Georgia, South Carolina) (Caltrans 2003; FDOT 2019; GDOT 2018; LADOTD 2005; MEDOT 2003; NCDOT 2018; SCDOT 2006). Louisiana also includes areas with a history of corrosive damage (LADOTD 2005). Florida, California, and North Carolina all have different levels of corrosion prevention requirements based on parameters including distance from the nearest coastline and level of parts-per-million (ppm) chloride content (Caltrans 2003; FDOT 2019; NCDOT 2018).

Common mitigation methods are designated as either physical, passive, or active systems, and each can be used in conjunction with another. A physical method would be a matter of design geometry, such as increased concrete cover and epoxy coating on the embedded steel or concrete surface. This acts as a way of increasing the time to corrosion initiation by providing a physical barrier between reinforcing steel and chlorides. A passive system would be the inclusion of admixtures, such as fly ash and other pozzolans. Passive methods work by decreasing the permeability of the concrete, therefore slowing the rate of chloride ingress. An active system would be the act of chemically raising the corrosion threshold of the steel. This is commonly achieved through the use of corrosion inhibitors (Rochelle 2000).

2.3.1 Minimum Concrete Cover

One of the simplest mitigation techniques used by many states is the specification of a minimum depth of concrete cover above the reinforcing steel, commonly defined for the top or bottom surface of the bridge deck. Some states also include a specification for exposed or submerged piers and bents. The most common minimum specification for top of bridge deck concrete cover is 2.5 inches, which is what North Carolina currently specifies (NCDOT 2018).

Alabama, Louisiana, and Maine specify 2 inches for the minimum cover (ALDOT 2017; LADOTD 2005; MEDOT 2003). Florida and Georgia specify 2 inches if the bridge meets certain requirements, but typically specify a larger minimum value (FDOT 2019; GDOT 2018). While 2.5 inches is a common specification among multiple states, it appears that this is a moderately conservative value, as some states specify a minimum value as low as 2 inches (states mentioned above) and others, such as Delaware, specify a minimum value of up to 3 inches (DelDOT 2017).

2.3.2 Reinforcing Steel

The most common steel choices specified for high potential corrosion areas included epoxy coating, galvanized, and stainless steel. Based on observation of United States (US) coastal states' bridge design manuals, the most common type of reinforcing steel specified for corrosion resistance or mitigation is epoxy coated.

2.3.2.1 Epoxy Coated Steel

Epoxy coated steel is one of the primary mitigation methods employed by North Carolina as well as many other states. This type of coating would be considered a physical mitigation method as it provides a physical barrier between the pore solution

within the concrete and the reinforcing steel. The benefit of using epoxy coated steel is that it has been used in both laboratory and field testing for decades, and has proven to be successful in delaying the onset of corrosion due to chlorides (ACI 2019).

A downside of using this method is that the coating can significantly lose its mitigation properties if it is damaged. This is a considerable concern since damage is very likely to occur on a construction site. It is specified that if damage occurs during construction then it is to be repaired before moving forward. The concern with this is that it would be fairly easy for damage to occur and go unnoticed or unreported.

At the time of this research, there were only 6 of the 19 states being reviewed that either do not specify or do not permit the use of epoxy coating. These states include Alabama, Florida, Mississippi, Oregon, South Carolina, and Virginia (ALDOT 2017; FDOT 2019; MDOT 2010; ODOT 2018; SCDOT 2006; VDOT 2011).

2.3.2.2 Galvanized Steel

Galvanized, or zinc-coated, steel is another commonly specified requirement for reinforcement found in environments designated as having a high corrosion potential. This type of coating is an example of a sacrificial protection. This means that the zinc coating undergoes corrosion and acts as the anode in the galvanic couple rather than the steel. An alternative protection method would be non-sacrificial, in which the coating will protect the steel as long as it remains undamaged. Non-sacrificial coatings include copper and nickel, however, zinc-coated reinforcing bars are most commonly available (ACI 2019).

Similar to epoxy coated steel, galvanized steel has been used in structures for decades. However, dissimilar to epoxy coated steel, the performance results of galvanized

reinforcement under corrosive conditions have shown conflicting results. Some lab studies show an increase in the time required to crack (Cornet and Bresler 1996) while others show a reduction in the time required to crack (Griffin 1969). A field study of galvanized steel reinforcement that had been in service for multiple years did not show significant deficiencies, however, it was noted that the chloride concentrations at the depth of the reinforcing steel were fairly low so it could not be conclusively determined that the galvanized bars were working effectively (Cook and Radtke 1977). Additionally, marine and accelerated field studies showed that galvanized steel reinforcement was successful in delaying the onset of corrosion related damage, such as delaminations or spalling, but will not prevent them entirely (Arnold 1976; Sopler 1973).

At the time of this research, very few coastal states specify or allow the use of galvanized steel, with Massachusetts, New York, and Texas being the only ones (MassDOT 2013; NYDOT 2017; TXDOT 2018). Virginia explicitly states that it should not be used (VDOT 2011).

2.3.2.3 Stainless Steel

Stainless steel as reinforcement was first introduced in the 1930s, though is not used often due to limited availability and high cost. It is currently being used more frequently as reinforcement for structures in environments with a higher corrosion potential due to its demonstrated improved ability to resist corrosion relative to conventional steel (ACI 2019). Stainless steel has also been used in conjunction with carbon steel in an effort to maintain a cost-effective design. This design methodology involves placing stainless steel in areas where corrosion is to be expected, such as the top

layer of a bridge deck where water containing chlorides may sit for extended periods, and placing carbon steel where corrosion is less likely to occur (ACI 2019).

Currently, there are three states (New York, Oregon, Texas) that offer stainless steel as an option for reinforcement (NYDOT 2017; ODOT 2018; TXDOT 2018). New York allows the use of epoxy coated steel, stainless steel, or galvanized steel for bridge reinforcement (NYDOT 2017). Oregon specifically states stainless steel should be used and epoxy coated steel is not permitted (ODOT 2018). Texas specifies the use of epoxy coated steel or galvanized steel, with stainless steel being required for areas of severe exposure (TXDOT 2018).

2.3.3 Admixtures

The most common admixtures specified in the different coastal states' bridge design manuals included Calcium Nitrite, fly ash, granulated blast furnace slag, and silica fume. These work in different ways and each fall under the category of either a corrosion inhibitor or a pozzolan.

2.3.3.1 Corrosion Inhibitors

A corrosion inhibitor is a chemical admixture that reduces the rate of corrosion on the reinforcing steel without actually reducing the concentration of the corrosive species. Corrosion inhibitors effectively raise the corrosion threshold level, requiring that a higher level of chlorides be present on the surface of the reinforcing steel in order for corrosion to initiate. Calcium nitrite is an example of a corrosion inhibitor and is currently used as a corrosion protection measure in Florida, Louisiana, Maine, New York, North Carolina, and Virginia (FDOT 2019; LADOTD 2005; MEDOT 2003; NCDOT 2018; NYDOT 2017; VDOT 2011).

2.3.3.2 Pozzolans

A pozzolan is a mineral admixture that is used to refine and reduce the concrete porosity by filling in the smaller gaps found between aggregates. By filling these gaps with very fine minerals, concrete demonstrates significantly enhanced resistance to chloride penetration (ACI 2019). However, the use of mineral admixtures can be counterproductive if too much is added. There are calcium hydroxides ($Ca(OH)_2$) formed when portland cement hydrates which creates a buffer for the pore solution, helping to maintain a constant pH level. When too much of a mineral admixture is introduced, all of the calcium hydroxides will be used in the pozzolan reaction (ACI 2019). This eliminates its ability to act as a buffer and allows the pH to get to a lower level where the steel will no longer be passivated. Fly ash, granulated blast furnace slag, and silica fume are examples of pozzolans that are currently being used as a corrosion protection measure in California, Florida, Louisiana, Maine, North Carolina, Oregon, and Rhode Island (Caltrans 2003; FDOT 2019; LADOTD 2005; MEDOT 2003; NCDOT 2018; ODOT 2018; RIDOT 2007).

2.4 Review of Coastal States Corrosion Policies

As a method of determining the state-of-the-art in terms of corrosion prevention policies, multiple states' DOT bridge design manuals were analyzed. For completeness, all states that have a coastal boundary were involved in this study. The states included were Alabama, California, Connecticut, Delaware, Florida, Georgia, Louisiana, Maine, Massachusetts, Mississippi, New Jersey, New York, North Carolina, Oregon, Rhode Island, South Carolina, Texas, Virginia, and Washington. Maryland was not included in this study due to difficulties locating the correct design manuals.

This section is divided into two subsections. The first subsection presents a complete table (Tables 2.1.a through 2.1.d) displaying each coastal state and their policy, if any, regarding the given header. The second subsection includes a more in-depth description of a select few states that employ more advanced corrosion related policies. The states that are discussed here include California, New Jersey, and Delaware.

Table 2.1.a. Comparison of Coastal States' Corrosion Policies.

State	Alabama	California	Connecticut	Delaware	Florida
Definition of Corrosive Zone	-	Based on ppm Cl (>500 ppm is corrosive)	-	Corrosive environments [2]	Based on distance from water and ppm Cl (Multiple zones)
Top of Deck Concrete Cover (in.)	2 [1]	2.5	AASHTO, unless noted	3 (coastal regions)	2 (bridges <100') 2.5 (bridges >100')
Required Steel Type	-	Engineers Discretion	Epoxy required on certain elements (deck)	Epoxy Coating	Explicitly stated NOT to use epoxy coating
Corrosion Inhibitor	-	-	-	-	Engineers Discretion
Corrosive Water	-	>500 ppm Cl	-	-	>2000 ppm Cl - Marine structure (varies by amount and location)
Expected Service Life (Years)	-	75	-	Existing 75 New 100	-
Common Admixtures	-	ASTM C618 Type F or N (Fly ash)	-	-	Fly ash, slag, silica fume, metakaolin
Chloride Testing	-	-	-	AASHTO C856, T-24, & T260, ASTM C876 & C1202, half-cell test	-

[-] No mention in appropriate DOT design manual.
[1] Not explicitly defined for corrosion prevention.
[2] Not explicitly defined in appropriate DOT design manual.
[3] No distinction between bridges in areas of high vulnerability to corrosion and those in areas of low vulnerability.
[4] Provision is defined more for deicing operations than seawater corrosion prevention.

Table 2.1.b. Comparison of Coastal States' Corrosion Policies (continued).

State	Georgia	Louisiana	Maine	Massachusetts	Mississippi
Definition of Corrosive Zone	Coastal Counties	Coastal splash zones, deicing areas, history of corrosion	All salt-water crossings	-	-
Top of Deck Concrete Cover (in.)	2 (Above Fall Line) 2.25 (Below F.L) [4]	2 [1]	2 (unless noted) [1]	-	-
Required Steel Type	Epoxy coating for top of deck steel	Epoxy coating in Divisions using deicing agents [4]	Engineers Discretion (recommend not using epoxy)	Epoxy coating or galvanized [1,2]	-
Corrosion Inhibitor	-	Calcium Nitrite (0.0748 - 0.2245 gal/ft^3)	Calcium Nitrite in PSC units (5.5 gal/yd^3)	-	-
Corrosive Water	-	-	-	-	-
Expected Service Life (Years)	-	-	-	New, 75	-
Common Admixtures	-	Silica fume, fly ash	Silica fume in class LP (low permeability) concrete	-	-
Chloride Testing	-	-	Cl Content at 1" intervals starting at ½" depth	Cl Core Analysis	-

[-] No mention in appropriate DOT design manual.
[1] Not explicitly defined for corrosion prevention.
[2] Not explicitly defined in appropriate DOT design manual.
[3] No distinction between bridges in areas of high vulnerability to corrosion and those in areas of low vulnerability.
[4] Provision is defined more for deicing operations than seawater corrosion prevention.

Table 2.1.c. Comparison of Coastal States' Corrosion Policies (continued).

State	New Jersey	New York	North Carolina	Oregon	Rhode Island
Definition of Corrosive Zone	Zones 1, 2, 3A, 3B	-	Two corrosive boundary lines	Marine Environment (distance from ocean, nearby geography)	Designated coastal environments [2]
Top of Deck Concrete Cover (in.)	2.5	2.25	2.5 [3]	2.5 (minimum of 2 in Marine)	2 (wearing surface), 3 (exposed deck) [3]
Required Steel Type	Epoxy coating for all deck steel	Epoxy, stainless steel, or galvanized for all deck steel	Epoxy coating	Stainless Steel (Epoxy not permitted)	Epoxy Coating [3]
Corrosion Inhibitor	-	Calcium Nitrite in PSC	Calcium Nitrite	-	-
Corrosive Water	-	-	-	-	-
Expected Service Life (Years)	100	100 for stainless steel, 50-75 for chromium steel, 40 for galvanized or epoxy, 20 for plain	100	-	-
Common Admixtures	-	-	Fly ash, silica fume, granulated blast furnace slag	Microsilica	Engineers Discretion [2]
Chloride Testing	Cl Analysis, half-cell test, Cl permeability	-	-	AASHTO T260, Cl Core Analysis, ASTM C1152	-

[-] No mention in appropriate DOT design manual.
[1] Not explicitly defined for corrosion prevention.
[2] Not explicitly defined in appropriate DOT design manual.
[3] No distinction between bridges in areas of high vulnerability to corrosion and those in areas of low vulnerability.
[4] Provision is defined more for deicing operations than seawater corrosion prevention.

Table 2.1.d. Comparison of Coastal States' Corrosion Policies (continued).

State	South Carolina	Texas	Virginia	Washington
Definition of Corrosive Zone	Coastal Counties (NW part of state for deicing)	District-specific	Corrosive environment, Marine [2]	Coastal/corrosive environments [2]
Top of Deck Concrete Cover (in.)	2.5 [3]	2.5 [4]	2.5	AASHTO, unless noted
Required Steel Type	-	Epoxy coating or galvanized. Stainless steel for severe exposure	References to current IIM-S&B-81). Epoxy or galvanized not permitted	Epoxy coating
Corrosion Inhibitor	-	-	Apply to prestressed tendons if approved	-
Corrosive Water	-	-	-	-
Expected Service Life (Years)	-	-	-	-
Common Admixtures	-	-	Not specified for concrete	-
Chloride Testing	Cl Analysis	-	Not specified for concrete	-

[-] No mention in appropriate DOT design manual.
[1] Not explicitly defined for corrosion prevention.
[2] Not explicitly defined in appropriate DOT design manual.
[3] No distinction between bridges in areas of high vulnerability to corrosion and those in areas of low vulnerability.
[4] Provision is defined more for deicing operations than seawater corrosion prevention.

2.4.1 California DOT Bridge Design Manual

California is distinguished due to its strict and specific policies related to corrosion protection and prevention. The focus of this section is on the specifications related to minimum concrete cover.

California employs the use of a very detailed table to determine what the minimum concrete cover thickness is to be for a particular project in order to attain a service life of 75 years. The table, which is shown on the following page in Table 2.2, is organized by rows displaying the structural element of interest and columns displaying the minimum cover thickness based on the exposure condition. The following paragraph defines the terms used in the table to better understand what is being displayed.

The following definitions are all paraphrased from California's DOT bridge design specifications (Caltrans 2003). Marine atmosphere includes the atmosphere over land that is within 1,000 feet of ocean water or tidal water and the atmosphere directly above the splash zone. Tidal water is defined as being any body of water with a chloride content of at least 500 parts-per-million (ppm). 500 ppm is also the minimum threshold value defined for corrosive water. The splash zone is described as being the region between the Mean Lower Low Water (MLLW) elevation and up to 20 feet above the Mean Higher High Water (MHHW) elevation as well as a horizontal distance of 20 feet from the edge of the water (Caltrans 2003). Additionally, it is noted that for structural elements in direct contact with ocean spray the concrete cover shall be determined based on the requirements for a chloride concentration of greater than 10,000 ppm in the corrosive splash zone.

Table 2.2. Minimum Concrete Cover for 75-year Design Life.
(Originally Table 8.22.1 in Caltrans Bridge Design Specifications (Caltrans 2003))

	Exposure condition									
	Non-corrosive Atmosphere/ soil/water	Marine Atmosphere	Corrosive soil above MLLW level			Corrosive soil below MLLW level	Corrosive water permanently below MLLW level	Corrosive splash zone		Deicing salt, snow run-off, or snow blower spray
			Chloride Concentration (ppm)					Chloride concentration (ppm)		
			500 – 5,000	5,001 – 10,000	Greater than 10,000			500 – 5,000	5,001 – 10,000	Greater than 10,000	
			(a)	**(a)**	**(a)**	**(a)**	**(a),(b)**	**(a),(b)**	**(a),(b)**	**(a),(b)**	**(a),(c),(e)**
Footings & pile caps	3	3	3	4	5	3	2	2	3	3.5	2.5
Walls, columns & cast-in-place piles	2	3	3	4	5	3	2	2	3	3.5	2.5
Precast piles and pile extensions	2	2[d]	2[d]	2[b),(d)]	3[b),(d)]	2[d]	2	2	2[d]	2.5[d]	2[d]
Top surface of deck slabs	2	2.5						2.5	2.5	2.5[d]	2.5
Bottom surface of deck slabs	1.5	1.5						2	2.5	2.5[d]	2.5
Bottom slab of box girders	1.5	1.5						2	2.5	2.5[d]	1.5
Cast-in-place "I" and "T" girders; cast exposed faces of box-girder webs, ben caps, diaphragms, and hinged joints (f)	1.5	3						2	2.5	2.5[d]	3
Curbs & railings	1	1[b]						1	1	1[d]	1
Concrete surface not exposed to weather, soil or water	Principal reinforcement: 1.5 inches Stirrups, ties and spirals: 1.0 inch										

General Notes: 1. Mineral admixtures conforming to ASTM Designation C618 Type F or N, are required for all exposure conditions, except for 'non-corrosive' exposure conditions.
2. For protection of bundled bars, ducts and /or prestressing steel, see Articles 8.22.2, 8.22.3 and 8.22.4.
3. The minimum cover at the corners, beveled edges, and curved surfaces shall be the same as that in the corresponding structural elements.

Footnotes: (a) The maximum water to cementitious material ratio shall not exceed 0.40.
(b) Use pre-fabricated epoxy coated reinforcing bars (ECR).
(c) Use post-fabricated ECR.
(d) Mineral admixtures conforming to ASTM Designation C1240 and/or ASTM Designation C618 Type F and/or N, may be required.
(e) The minimum concrete cover and other requirements in structural elements exposed to de-icing salt, snow run-off, or snow blower spray shall be adopted only where the structural elements are directly exposed to these corrosive conditions, otherwise the requirements specified for non-corrosive conditions shall be adopted.
(f) For precast "I" and "T" girders, the minimum cover may be reduced (depending on site conditions).

Additionally, as shown in the general notes in Table 2.2, it is specified that mineral admixtures following ASTM C618 Type F or N are required for all exposure conditions, with the exception of non-corrosive conditions. Type F and N are both referring to a class of fly ash as designated within ASTM C618 (ASTM 2019). This means that all structures meeting any of the requirements to be considered within a corrosive area are required to include fly ash as a protective measure.

2.4.2 New Jersey DOT Bridge Design Manual

The New Jersey Department of Transportation (NJDOT) is distinguished from other states' corrosion related policies in that they provide a very detailed description of analyzing the extent of corrosion and defining what steps to take upon identification of corrosion related damage. This section will focus on the process utilized by the NJDOT to identify and remediate corrosion damage on bridge decks.

The field survey performed by the NJDOT includes visual observations, delamination detection, concrete sampling for chloride testing, half-cell potential testing, and a pachometer survey. This testing strategy is used to determine existing defects and areas of bridge decks that are actively deteriorating. The combined results of each section are then used to assist engineers in evaluating the current condition of a bridge deck. The following subsections provide a brief description of each step of the analysis.

The visual survey is used to identify the extent of damage such as spalling or cracking. The extent of spalling is generally reported as a percentage of the total deck area. The information gained from the visual survey is then used to determine specific areas of the bridge that may require additional investigation or testing. In addition to identifying locations that are spalling or cracking, a delamination survey is also

performed to determine the subsurface condition of concrete bridge decks. This can be completed by either performing a chain drag or using a ground penetrating radar (GPR) (NJDOT 2016).

A chloride analysis is performed to provide a quantitative measure of the chloride levels within the concrete at varying depths. The threshold chloride content, or amount needed for corrosion to initiate, that the NJDOT defines is approximately 2 pounds of chloride per cubic yard of concrete (NJDOT 2016). The number of samples from each bridge should be randomly selected using statistical methods and the locations should be plotted on a plan view of the deck. The minimum requirement is that there be at least 10 locations tested for every 6,000 square yards of deck area (NJDOT 2016).

The half-cell potential test is performed to determine areas of the deck where there is active corrosion. The NJDOT Design Manual defines the following ranges for half-cell potential readings: a potential difference more negative than -0.35 volts (V) indicates a high probability of active corrosion; potential readings between -0.35 V and -0.20 V indicate the possibility of active corrosion; potential readings less negative than -0.20 V indicate the probability of inactive or no corrosion (NJDOT 2016). Additionally, it is specified that the ambient air temperature has been above 40°F for a minimum of 72 hours before performing the test.

A pachometer survey of the bridge deck is the final step in the deck survey process. The pachometer survey is used to identify the depth of the steel from the surface of the concrete deck, or the cover thickness. This can then be compared against the required minimum cover depth.

Following the investigation as described above, the bridge deck is then placed into one of the following categories (NJDOT 2016):

- Category 1 – Extensive Active Corrosion
    - 5% or more of the total deck area is spalled
    - OR 40% or more of the deck area has deteriorated or has been contaminated by any combination of the following: spalls, delamination, corrosion potentials more negative than -0.35 V
    - OR 40% or more of the area of the bridge deck indicated by random chloride sampling contains greater than 2.0 pounds of chloride per cubic yard of concrete at the level of the top reinforcing steel
- Category 2 – Moderate Active Corrosion
    - 0 to 5% of the total deck area is spalled
    - OR 5 to 40% of the deck area has deteriorated or has been contaminated by any combination of the following: spalls, delamination, corrosion potentials more negative than -0.35 V
    - OR 5 to 40% of the area of the bridge deck indicated by random chloride sampling contains greater than 2.0 pounds of chloride per cubic yard of concrete at the level of the top reinforcing steel
- Category 3 – Light to No Active Corrosion
    - No spalls
    - OR 0 to 5% of the deck area has deteriorated or has been contaminated by any combination of the following: spalls, delamination, corrosion potentials more negative than -0.35 V

- OR 0 to 5% of the area of the bridge deck indicated by random chloride sampling contains greater than 2.0 pounds of chloride per cubic yard of concrete at the level of the top reinforcing steel

Once the bridge deck has been investigated and placed into the appropriate category, the recommended remediation procedures can be found in the following table, Table 2.3, which was created by the NJDOT.

Table 2.3. Restoration Procedures for Structures Affected by Corrosion. (Originally Table 9.1 in NJDOT Design Manual (NJDOT 2016))

Category	**Procedures**	**Restoration** (Considered Permanent)	**Restoration** (Estimated extended life 10 to 15 yrs)
Structurally Inadequate		Complete Deck Replacement (Unless restorable)	
1. Extensive Active Corrosion	Required Restoration Work	Complete Deck Replacement	Removal of all deteriorated concrete. Follow the repair procedure approved for the protective system selected.
	Testing Steps (see below)	Steps 1 through 4 as necessary. (Probably only step 1)	Step 1 only, except all the testing steps on the first five (5) bridge decks (spans) plus 10% of the remaining bridge decks.
	Suggested Protective Systems	Membrane with HMA overlay*; Concrete Thin (less than 1") Overlay Protective System. *	Membrane with HMA overlay**; Concrete Thin (less than 1") Overlay Protective System. **
2. Moderate Active Corrosion		Same as Category 1 above or Same as Category 3 below, as determined by the State.	Same as Category 1
3. Light To No Active	Required Restoration Work	Removal and Replacement of all areas of deterioration and chloride contaminated concrete as determined by corrosion potentials and/or chloride sampling. (Less than 5% of the deck area is bad).	Same as Category 1 Note: For this category of condition, permanent restoration is recommended.
	Testing Steps	Steps 1 through 4.	Same as Category 1
	Suggested Protective System	Membrane with HMA overlay*; Concrete Thin (less than 1") Overlay Protective System. *	Membrane with HMA overlay**; Concrete Thin (less than 1") Overlay Protective System. **

* When approved prior to Preliminary Plan ** Submission on a project to project basis

Testing Steps:

1.	Visual	3.	Half-Cell Test		
2.	Chloride Analysis	4.	Pachometer Test		

2.4.3 Delaware DOT Bridge Design Manual

Delaware is distinguished in their specifications related to the testing and inspections of concrete bridge decks that are showing potential signs of active corrosion. The description of testing and inspections falls under the chapter of Bridge Preservation Strategies in the Delaware Department of Transportation (DelDOT) bridge design manual which includes two types of projects, either bridge rehabilitation or preventative maintenance (DelDOT 2017). This section will focus on the many considerations when determining the current condition of a bridge deck and what type of remediation is appropriate.

The DelDOT defines the test specifications to be used when performing a bridge inspection, which include both ASTM and AASHTO standardized test methods. The following table, Table 2.4, describes which test is to be performed based on what is required of the inspection.

Table 2.4. Specifications for Testing of Field Materials.
(Originally Table 109-1 in DelDOT Design Manual (DelDOT 2017))

Specification	Description
Tests performed by DelDOT Materials & Research (M&R) Section	
AASHTO T24 (ASTM C42)	Obtaining and Testing Drilled Cores and Sawed Beams of Concrete
ASTM C856 (Annex A only)	Petrographic Examination of Hardened Concrete
AASHTO T260	Sampling and Testing for Chloride Ion in Concrete and Concrete Raw Materials
ASTM C1583	Tensile Strength of Concrete Surfaces and the Bond Strength or Tensile Strength of Concrete Repair and Overlay Materials by Direct Tension (Pull-off Method)
ASTM C457	Microscopical Determination of Parameters of the Air-Void System in Hardened Concrete
Tests performed by Outside Agencies	
ASTM C856	Petrographic Examination of Hardened Concrete
ASTM C876	Corrosion Potentials of Uncoated Reinforcing Steel in Concrete
ASTM C1202	Electrical Indication of Concrete's Ability to Resist Chloride Ion Penetration

The DelDOT defines a procedure for determining the current condition of concrete bridge decks. This procedure involves a visual inspection, delamination survey, reinforcement corrosion survey, pachometer survey, and deck coring. Each section of the inspection is briefly described in the following paragraphs.

The visual inspection involves the assessment of the following five conditions: cracking, spalling, scaling, wear, and efflorescence (DelDOT 2017). The entire bridge deck, both the top surface and the underside, should be inspected for signs of the previously mentioned conditions.

The delamination survey can be completed using either the chain-drag or hammer-sound testing methods. The location, size, and amount of delamination should be documented on a plan drawing of the bridge being inspected. Generally, the DelDOT suggests surveying the entire deck surface, however, it is permitted to test select areas of larger decks that can be used to estimate the condition of the entire deck. These areas should be selected to include sections that experience the most heavy-truck traffic or deicing exposure and the pier and joint locations. In the case that the entire deck is not surveyed, the locations should be representative to provide a balanced report of the deck condition (DelDOT 2017).

The reinforcing corrosion survey consists of performing a half-cell potential survey of the bridge deck. The DelDOT suggests that the entire deck should be surveyed, however, if it is not practical then a sufficient number of typical areas should be tested to provide a complete picture of the current condition. In addition to the half-cell readings, the tester should note whether epoxy coated reinforcement is present in the top layer only or in both the top and bottom layer. The results of the half-cell potential testing should be

plotted on a contour map to make it easier to identify regions where there is a high probability of active corrosion. Finally, it is suggested that cores in areas where active corrosion is predicted as well as areas where no active corrosion is predicted should be collected and visually inspected to confirm the predicted conditions (DelDOT 2017).

A pachometer survey is performed to determine the actual depth of steel cover where other tests have been performed. The DelDOT notes that this information is useful when determining the significance of the results from chloride content testing.

Finally, concrete core samples are collected from a bridge and are then either returned to a DelDOT research laboratory or sent to an external testing agency. One of the tests performed with concrete cores is a chloride content analysis (AASHTO T260, 2016). The range that is specified for a corrosion threshold is approximately 0.02 to 0.03% by weight of concrete, or 1.0 to 1.5 pounds of chloride per cubic yard, for uncoated steel in non-carbonated concrete (ACI 2008; DelDOT 2017). The following paragraph will describe the process used to perform chloride content testing.

The chloride content test is recommended to be determined and plotted against the depth of concrete where the sample was taken. The DelDOT suggests testing 0.25-inch (in.) slices from a 4-in. diameter concrete core at depths of 0.375 in., 1 in., 2 in., and 3 in. It is recommended that the test be performed at depths greater than 3 inches if there is significant chloride contamination at the 3-inch depth. Additionally, it is recommended that the background chloride concentration is determined by using at least two samples and testing at a depth that the chloride content would not be affected by chloride ingress from the concrete surface. The number of cores that should be taken for testing is

approximately one core per 2,000 square feet of total deck area, however, there should be a minimum of three cores taken for chloride content testing.

Following the full inspection of a bridge deck as described above, the DelDOT performs a deck characterization. This is a process that is used to identify the current condition of a bridge deck and determines what type of remediation is required. The deck characterization process is based on the following four factors:

- Percent deck distress and visual condition ratings;
- Estimated time-to-corrosion;
- Deck surface condition;
- Concrete quality.

Based on how a bridge is scored in each of the above categories, the table on the following page (Table 2.5) is used to determine what type of remediation is required, if any. This is the final step in the full investigation process of a bridge deck.

Table 2.5. Remediation Choices Based on Deck Characterization.
(Originally Table 109-3 in DelDOT Design Manual (DelDOT 2017))

Table 109-3. Deck Repair Evaluation Matrix

Factors Repair	Deck Distress		Time-to-Corrosion Initiation	Deck Surface Problems	Concrete Quality Problems
Do Nothing	% Distress	< 1%	> 10 years	none	none
	% Distress + half cell	< 5%			
	NBI deck rating	≥ 7			
	underside rating	≥ 7			
Maintenance	% Distress	1 – 10%	> 5 years or > 10 years	none	none
	% Distress + half cell	1 – 15%			
	NBI deck rating	≥ 5			
	underside rating	≥ 5			
Overlay	% Distress	2 – 35%	Ongoing to < 5 years	yes	yes
	% Distress + half cell	10 – 50%			
	NBI deck rating	≥ 4			
	underside rating	≥ 5			
Rehabilitation	% Distress	> 35%	Ongoing	yes	yes
	% Distress + half cell	> 50%			
	NBI deck rating	≤ 3			
	underside rating	≤ 4			

NBI = National Bridge Inventory

2.5 Test Methods and Properties

A portion of this project included performing field investigations of structures located within the NCDOT defined corrosive zones (discussed in Section 1.1.1). These field visits included the collection of corrosion rate data, surface resistivity data, and powder samples. This section includes the process for selecting the corrosion rate and surface resistivity testing device, the methodology of the testing device, and a discussion of surface resistivity and corrosion rate. The powder samples were analyzed by Ross Newsome, a fellow UNC Charlotte graduate student, and were discussed in detail in his thesis (Newsome 2020), therefore they will not be discussed here.

2.5.1 Corrosion Measurement Device Selection

To obtain data about ongoing corrosion during field visits, a corrosion rate measurement device was used. These devices are capable of making several different measurements, some of them simultaneously, such as corrosion rate, polarization resistance of rebar, electrical resistivity of concrete, and half-cell potential. Two similar devices, the Giatec iCOR made by Giatec Scientific Inc. and the GalvaPulse made by Germann Instruments, were available on the market. The selection of the Giatec iCOR was made following a field trial of both devices by Jeffery Poe Jr., a fellow UNC Charlotte graduate student (Poe 2019).

The Giatec iCOR was the device selected to conduct field testing. While both devices are capable of performing the same measurement type, the iCOR was favored because it is a non-destructive testing (NDT) device. The GalvaPulse requires a physical connection to the reinforcing steel, which is not ideal as it leaves a direct path to allow chlorides to enter at an increased rate. The iCOR also benefits from a more user-friendly

interface, which includes a tablet that is wirelessly connected to the transducer. Additionally, testing indicated that the iCOR has a smaller margin of error and reported more precise measurements than the GalvaPulse (Poe 2019).

2.5.2 CEPRA Method of the Giatec iCOR

The iCOR makes use of Giatec Scientific's patented technology called Connectionless Electrical Pulse Response Analysis (CEPRA). CEPRA is what differentiates the iCOR from other corrosion measurement devices that were commercially available at the time of this study because it is not necessary to expose the reinforcing steel to take measurements. Using four electrodes, the electrical response of reinforcing steel in concrete can be determined. This is depicted in Figure 2.1 below. An AC current is applied to the surface of the concrete between the two outer electrodes while the voltage between the two inner electrodes is measured.

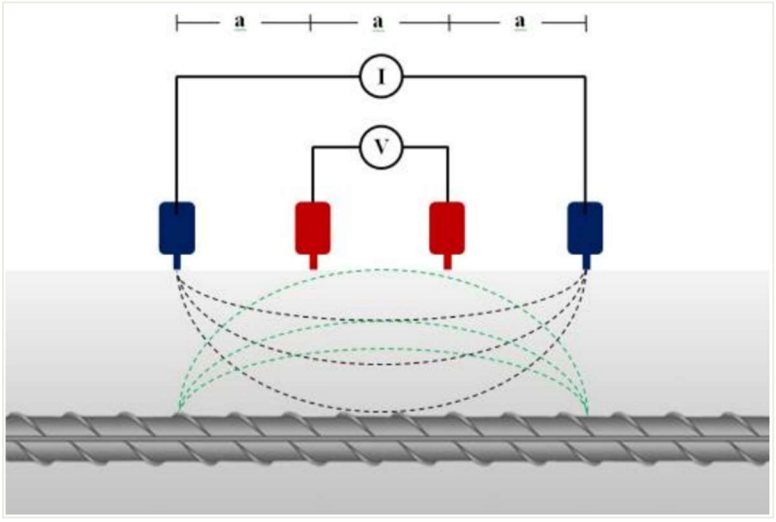

Figure 2.1. Layout of Electrodes Utilized by Giatec iCOR.
(Originally Figure 3 from Giatec iCOR Manual (Giatec 2019))

During testing, the applied AC current is varied between a low frequency and a high frequency while the voltage at the inner electrodes is recorded. The use of varying frequencies is key due to the difference in response between a corroding bar and a non-corroding bar. The voltage response of a non-corroding bar increases when a lower frequency is applied while the voltage response remains nearly constant with varying frequencies for a bar that is corroding (Giatec 2019). This relationship is depicted in Figure 2.2 below.

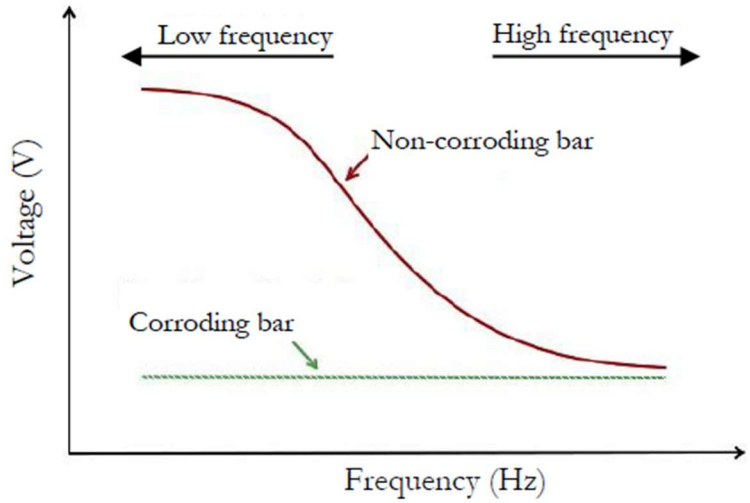

Figure 2.2. Graph Demonstrating Different Voltage Responses between a Corroding and Non-Corroding Bar (Originally Figure 4 from Giatec iCOR Manual (Giatec 2019)).

While the voltage response varies between a corroding and non-corroding bar under the application of various frequencies, direct measurement of this low-frequency response is time consuming and is vulnerable to noise corruption (Giatec 2019). This makes it highly impractical to apply this technique to measure the corrosion rate of steel embedded in concrete in a field setting. The Giatec iCOR avoids these issues by applying a narrow DC/AC current pulse over a short time period (6-10 seconds) while using a high sampling rate (3 samples per second) to record the voltage response (Giatec 2019).

The iCOR makes use of a complex electrical circuit model, shown in Figure 2.3 below, to predict various properties of the concrete and embedded steel. The companion tablet has a mathematical algorithm built into its software. This algorithm is responsible for performing the analysis of the recorded current and voltage data over time to determine various properties such as electrical resistivity and corrosion rate. These properties are discussed in Section 2.5.4.

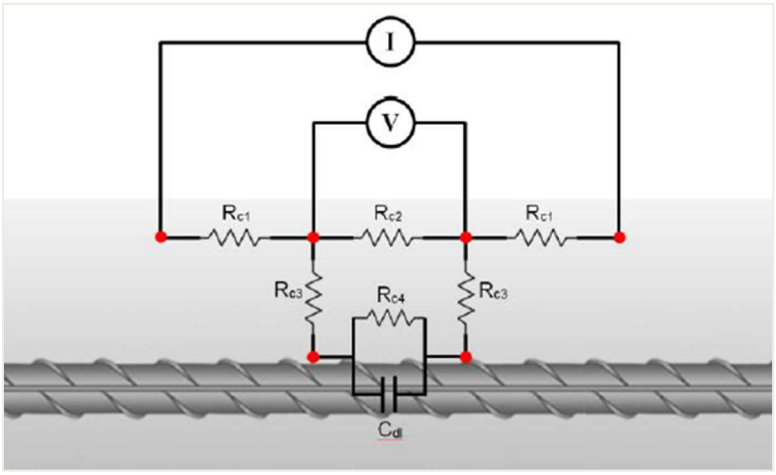

Figure 2.3. Electrical Circuit Utilized by Giatec iCOR.
(Originally Figure 5 from Giatec iCOR Manual (Giatec 2019))

2.5.3 Complications and Limitations of Giatec iCOR

The Giatec iCOR is capable of performing multiple tests such as half-cell potential, electrical resistivity of concrete, and corrosion rate. For the scope of this thesis, only the electrical resistivity, also called surface resistivity, and the corrosion rate were measured. The half-cell potential test was not be performed because it requires direct contact with the steel.

The limitations of the device that will ultimately determine the extent of testing that can be performed include the inability of the device to test epoxy coated steel,

galvanized steel, or prestressed post tensioned tendons that are placed in a protective tube. Additionally, the results can be affected by temperature, moisture, concrete cover thickness and material properties, and the availability of oxygen.

The interpretation of results is largely driven by the coefficient of determination, or R-squared value, which is the proportion of observed variation explained by the regression model (Devore 2010). The R-squared value ranges from 0.0 meaning no correlation to 1.0 meaning a perfect correlation. After each individual test is performed, the software plots a graph of change in voltage over the total test period and generates a best fit curve along with the corresponding R-squared value. At this stage, the data can either be saved if the R-squared value is acceptable or deleted so that the test may be performed again. The R-squared values that were accepted in the field are discussed in the following chapter (Chapter 3: Field Investigation).

2.5.4 Test Properties and Giatec iCOR Testing Methodology

As mentioned above, the Giatec iCOR was chosen for the field-testing portion of this thesis. The properties that were determined using the iCOR include the surface resistivity of the concrete and the corrosion rate of the embedded reinforcing steel. The following subsections (2.5.4.1 through 2.5.4.3) will describe each of these properties as well as the methodology utilized by the iCOR to determine the property.

2.5.4.1 Surface Resistivity

Surface resistivity is a measure of the ability for an electrical current to flow within a material and can be used as a parameter to describe the ability of concrete to resist the ingress of chloride ions (Lataste 2010). Resistivity can be influenced by several factors such as water content, cement type, water-to-cement ratio (w/c), and the presence

of chlorides. While some factors work to decrease the resistivity and therefore increase the risk of corrosion, some factors such as a low w/c ratio or the addition of a pozzolan (see Section 2.3.3.2 for examples) work to increase the resistivity, therefore decreasing the risk of corrosion (Bertolini et al. 2013). It has been shown that the addition of a pozzolan, such as silica fume (a common pozzolan used by the NCDOT), can reduce the electrical conductivity of concrete by more than 90% when compared against a conventional mixture with portland cement (Ramezanianpour et al. 2011; Shi et al. 1998). Surface resistivity is inversely related to electrical conductivity, meaning that as the conductivity is reduced, the resistivity is increased.

The resistivity of concrete can range in value from less than ten to hundreds of kiloohm-centimeters (tens to thousands of ohm-meters) with lower values indicating a higher risk of chloride ingress and higher values indicating a lower or negligible risk of chloride ingress (Bertolini et al. 2013). The following table (Table 2.6) presents global reference values for the surface resistivity of mature (age > 10 years), dense-aggregate concrete measured at 20°C (68°F) (Cox et al. 1997; Polder et al. 2000).

Table 2.6. Global Reference Values at 20°C for Resistivity of Mature (>10 years) Concrete. (Cox et al. 1997; Polder et al. 2000)

Environment	Concrete resistivity (Ω m)	
	Ordinary portland cement (CEM I)	Blast furnace slag cement CEM III/B (>65% slag) or fly ash cement CEM II/B-V (>25%) or with silica fume (>5%)
Very wet, submerged, splash zone (fog room)	50–200	300–1000
Outside, exposed	100–400	500–2000
Outside, sheltered, coated, hydrophobized (not carbonated) (20 °C/80% R.H.)	200–500	1000–4000
Ditto, carbonated	1000 and higher	2000–6000 and higher
Indoor climate (carbonated) (20 °C/50% R.H.)	3000 and higher	4000–10 000 and higher

There have been multiple recent projects completed at UNCC in which surface resistivity specifications were recommended for use by the NCDOT (Biggers 2019; Cavalline et al. 2020). However, Biggers' (2019) and Cavalline et al.'s (2020) recommendations were not followed here as they are primarily related to early age surface resistivity testing and all structures investigated for this thesis were within 10 to 15 years old at the time of testing. For the purpose of the field work, the ranges below (Table 2.7) were used to interpret the surface resistivity data. This table has been suggested for use by Feliu et al. (1996) and Polder et al. (2000).

Table 2.7. Classification of Surface Resistivity Results. (Feliu et al. 1996; Polder et al. 2000)

Color Code	Resistivity (kohm.cm)	Classification
Green	> 100	Very High
Yellow	50 - 100	High
Orange	10 - 50	Moderate
Red	< 10	Low

The Giatec iCOR is capable of determining the surface resistivity of concrete by making use of the following equation (Giatec 2019):

$$\rho = 2\pi a \times R \qquad (2.6)$$

In Equation 2.6, ρ is the surface resistivity, a is a constant parameter based on the geometry of the electrodes, and R is the equivalent resistance of the concrete. R is calculated from R_{c2}, R_{c3}, and R_{c4} which were previously defined in Figure 2.3. The iCOR user manual notes that by using this approach the effect of rebar would be minimized whereas other AC measurement techniques will have inherent error (Giatec 2019). It should be noted that the variables described above are all determined by the iCOR's companion tablet and the equation is solved automatically after testing a particular grid point.

2.5.4.2 Variability Associated with Surface Resistivity

Field testing of surface resistivity, regardless of testing device, has inherent variance due to constantly changing conditions such as fluctuations in the weather and tides. Presuel-Moreno et al. (2010) performed a field study of more than 60 new and old bridges located in coastal environments in Florida. The study included the creation of surface resistivity profiles at varying elevations of partially submerged reinforced concrete substructures at and above the mean water elevation. The field testing of surface resistivity was performed using a commercial Wenner probe with electrode spacings of 3 centimeters (cm) and 5 cm. The profiles demonstrated a surface resistivity gradient from low to high starting within the submerged zone and extending upwards to an elevation outside of the splash zone, which Presuel-Moreno et al. (2010) attributed to the elevation

dependence of moisture saturation (higher moisture content at lower elevations for example).

Concrete has an outer surface layer that can have a surface resistivity value different than that of the bulk material. This layer could be the result of chloride ingress, carbonation, or differential moisture content and can range in depths from a fraction of a millimeter to a few centimeters (Presuel-Moreno et al. 2010). It was found that the relative humidity at depths of 3 centimeters or greater is constant, which would result in a constant surface resistivity unless chlorides have penetrated deep enough (greater than 3 centimeters) (McCarter et al. 2000; Pruckner and Gjorv 2001; Saleem et al. 1996).

In addition to the field study, Presuel-Moreno et al. (2010) collected nominal 2-inch cores in the same vicinity as the surface resistivity profiles were tested and performed surface resistivity measurements in a controlled laboratory setting. Prior to performing the laboratory measurements, the cores were placed in a high humidity chamber for a few weeks (exact timeframe not specified). These resistivity measurements were considered to be wet while the resistivity measurements made in the field were considered to be dry. The wet and dry measurements were correlated, and it was discovered that the dry (field tested) resistivity values were about 3 times higher than the wet (laboratory conditions) resistivity values (Presuel-Moreno et al. 2010).

2.5.4.3 Corrosion Rate

The corrosion rate is usually described as the penetration rate and is typically expressed in μm/year (micrometers per year). There are many factors that can influence the magnitude of the corrosion rate such as temperature or humidity (Bertolini et al.

2013). Bertolini et al. (2013) suggest the following ranges for interpreting corrosion rate recordings:

- Negligible: Less than 2 µm/year
- Low: 2 – 5 µm/year
- Moderate: 5 – 10 µm/year
- Intermediate: 10 – 50 µm/year
- High: 50 – 100 µm/year
- Very high: Greater than 100 µm/year

Alternatively, the table below is suggested for use within the Giatec iCOR User Manual (Giatec 2019). For the purpose of the field work presented in this thesis, the ranges suggested within the iCOR User Manual (Table 2.8) were used to create the heat maps. In the discussion and analysis of the corrosion rates, both ranges were considered.

Table 2.8. Classification of Corrosion Rate Results (Giatec 2019).

Color Code	Corrosion Rate (µm/year)	Classification
Green	< 10	Passive/Low
Yellow	10 - 30	Moderate
Orange	30 - 100	High
Red	> 100	Severe

The iCOR is capable of calculating the corrosion rate by first determining the polarization resistance of rebar, or R_P, by making use of the following equations (Giatec 2019):

$$\mathrm{R}_P = A_P \times R_{c4} \qquad (2.7)$$

$$\mathrm{i}_{corrosion} = \frac{B}{R_P} \qquad (2.8)$$

In Equations 2.7 and 2.8, A_P is the polarized area of steel, R_{c4} is the charge transfer resistance of the steel (defined previously in Figure 2.3), $i_{corrosion}$ is the corrosion rate of the steel, and B is a constant parameter that is determined experimentally (Giatec 2019). It should be noted that the variables described above are all determined by the iCOR's companion tablet and the equations are solved automatically after testing a particular grid point.

2.5.5 Verification of Giatec iCOR Results

The Giatec iCOR makes use of the CEPRA method, described above, that was developed by Giatec Scientific. Fahim et al. (2018) performed a study which compared the corrosion rate measurements using five different techniques. The techniques included in the study are as follows: galvanostatic pulse technique, potentiodynamic technique, coulostatic technique, electrochemical impedance spectroscopy (EIS), and the CEPRA technique.

The reinforced concrete specimens prepared for the study were placed in sealed containers with a small layer of water to ensure the required oxygen and moisture was available for corrosion to initiate. With the exception of EIS, the corrosion rate measurements with each technique were collected weekly for 7 months. The EIS test was only performed after 3 and 4 months of exposure once the corrosion rates had stabilized due to the length required for a measurement. At the end of the testing period, the steel rebar was removed from the concrete specimens to allow for the calculation of the ratio of corroded area to total area. The mass loss of reinforcement was determined using ASTM G1 (ASTM 2003). Finally, using Faraday's law, the average corrosion rates were calculated from the mass loss results (Fahim et al. 2018).

The results of the study indicated that for the actively corroding specimens, the corrosion rates determined using the CEPRA method agreed well with the actual corrosion rates (Fahim et al. 2018). Fahim et al. (2018) reported that results for 21 out of 24 specimens fell within the range that is typically accepted in the literature, while the remaining 3 specimens underestimated the corrosion rate. The underestimation found was attributed to errors associated with the polarized area assumption. It was noted that the CEPRA method overestimated the corrosion rate in the case of passive corrosion of small diameter reinforcement, though it was also stated that this type of overestimation is common in other more conventional methods such as the galvanostatic pulse method (Fahim et al. 2018). In summation, Fahim et al. (2018) state that the CEPRA method produced good correlations between the predicted and actual corrosion rates for cases of actively corroding steel and that the results were very similar to those shown using the well-established techniques.

Since the previously discussed study focused primarily on the accuracy of the corrosion rate measurement ability of the CEPRA method, a study was performed to determine the similarity of surface resistivity results between the Giatec iCOR and a well-established surface resistivity device, the Proceq Resipod. The study concluded that the iCOR produced results similar to that of the Resipod and resulted in an improvement in the testing process. This comparison study and the results are discussed in detail in the following chapter (Chapter 3, Section 3.1.4.1).

CHAPTER 3: FIELD INVESTIGATION

This project included three field visits over which eight bridges were investigated. The visits were performed over the dates of August 5, 2019, November 1-3, 2019, and February 20-23, 2020. Each field investigation consisted of a review of existing information on the bridge (such as recent inspection reports and data available in the Bridge Management System), visual assessment of accessible surfaces, and at selected locations, surface resistivity tests, corrosion rate tests, and the collection of powder samples. The review of background information was performed before travelling to each bridge site. The Giatec iCOR was used in-situ for surface resistivity and corrosion rate testing. The powder samples were returned to a UNCC laboratory where they were tested for chloride content. Following the first field visit, it was decided to additionally investigate the corrosion inhibitor content using powder samples on the remaining structures. The collection and analysis of powder samples is not discussed here as that portion of the project was completed by Ross Newsome, a fellow graduate student at UNCC, and is discussed in detail in his thesis (Newsome 2020).

This chapter begins by providing an overview of each stage of the field investigation as introduced above followed by a summary and discussion of the results.

3.1 Methodology of Field Investigations

The following subsections will provide an overview of each aspect of the investigations. This includes bridge selection, background information review, visual

assessment, and surface resistivity and corrosion rate testing. Additionally, a comparison study to assess the accuracy of the Giatec iCOR's surface resistivity results is discussed.

3.1.1 Bridge Selection

The bridges selected for investigation were chosen due to their age, location, relative proximity to each other (to assist with fieldwork scheduling and logistics), and accessibility. For this research, only bridges constructed within the last 10 to 15 years (2003 to 2008) and located within either the corrosive or highly corrosive zone were considered. This age range allows only bridges with a minimum of 10 years of exposure and constructed under the NCDOT's corrosion policy to be selected. From there, the relative proximity between prospective bridges was considered to allow visits to the coast to be more efficient. As a final criterion, it was determined which bridges would provide the easiest access to the elements of interest (such as the piers or caps).

3.1.2 Background Information Review

A review of background information was performed for each bridge before going to the field. This was facilitated by looking at the most recent inspection reports, which were provided for each site by the NCDOT. These reports include substructure and superstructure element type (precast concrete, cast-in-place concrete, steel, etc.), multiple recent photographs of the structure, identification of visual defects or signs of corrosion, suggestions for maintenance, year constructed, and geometric properties (length, number of lanes, number of spans, etc.), among other information from the inspection that was not pertinent to this study. From this information, it was determined what kind of equipment was required, such as a ladder, waders, or a boat, and what tests were able to be performed on what elements.

3.1.3 Visual Assessment

Visual assessment was used to identify areas of the structural components that appear to be showing signs of deterioration and judge whether they are corrosion related. It also provided guidance as to where the most significant damage is, what the cause of the damage is, and what plan of action is required for repair. For the purpose of this project, the concern was more directed towards what the current state of each bridge is and identifying the level of corrosion rather than developing a plan of action for repair.

Some of the most common signs of corrosion related deterioration are cracks parallel to the reinforcement, spalling of the concrete cover, and rust staining (Bertolini et al. 2013). These are typically the most important signs of deterioration to identify and take note of. Additional signs to look for and take note of are cracks and signs of ponding or water runoff patterns. At each structure, pictures were taken of the entire structure and visible signs of corrosion.

3.1.4 Surface Resistivity and Corrosion Rate Testing

The Giatec iCOR was used to test for the corrosion rate and surface resistivity. As discussed previously, this device is capable of performing both tests simultaneously. The testing locations were selected to obtain data at different levels of exposure. Data was collected at elevations ranging from within the splash zone, which receives the highest exposure to chloride-rich waters, to the underside of the cored slabs, which typically receives very low exposure depending on the structure's height above the water. The elements tested included the piers and bent caps, if accessible, underside of the cored slabs, and the bridge deck where applicable (the iCOR is not able to test through asphalt or epoxy overlays). To ensure consistency of results at each structure, it was attempted to

obtain a similar number of readings from each element of interest at each structure. This was not always possible due to accessibility (i.e. cap too high above water or piers that are entirely submerged).

The software associated with the iCOR includes an R-squared value with each set of results. This allows the user to either accept or reject a particular data point while in the field. During the first field visit, results with an R-squared value of 0.70 or higher were accepted. A lower R-squared value allows for higher variability in the results. To decrease the variability of the results collected during the second and third field visit, the minimum acceptable R-squared value was increased to 0.90. Due to concerns relating to the accuracy of the Giatec iCOR's surface resistivity readings during the first and second field visit, a comparison study was developed to confirm the results. The details and results of the experiment are discussed in the following subsection.

3.1.4.1 Giatec iCOR and Proceq Resipod Comparison Study

To confirm the surface resistivity readings obtained using the Giatec iCOR, a comparison study was performed with the iCOR and the Proceq Resipod. The goal of this study was to compare the results of each device using the same testing grid, shown below in Figure 3.1, in order to justify the surface resistivity results collected during field visits one and two. The results of this study also provided justification of the surface resistivity readings obtained during the third field visit. Additionally, the study led to an improved testing methodology that was adopted for field visit three.

Figure 3.1. Test Grid for iCOR versus Resipod Comparison Study.

The testing grid shown in Figure 3.1 is an exterior vertical barrier wall located in the East Deck parking garage on the UNCC campus. The wall was located outside but is on a midlevel and is therefore sheltered from above. The test was performed on December 17, 2019. The temperature during testing was 61°F and the relative humidity was 91%.

The testing included utilizing a pachometer to locate the steel followed by the marking of the six individual test locations. Each location was saturated using the same process performed in the field during field visits one and two. This process consisted of spraying the locations of interest with water and allowing it to soak for approximately 10 minutes before beginning the test. After thoroughly wetting the surface, each location was tested with both the iCOR and Resipod every 10 minutes for a total of 60 minutes. The Resipod was tested perpendicular to the embedded rebar to minimize the effect of the steel. The following graphs (Figure 3.2 (a) through (f)) were created by plotting the results of both devices at each location.

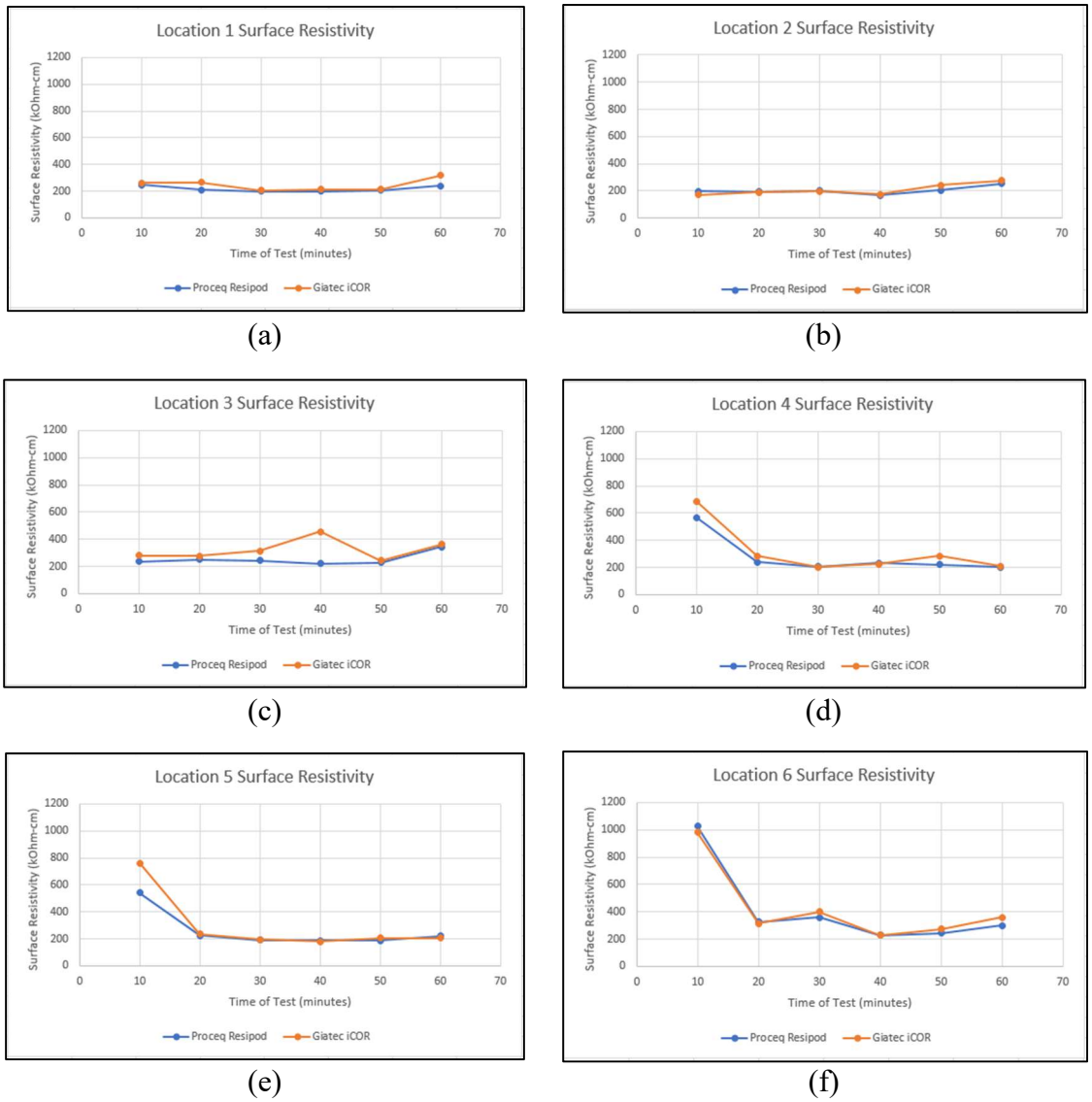

Figure 3.2.(a) – (f). Surface Resistivity Results from Comparison Study.

With the exception of a few outliers, such as Location 3 at 40 minutes (Figure 3.2.(c)) or Location 5 at 10 minutes (Figure 3.2.(e)), the results obtained from each device follow the same trends and are close in magnitude throughout the entire 60-minute testing period. From the graphs above, it was concluded that the surface resistivity results obtained from the Giatec iCOR are very similar to the resistivity results obtained using the Proceq Resipod at any time within a 60-minute testing period. Based on the results of

this comparison study, the resistivity measurements obtained during field visits one and two into the final analysis of the current condition of structures at the coast.

As an additional accuracy check while in the field, alongside the R-squared value discussed above, the Proceq Resipod was included in the iCOR testing procedure on field visit three. This additional check was performed by first testing a grid point using the iCOR. The companion tablet provided immediate resistivity results along with the R-squared value. If the R-squared value was acceptable (R-squared > 0.90), the Resipod was then used at the same grid point to obtain a secondary confirmation that the resistivity value determined using the iCOR was accurate. This method ensured that outliers were noticed in the field and allowed the grid point to be retested.

3.2 Field Investigation Results

This section presents summary results for the corrosion rate and surface resistivity measurements of each structure. Additionally, the individual results for each structure visited as well as a brief discussion of the visual inspection are presented. In many of the photographs in the following subsections, an "L" followed by a number is shown; this is a callout showing where powder samples were collected. The heat maps were created using the ranges presented in Table 2.8 (see Section 2.5.4.3). The discussion will use these same ranges to categorize results, although the categories based on ranges suggested by Bertolini et al. (2013) (see Section 2.5.4.3) were included in parentheses and considered in the final analysis of current condition.

A detailed narrative of each field investigation along with photographs can be found in Appendix A. Additionally, the raw corrosion rate and surface resistivity data for each structure is in Appendix B.

3.2.1 Summary Results

The following table presents the minimum, median, and maximum corrosion rate and surface resistivity results for each structure. It should be noted here that low corrosion rate values indicate a lower likelihood of active corrosion while high surface resistivity values indicate a lower likelihood of chloride ingress therefore a lower likelihood of active corrosion. This is reflected by the color coding in the table. Additionally, information related to the structure location, age, and testing location is included. The table is organized from top to bottom by corrosive zone with the highly corrosive zone first and then by age from oldest to newest.

Table 3.1. Field Investigation Summary Table.

Structure Number	Zone	Year Built	Corrosion Rate µm/year		Location on Structure	Surface Resistivity kOhm.cm		Location on Structure
660091	Highly Corrosive	2005	Low	0.03	Cored Slab, Above Splash Zone	High	459.6	End Bent, Above Splash Zone
			Median	8.9	-	Median	80.9	-
			High	54	End Bent, Above Splash Zone	Low	39	Cored Slab, Above Splash Zone
090061	Highly Corrosive	2005	Low	0.6	Pier, Above Splash Zone	High	403	Pier, Above Splash Zone
			Median	13.5	-	Median	51	-
			High	274	Pier, In Splash Zone	Low	6.7	Pier, In Splash Zone
660021	Highly Corrosive	2005	Low	0.23	Pier, Above Splash Zone	High	646	Bent Cap, Above Splash Zone
			Median	2.7	-	Median	128.5	-
			High	10	Pier, In Splash Zone	Low	45	Cored Slab, Above Splash Zone
640010	Highly Corrosive	2006	Low	0.03	Bent Cap, Above Splash Zone	High	801	Bent Cap, Above Splash Zone
			Median	6.15	-	Median	86	-
			High	77	Pier, In Splash Zone	Low	7.2	Cored Slab, Above Splash Zone
150026	Highly Corrosive	2006	Low	0.13	Bent Cap, Above Splash Zone	High	775	Bent Cap, Above Splash Zone
			Median	3.9	-	Median	246	-
			High	52	Wing Wall, Above Splash Zone	Low	123	Cored Slab, Above Splash Zone
260007	Highly Corrosive	2007	Low	0.34	Cored Slab, Above Splash Zone	High	315	Bent Cap, Above Splash Zone
			Median	11	-	Median	137	-
			High	67	Bent Cap, Above Splash Zone	Low	42	Bent Cap, Above Splash Zone
150020	Corrosive	2008	Low	0.43	Bent Cap, Above Splash Zone	High	866	Pier, Above Splash Zone
			Median	14	-	Median	38.6	-
			High	52	Cored Slab, Above Splash Zone	Low	21	Cored Slab, Above Splash Zone
660019	Corrosive	2008	Low	0.82	Pier, Above Splash Zone	High	190	Pier, Above Splash Zone
			Median	9.8	-	Median	52	-
			High	136	Pier, In Splash Zone	Low	26	Cored Slab, Above Splash Zone

3.2.2 Structure Number 150020 Results

Figures 3.4 through 3.7 below show heat maps of a section of an interior bent and three separate piers at varying elevations. Figure 3.3 below shows the location of each pier shown in subsequent figures and how they are labeled. These piers appeared to only experience wetting during large storm events when the water level reaches higher elevations than typical tidal fluctuations.

Figure 3.3. Location of Piers in Figures 3.4 through 3.7

(a) (b)

Figure 3.4. (a) Pier #1: Corrosion Rate Heat Map
(b) Pier #1: Surface Resistivity Heat Map

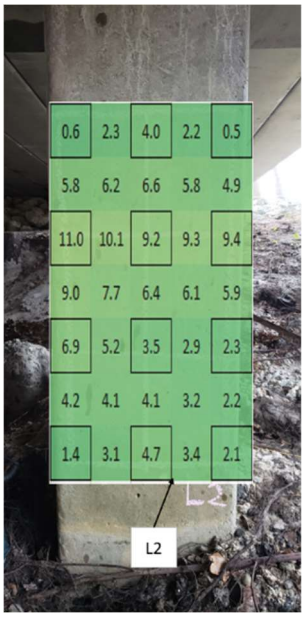

(a)

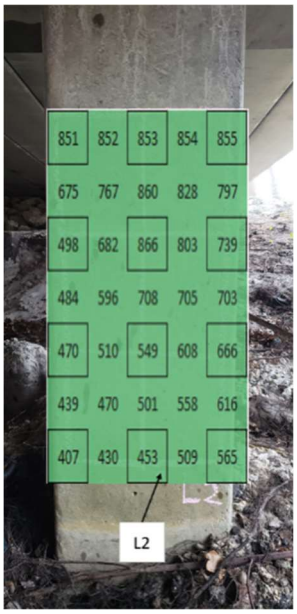

(b)

Figure 3.5. (a) Pier #2: Corrosion Rate Heat Map
(b) Pier #2: Surface Resistivity Heat Map

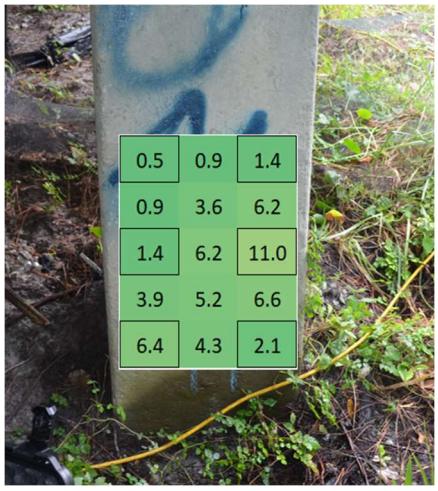

(a)

(b)

Figure 3.6. (a) Pier #3: Corrosion Rate Heat Map
(b) Pier #3: Surface Resistivity Heat Map

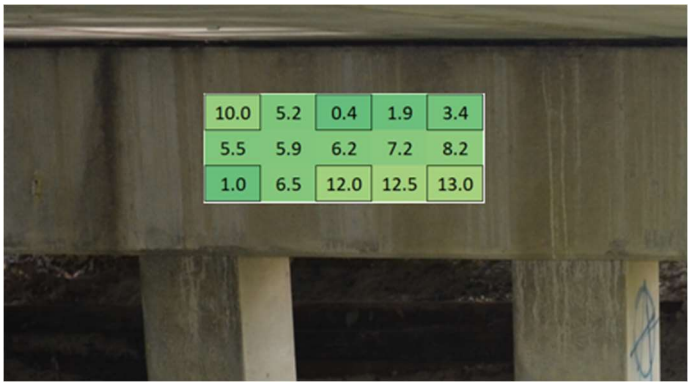

(a)

(b)

Figure 3.7. (a) Cap: Corrosion Rate Heat Map
(b) Cap: Surface Resistivity Heat Map

The visual inspection of structure number (SN) 150020 showed little to no sign of active corrosion. The only exception to this was on two side-by-side central piers at the same elevation that showed efflorescence. This can be seen in the following photographs (Figure 3.8 (a) and (b)). One location appeared to be a patched drill hole (Figure 3.8 (b)) where powder samples had previously been collected.

(a)

(b)

Figure 3.8. Signs of Efflorescence on Two Central Piers.

3.2.3 Structure Number 660091 Results

Figures 3.9 and 3.10 below show heat maps of two separate locations along an end bent well above the splash zone. There were no piers or interior bent caps analyzed on this structure due to it being a single span bridge.

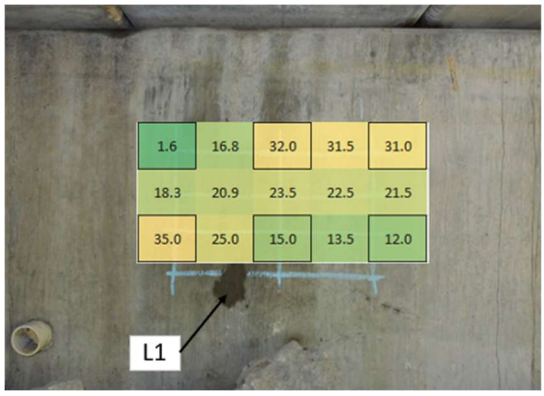

(a)

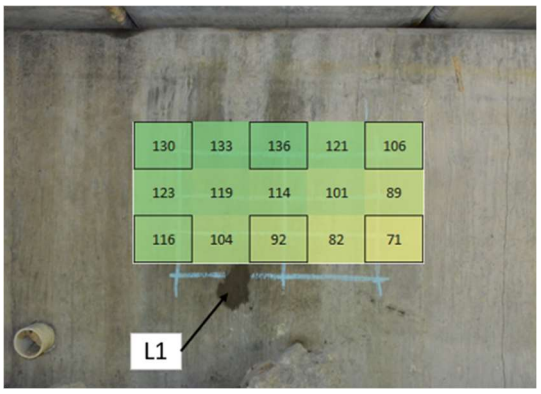

(b)

Figure 3.9. (a) End Bent Location 1: Corrosion Rate Heat Map
(b) End Bent Location 2: Surface Resistivity Heat Map

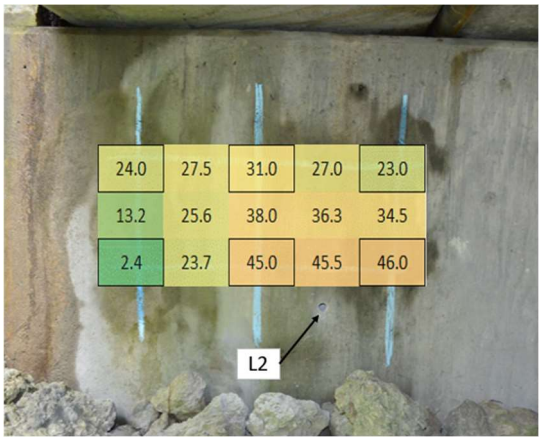

(a)

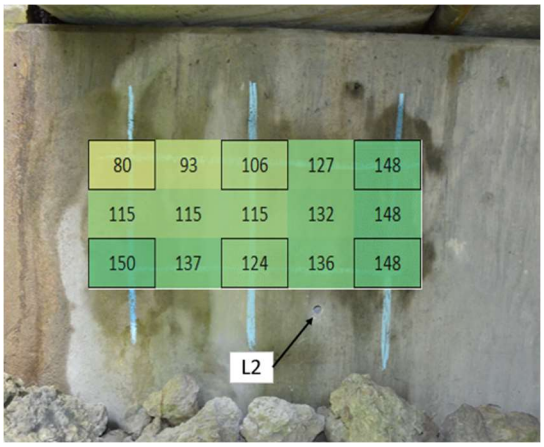

(b)

Figure 3.10. (a) End Bent Location 2: Corrosion Rate Heat Map
(b) End Bent Location 2: Surface Resistivity Heat Map

The visual inspection of SN 660091 identified many locations with significant efflorescence staining on the sides and underside of the cored slabs, a large section of honeycombing on the underside of a cored slab exposing a corroded prestressed strand, and large cracks that had been repaired (i.e. filled in) on the underside of multiple cored slabs. Photographs of these potential signs of corrosion can be seen below.

(a)

(b)

Figure 3.11. (a) Efflorescence on Side Face of Cored Slab.
(b) Efflorescence on Underside of Cored Slab.

(a)

(b)

Figure 3.12. (a) Zoomed Out View of Honeycomb.
(b) Close Up Showing Exposed Prestressed Strand.

Figure 3.13. Example of Large Cracked and Repaired Section on Underside of Cored Slab.

3.2.4 Structure Number 660019 Results

Figures 3.14 and 3.15 below show heat maps of side-by-side piers with readings at the bottom beginning in the splash zone. No readings were collected from the interior bent cap due to the lack of accessibility.

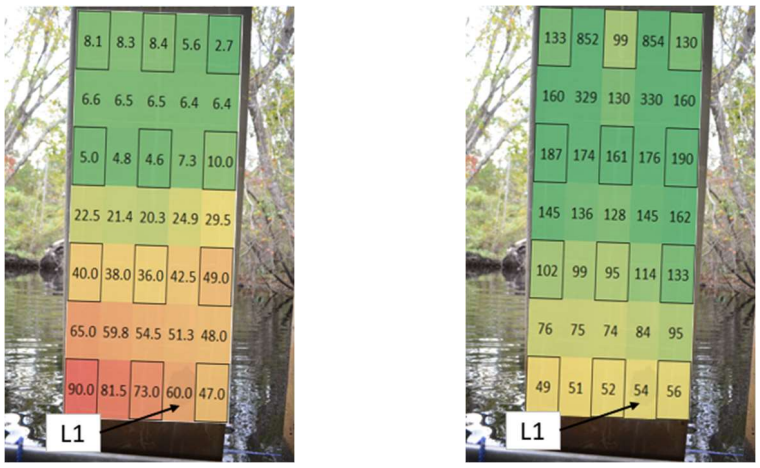

(a) (b)

Figure 3.14. (a) Pier 1: Corrosion Rate Heat Map
(b) Pier 1: Surface Resistivity Heat Map

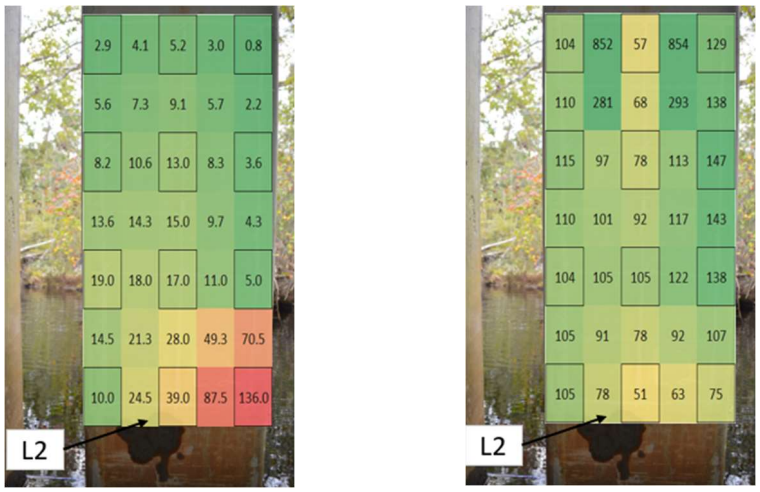

(a) (b)

Figure 3.15. (a) Pier 2: Corrosion Rate Heat Map
(b) Pier 2: Surface Resistivity Heat Map

The visual inspection of SN 660019 revealed little to no sign of active corrosion. The only exception to this was efflorescence below the high tide line on all the piers. A photograph of this potential sign of corrosion can be seen below.

Figure 3.16. Efflorescence within Splash Zone of Piers.

3.2.5 Structure Number 090061 Results

Figure 3.17 below shows heat maps on two side-by-side piers with readings at the bottom beginning in the splash zone. No readings were collected from the interior bent caps due to the lack of accessibility.

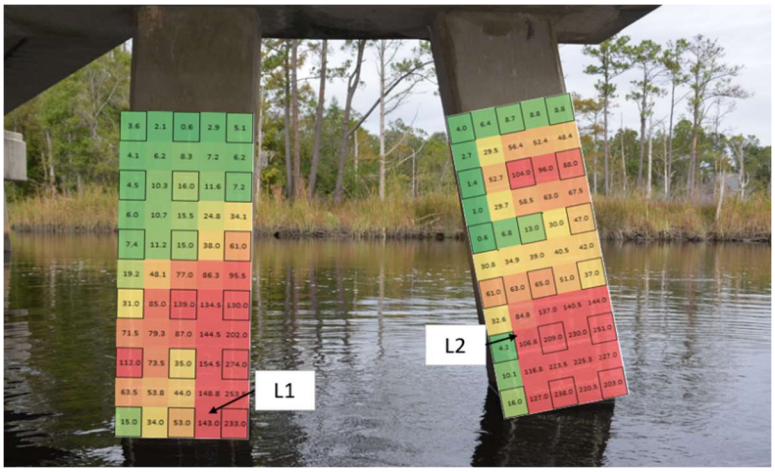

(a)

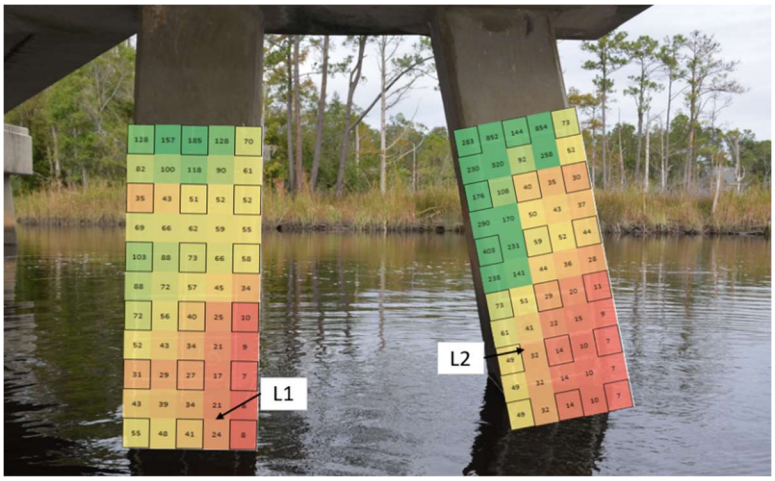

(b)

Figure 3.17. (a) Piers: Corrosion Rate Heat Map
(b) Piers: Surface Resistivity Heat Map

The visual inspection of SN 090061 revealed little to no sign of active corrosion. The only exception to this was efflorescence below the high tide line on all the piers. There was no efflorescence or honeycombing discovered on the cored slabs. A photograph of this potential sign of corrosion can be seen below.

Figure 3.18. Efflorescence at High Tide Line on all Piers.

3.2.6 Structure Number 640010 Results

Figures 3.19 and 3.20 below show heat maps of two interior bent caps and a pier within the splash zone.

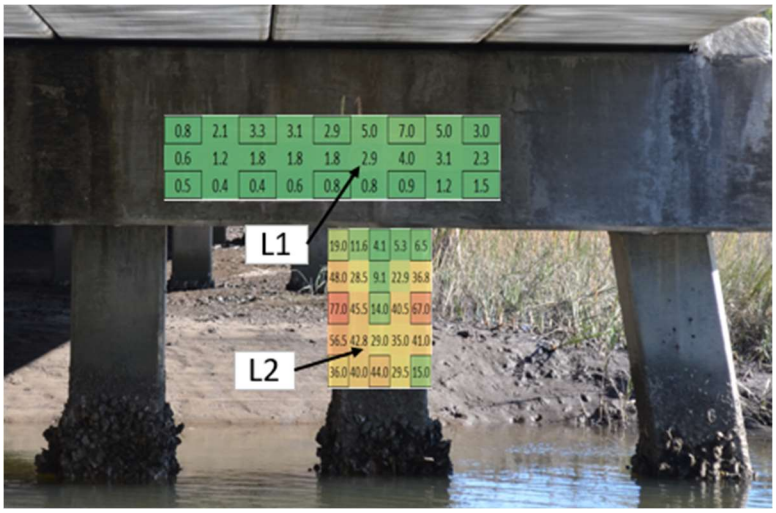

(a)

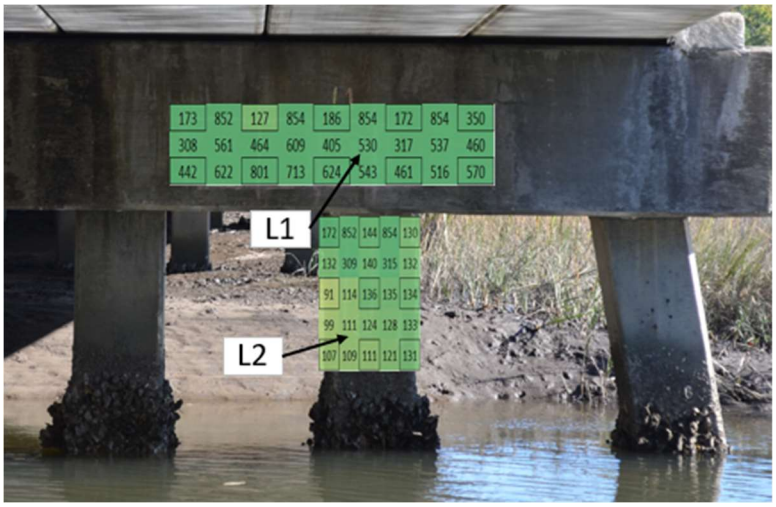

(b)

Figure 3.19. (a) Interior Bent Cap and Pier: Corrosion Rate Heat Map
(b) Interior Bent Cap and Pier: Surface Resistivity Heat Map

(a)

(b)

Figure 3.20. (a) Interior Bent Cap: Corrosion Rate Heat Map
(b) Interior Bent Cap: Surface Resistivity Heat Map

The visual inspection of SN 640010 revealed little to no sign of active corrosion. There was no evidence of efflorescence on the piers, caps, or cored slabs. Additionally, there were no signs of honeycombing on this structure. The only damage noted was a spalled section between a pier and interior bent cap connection that appeared to have been patched. It cannot be confirmed whether the origin of this spall is corrosion-related or is simply a construction defect, however, it was included here as a current defect that was identified during the visual inspection. This can be seen in Figure 3.21 below.

Figure 3.21. Spalled Section at Pier to Bent Cap Connection.

3.2.7 Structure Number 150026 Results

Figures 3.22 and 3.23 below show heat maps of the face of an interior bent cap and the face of a wing wall. The interior piers were not tested because the water level was even with the bottom of the interior bent cap.

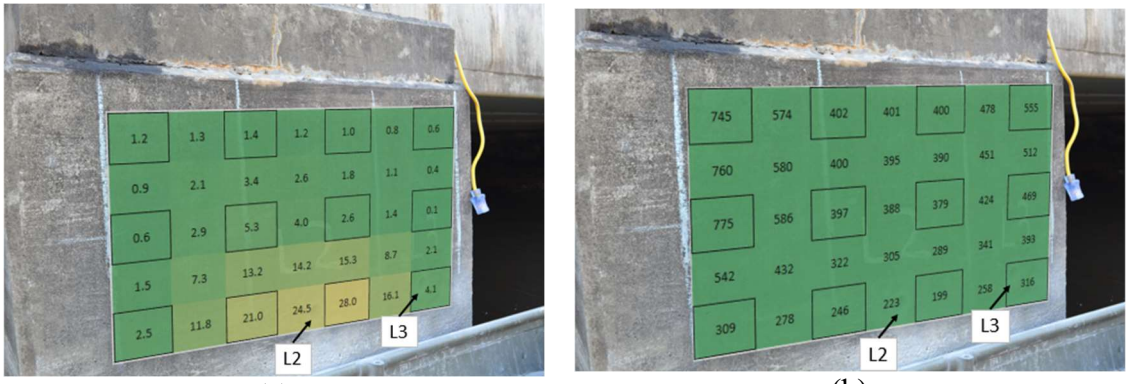

(a) (b)

Figure 3.22. (a) Cap Face: Corrosion Rate Heat Map
(b) Cap Face: Surface Resistivity Heat Map

(a) (b)

Figure 3.23. (a) Wing Wall: Corrosion Rate Heat Map
(b) Wing Wall: Surface Resistivity Heat Map

The visual inspection of SN 150026 revealed little to no sign of active corrosion. The only exception to this was efflorescence staining along the side of the exterior cored slabs. A photograph of this potential sign of corrosion can be seen below.

Figure 3.24. Efflorescence Staining on Side of Exterior Cored Slabs.

3.2.8 Structure Number 260007 Results

Figures 3.25 and 3.26 below show heat maps of a section on both an interior face and an end face of an interior bent cap. No piers were tested on this structure due to them all being either steel piles or steel encased concrete.

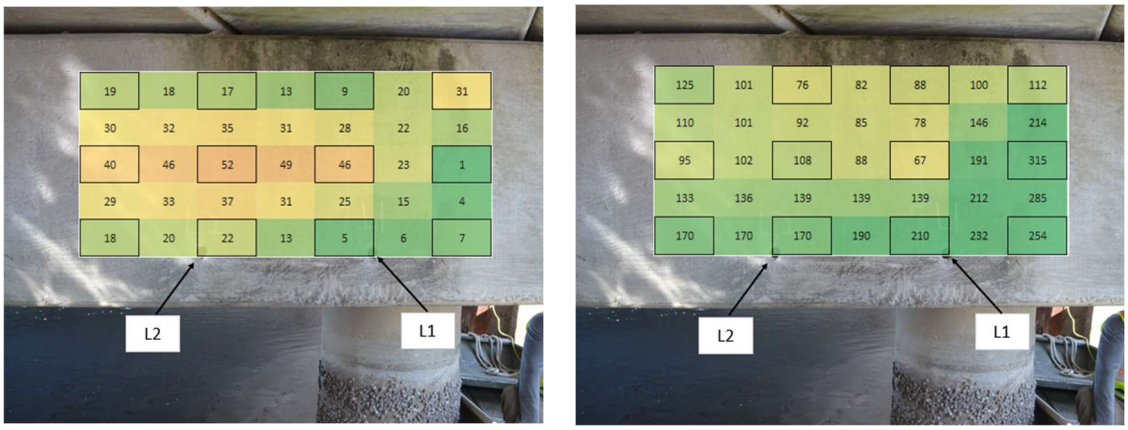

(a) (b)

Figure 3.25. (a) Face of Interior Bent Cap: Corrosion Rate Heat Map
(b) Face of Interior Bent Cap: Surface Resistivity Heat Map

(a) (b)

Figure 3.26. (a) End Face of Interior Bent Cap: Corrosion Rate Heat Map
(b) End Face of Interior Bent Cap: Surface Resistivity Heat Map

The visual inspection of SN 260007 revealed no active signs of corrosion on concrete elements, however, the steel sheet piles and steel bent piles appeared to be heavily corroded. The signs of corrosion can be seen in the photographs below.

Figure 3.27. Heavily Corroded Interior Bent Steel Piles.

Figure 3.28. Heavily Corroded Steel Sheet Piles.

3.2.9 Structure Number 660021 Results

Figure 3.29 below shows heat maps of two interior bent piles near the splash zone and on the face of the interior bent cap.

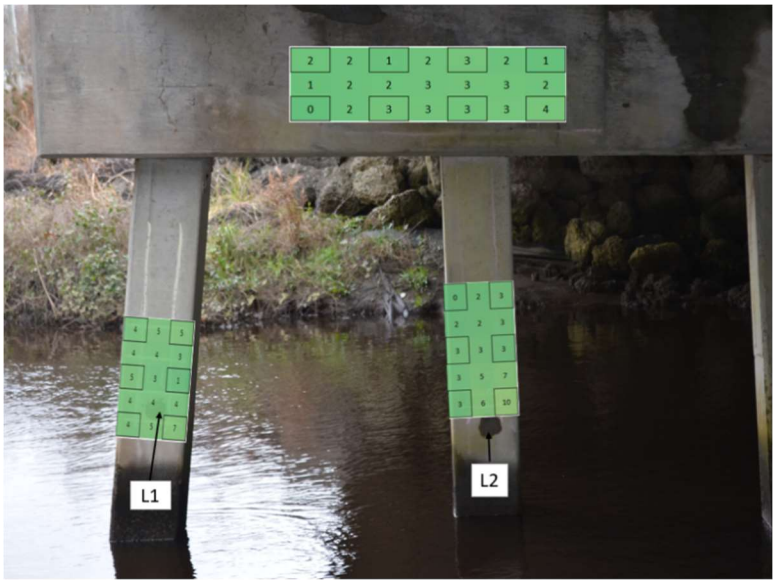

(a)

(b)

Figure 3.29. (a) Interior Bent Cap and Piles: Corrosion Rate Heat Map
(b) Interior Bent Cap and Piles: Surface Resistivity Heat Map

The visual investigation of SN 660021 revealed little to no sign of active corrosion. The only signs were efflorescence on the underside of the cored slabs and within the splash zone on the interior bent piles. Photographs of these potential signs of corrosion can be seen below.

Figure 3.30. Efflorescence on Underside of Cored Slab.

Figure 3.31. Efflorescence within splash zone on interior bent piles.

3.3 Field Investigation Discussion

The following subsections discuss the results presented above in the order of visual inspection, summary table (Table 3.1), and heat maps. The summary table and heat maps subsections will both be divided by corrosion rate results and surface resistivity results.

3.3.1 Visual Inspection

The two structures located within the corrosive zone, both constructed in 2005, showed little to no sign of active corrosion with the only exception being efflorescence on the piers. Additionally, the only efflorescence observed on these structures were located on elements within the splash zone. The piers appeared to be in good condition (i.e. no signs of active corrosion) above the splash zone and the cored slabs appeared to show no signs of active corrosion. This is an indication that the structures are performing well, relative to the prevention of corrosion, for elements located above the splash zone. Although the piers were showing signs of corrosion (efflorescence) within the splash zone, they are very minor signs indicating that they were still in good condition.

The remaining six structures were located within the highly corrosive zone and were constructed between 2005 and 2007. Apart from SN 660091, these structures showed little to no signs of active corrosion. The main sign on these was efflorescence on the piers within the splash zone. With the only exception being SN 660091, which is discussed in more detail in the following paragraph, the structures within the highly corrosive zone appeared to be in good condition. Similar to the structures in the corrosive zone, these structures appeared to be performing well for elements above the splash zone with only minor signs of corrosion (efflorescence) below the splash zone.

SN 660091 had more widespread efflorescence than the other structures visited and was seen on the side and underside of the cored slabs, well above the splash zone (water level at time of inspection was approximately 10 feet below bottom of cored slabs). Based on signs of erosion on the sides of the river, the water level did not appear to ever raise high enough for the cored slabs to be within the splash zone. In addition to efflorescence, there was a large section of honeycombing on the underside of a cored slab. It was approximately 2 feet long by 2 inches wide and in the deepest section showed a prestressed strand that was corroded (see Figure 3.12 in previous section). This was the only structure visited in either corrosive zone that showed multiple visual signs of active corrosion indicating that it could be an outlier, though the number of structures visited is too small to state that definitively.

3.3.2 Summary Table: Corrosion Rate

From the summary table (Table 3.1), four out of the eight structures visited showed the expected trend of high corrosion rates on elements within the splash zone and lower, negligible corrosion rates on elements above the splash zone. This is expected because the chloride loading of elements above the splash zone is lower than that of elements either within the splash zone or in direct contact with chloride-rich waters.

Although the high value for two of the structures fell under the category of a severe corrosion rate (very high based on Bertolini et al.'s (2013) ranges – see Section 2.5.4.3) and five of the structures fell under the category of a high corrosion rate (high based on Bertolini et al. (2013)), the median value for each of the structures was significantly lower. All eight structures' median corrosion rate was within the lower 33 percent of the full range of readings for each structure. The highest median corrosion rate

in the highly corrosive zone was 13.5 µm/year (moderate based on Table 2.8, intermediate based on Bertolini et al. (2013)) on SN 090061 while the highest median corrosion rate in the corrosive zone was 14 µm/year (moderate based on Table 2.8, intermediate based on Bertolini et al. (2013)) on SN 150020.

Overall, based on the summary of results (Table 3.1) it appears that the structures visited are experiencing relativity low corrosion rates. There appear to be a few hot spots of high corrosion rates, primarily on locations within the splash zone. SN 660021 in the highly corrosive zone had the lowest maximum corrosion rate reading at 10 µm/year which falls under the category of moderate (moderate based on Bertolini et al. (2013)).

In addition to these results, Ross Newsome (fellow UNCC graduate student) performed service live projections based on powder samples collected at the same set of structures. His projections indicated that most elements were on track to exceed the expected service life of 50 years with the main exceptions being on elements that experience frequent wetting by chloride-rich waters (Newsome 2020). More details related to service life projections can be found in Ross Newsome's thesis (Newsome 2020).

3.3.3 Summary Table: Surface Resistivity

The maximum and minimum readings of surface resistivity did not appear to show a tendency for a maximum within the splash zone and a minimum above the splash zone or vice versa. This was expected as surface resistivity is a material property and should be relatively consistent within the same element regardless of the environmental conditions.

There were only two structures (SN 090061 and 640010) that the lowest surface resistivity reading fell under the category of low (see Table 2.7 for categories). While SN 090061 and SN 640010 had the lowest readings of the eight structures visited, the median surface resistivity fell under the category of high for both SN 090061 and SN 640010. Similarly, there were five structures that the lowest reading fell under the category of moderate, however two of these structures had a median reading under the category of high and two had a median reading under the category of very high.

Based on the findings in the summary table (Table 3.1) it appears that all of the structures visited have high to very high surface resistivities indicating that they should be less prone to the ingress of chlorides and subsequently less prone to the corrosion of the embedded steel reinforcement. It should be noted that the very high readings recorded above the splash zone are likely inflated due to the lower moisture content than elements either fully submerged or within the splash zone. It should also be noted that each testing location was not able to be saturated to simulate laboratory conditions and the actual moisture content was not recorded. The Giatec iCOR companion software has a correction for moisture content, however, the user does not have control over this correction nor does the user manual describe how this function works.

As discussed in Section 2.5.4.2, Presuel-Moreno discovered that field tested values of surface resistivity can be up to three times higher than the same test being performed under laboratory conditions where the moisture content of the concrete can be controlled (Presuel-Moreno et al. 2010). In addition to this study, Cox et al. (1997) and Polder et al. (2000) created a table (see Table 2.6 in Chapter 2) that presents reference surface resistivity values for multiple different environmental conditions with either

ordinary portland cement or a pozzolan such as blast furnace slag, fly ash, or silica fume. This table (Table 2.6) shows a similar conclusion to the Presuel-Moreno et al. (2010) study, however, they suggest that the surface resistivity of concrete with a pozzolan is approximately five times higher than concrete with portland cement (Cox et al. 1997; Polder et al. 2000). Even when the high values of surface resistivity discussed in the previous paragraph are divided by three to account for the lower moisture content, they are still high and therefore should be slowing the ingress of chlorides.

3.3.4 Heat Maps: Corrosion Rate

The corrosion rate heat maps typically demonstrated a trend of high values in the splash zone with values decreasing as elevation above the splash zone increases. In most cases (16 out of 20), the corrosion rate decreased to low or negligible values (moderate, low, or negligible based on Bertolini et al. (2013)) above the splash zone. The only exceptions were SN 660091, 260007, 150020, and 660021. SNs 660091 and 260007 had corrosion rates mostly in the moderate to high category (intermediate to high based on Bertolini et al. (2013)) and did not appear to follow trends related to elevation above the splash zone. SNs 150020 and 660021 had fairly low readings (<13 μm/year and <10 μm/year, respectively) regardless of the elevation or location of the splash zone.

3.3.5 Heat Maps: Surface Resistivity

The surface resistivity heat maps demonstrated the same gradient style trend as the corrosion rate heat maps. The values were lowest in or near the splash zone and were highest above the splash zone. It was noted above (Section 3.3.3) that because surface resistivity is a material property it should be relatively consistent throughout an entire element. Presuel-Moreno (2010) (discussed in detail in Section 2.5.4.2) found that a

resistivity gradient can be observed when tested in the field due to differential moisture content. This is likely the explanation for the gradients seen on the surface resistivity heat maps as the lowest readings were typically observed in the splash zone while the highest readings were typically observed well above the splash zone.

CHAPTER 4: DEFECT MAPPING INVESTIGATION

The defect mapping portion of this thesis consisted of analyzing the NCDOT maintenance records from 2016 to determine whether there were trends between distance from the coast (i.e. corrosive zones) and corrosion related damages. The corrosion related damages that were included in the investigation were delamination and spalling, reinforced concrete cracking, and efflorescence. Each of these damages and how they relate to corrosion are discussed below. Additionally, the condition state of each maintenance record was analyzed. The structures included were limited to bridges near the North Carolina coast that are water crossings and have elements located directly in the water.

The investigation was divided into three groups based on proximity to the coast. These groups included the highly corrosive zone and corrosive zone as defined by the NCDOT and a subset of structures located west of the corrosive zone boundary line. By dividing the structures into these three zones, the investigation was able to aid in determining whether there were trends between location relative to the coastline and corrosion-related defects. In addition to dividing the structures into zones, they were also divided by whether they were constructed before or after the corrosion policy was enacted. This assisted in the determination of whether the current NCDOT specifications for structures constructed in corrosive environments are working as intended (i.e. extending the maintenance-free service lives). Also, this division assisted in the

determination of whether the current corrosive boundary lines are drawn in the most effective location.

This chapter is organized by first describing the methodology used to complete the investigation followed by a presentation and discussion of the results.

4.1 Methodology of Defect Mapping

The following subsections will describe the methodology used to prepare the dataset and perform the analysis.

4.1.1 Creating the Dataset

The dataset for this analysis was created using NCDOT bridge maintenance records from 2016. These records had been organized during a previous project for the NCDOT by Austin Lukavsky (Lukavsky 2019), however, the structures were filtered for the purpose of this investigation.

First, a set of structures was eliminated based on their proximity to the coast. Only structures located in either the highly corrosive zone or corrosive zone and an additional subset directly west of the corrosive zone boundary line were considered. This extra subset of structures was included to aid in determining if structures west of the corrosive boundary line were receiving more, less, or the same amount of corrosion related damage even though they are not necessarily exposed to the same type of environmental conditions. Next, certain maintenance records were eliminated by excluding elements that are not concrete and excluding reported defects that were likely not caused by corrosion. Once these filters were applied, the remaining defects included the following:

- Delamination/Spall
- Exposed Rebar

- Cracking (RC and Other)
- Efflorescence/Rust Staining
- Cracking (PSC)
- Exposed Prestressing

Exposed rebar, cracking (PSC), and exposed prestressing were eliminated from the analysis due to very low numbers of reported cases. The final analysis included delamination/spalling, cracking (RC and other), and efflorescence/rust staining, which are discussed below.

Cracking on the surface of reinforced concrete occurs as a result of embedded steel corrosion. As the steel rusts, it undergoes a volumetric expansion which in turn causes the concrete cover to crack. Once a crack has formed, it provides a direct path for chloride ingress to the embedded steel to occur at a rapid speed. As the corrosion process accelerates, it can lead to additional damages to the concrete cover such as delaminations and spalling (Zhao and Jin 2016). Efflorescence and rust staining are signs that corrosion is at an increased risk or is actively occurring because they are stains caused either by salts on the surface (which could lead to corrosion) or underlying rust (indicating that the steel is already corroding).

Once the dataset was reduced as described above, the structures were divided by both by location and by age. The location of the structures was divided by whether it was in the highly corrosive zone, corrosive zone, or neither zone (referred to as outside corrosive zone). The age of the structures was divided by whether they were constructed before or after the corrosion policy (enacted in 2003). It should be noted here that the age of structures in the post-policy category were 13 years old at the maximum with no

minimum age restriction while the age of structures in the pre-policy category were 14 years old at the minimum with no maximum age restriction. The defects analyzed for this study were from 2016 NCDOT maintenance records (these records were used as they had been previously sorted and organized in a thesis by Austin Lukavsky, a fellow UNCC graduate student (Lukavsky 2019)), therefore the structures constructed pre-policy had been in service for a longer time than post-policy structures at the time these defects were reported. This difference of time in service was not accounted for in the investigation, however it was considered as a potential factor in the discussion.

The final breakdown of structures included is shown in Table 4.1 below. The number of structures in each zone considered for this analysis was low due to only structures having defects reported in the year 2016 being included in the study.

Table 4.1. Breakdown of Structures Included for Defect Mapping.

Location	Number of Structures Included	
	Pre-Policy	Post-Policy
Highly Corrosive Zone	19	15
Corrosive Zone	6	17
Outside Corrosive Zone	31	141
Total	56	173

When a defect is reported, it is accompanied by a condition state which ranges from 1 to 4. Condition states are included to aid in defining the severity of a defect. The four states are generally described as good, fair, poor, and severe with 1 being good and 4 being severe (Ryan et al. 2012).

4.2 Defect Mapping Results

The summary results (Tables 4.2 through 4.4) presented in this section are conveyed using two different measures. The first measure is the number of structures affected in each zone. Since the number of structures included before and after the policy is different, this measure is represented by the percentage of structures affected by the specified defect compared to the total number of structures considered in that particular corrosive boundary. The second measure is the average condition state that is included with each report of a specific defect. As mentioned above, the condition state is included when a defect is reported that identifies whether the defect is in good (1), fair (2), poor (3), or severe (4) condition. Additionally, it should be noted that while these defects are commonly caused by corrosion, it cannot be confirmed or guaranteed that each reported defect included in this study was the result of corrosion.

Table 4.2. Summary of Delamination/Spall Reports.

Corrosive Zone	Percentage of Structures Affected		Average Condition State	
	Pre-Policy	Post-Policy	Pre-Policy	Post-Policy
Highly Corrosive Zone	63%	20%	2.50	2.14
Corrosive Zone	67%	53%	2.59	2.11
Outside Corrosive Zone	61%	25%	2.37	2.44

Table 4.3. Summary of Efflorescence/Rust Staining Reports.

Corrosive Zone	Percentage of Structures Affected		Average Condition State	
	Pre-Policy	Post-Policy	Pre-Policy	Post-Policy
Highly Corrosive Zone	42%	53%	2.28	2.53
Corrosive Zone	33%	59%	2.40	2.59
Outside Corrosive Zone	29%	55%	2.29	2.47

Table 4.4. Summary of Cracking (RC and Other) Reports.

Corrosive Zone	Percentage of Structures Affected		Average Condition State	
	Pre-Policy	Post-Policy	Pre-Policy	Post-Policy
Highly Corrosive Zone	58%	80%	2.22	2.15
Corrosive Zone	67%	71%	2.17	2.05
Outside Corrosive Zone	71%	78%	2.25	2.12

4.3 Defect Mapping Discussion

The following subsections discuss the results presented above in order of delamination and spalling, efflorescence and rust staining, and reinforced concrete cracking, followed by an overall discussion.

4.3.1 Delamination/Spall Discussion

The percentage of structures with reported delaminations or spalls in 2016 was significantly lower (reduced by over a third) for structures in the highly corrosive zone that were built after the enactment of the current NCDOT corrosion policy. There was also a decrease of structures affected in the corrosive zone, however, it is not as significant of a decrease as in the highly corrosive zone. This could be due to the differing and/or lack of corrosion-related construction specifications in the corrosive zone. Additionally, the very high percentages of structures affected in the pre-policy age group could be due to the low number of structures in each zone that were considered for this study.

Looking at the highly corrosive zone and outside corrosive zone before the corrosion policy was enacted, the highly corrosive zone had a slightly higher percentage of structures affected by delaminations or spalls. Following the enactment of the

corrosion policy, structures in the highly corrosive zone had a smaller percentage of structures affected than the outside corrosive zone by 5%.

The average condition state in the highly corrosive zone and corrosive zone both decreased, indicating that the defects reported were typically less severe on structures constructed under the corrosion policy, while the average condition state in the outside corrosive zone slightly increased, indicating that the defects reported were typically more severe. It should be noted that the structures located in the outside corrosive zone are not receiving any corrosion prevention treatments whether they were constructed before or after the policy was enacted as the policy only applies to structures located in the highly corrosive zone and corrosive zone.

4.3.2 Efflorescence/Rust Staining Discussion

The percentage of structures affected by efflorescence or rust staining increased in all three zones from pre-policy to post-policy. Although this is the opposite of the trend seen in Table 4.2 with delamination and spalling reports, the increase in reports between pre-policy and post-policy in the highly corrosive zone (11% increase) is significantly lower than the increase in the corrosive zone (26% increase) and outside corrosive zone (26% increase). Looking at only the post-policy percentages, the highly corrosive zone shows a lower percentage of structures affected than the corrosive zone and outside corrosive zone although all three are relatively close.

Similar to the trend shown in the percentage of structures affected, the average condition state of the reported efflorescence or rust staining increased in all three zones from pre-policy to post-policy. Although the average severity (condition state) of this defect increased for post-policy structures, the distribution between the highly corrosive,

corrosive, and outside corrosive zone remained relatively the same when compared to pre-policy structures.

4.3.3 Cracking (RC and Other) Discussion

The percentage of structures affected by reinforced concrete cracking increased in all three zones from pre-policy to post-policy. The percentages affected in the highly corrosive zone and corrosive zone were lower than the percentage affected in the outside corrosive zone before the corrosion policy was enacted. Following the enactment of the policy, the corrosive zone still maintained a lower percentage of structures affected than the outside corrosive zone, while the highly corrosive zone surpassed the outside corrosive zone.

The average condition state of the reported reinforced concrete cracking decreased in all three zones from pre-policy to post-policy, indicating that this defect was typically less severe following the enactment of the policy. This was the only defect analyzed that showed a decreased average condition state even though the percentage of structures affected increased from pre-policy to post-policy.

4.3.4 Overall Discussion

The percentage of defects reported in each zone, as well as west of the zones, appears to be roughly equal before and after the policy was enacted. This was also true for the average condition state, or severity. Additionally, due to the structures considered in the pre-policy category having been in service longer than those in the post-policy category and the defects considered for both being from 2016, it was difficult to draw strong conclusions on whether structures constructed post-policy were performing better or worse than those constructed pre-policy.

While this study included the condition state as a portion of the analysis, the actual severity of defects could not be adequately captured with the information available (i.e. four level measure of severity). It could be that although post-policy structures appeared to be experiencing a larger percentage of defects, the defects were typically less severe, or vice versa. With the records available for this analysis, it was not possible to determine this with a high level of certainty.

CHAPTER 5: DETERIORATION MODELING INVESTIGATION

The deterioration modeling portion of this thesis consisted of analyzing substructure and superstructure condition rating records sourced from the National Bridge Inventory (NBI). The outcomes of this investigation included the creation of multiple deterioration models and findings determined from a statistical analysis using Minitab. Comparisons were made for each set of results based on bridge component (substructure versus superstructure bridge component), geographic location in relation to the NCDOT corrosive zone map (highly corrosive zone, corrosive zone, or neither), and structure age (built before or after current NCDOT corrosion policy). These analyses aided in the determination of whether the current NCDOT corrosion specifications are working as intended to extend the corrosion related maintenance-free service lives of structures located near the coast.

This chapter is organized by first describing the methodology used to complete each stage of the analysis followed by a presentation and discussion of the results.

5.1 Methodology of Deterioration Modeling

The following subsections will describe the methodology used to prepare the dataset, create the deterioration models, and perform the statistical analysis.

5.1.1 Creating the Dataset

The dataset for this analysis was created using records sourced from the National Bridge Inventory (NBI) for North Carolina ranging from 1992 to 2018. After

downloading the NBI characteristic and inspection data for all available years, the information necessary to complete the deterioration modeling and statistical analyses was compiled into a single Excel spreadsheet. This spreadsheet included the structure number, latitude and longitude, year built, substructure condition rating, superstructure condition rating, and crossing type. The condition ratings for both the substructure and superstructure follow the general guidelines below (Ryan et al. 2012):

Code	Description
N	NOT APPLICABLE
9	EXCELLENT CONDITION
8	VERY GOOD CONDITION – no problems noted.
7	GOOD CONDITION – some minor problems.
6	SATISFACTORY CONDITION – structural elements show some minor deterioration.
5	FAIR CONDITION – all primary structural elements are sound but may have minor section loss, cracking, spalling, or scour.
4	POOR CONDITION – advanced section loss, deterioration, spalling, or scour.
3	SERIOUS CONDITION – loss of section, deterioration, spalling, or scour have seriously affected primary structural components. Local failures are possible. Fatigue cracks in steel or shear cracks in concrete may be present.
2	CRITICAL CONDITION – advanced deterioration of primary structural elements. Fatigue cracks in steel or shear cracks in concrete may be present or scour may have removed substructure support. Unless closely monitored it may be necessary to close the bridge until corrective action is taken.
1	“IMMINENT” FAILURE CONDITION – major deterioration or section loss present in critical structural components, or obvious vertical or horizontal movement affecting structure stability. Bridge is closed to traffic but corrective action may put bridge back in light service.
0	FAILED CONDITION – out of service; beyond corrective action.

The initial dataset consisted of 18,377 bridges and culverts across North Carolina. Since the scope of this thesis is focused primarily on structures near the coastline, a large

portion of this initial dataset was not of interest. To limit the records contained in the spreadsheet to those only associated with structures falling within the scope of this thesis, several filters were applied including proximity to coast, structure type, structure crossing type, year built, and accuracy and length of available records.

The first filter applied was the structure crossing type, which limited the structures to only those crossing over water (coded as 5 under SERVICE_UND_042B in NBI records). Next, the proximity to the coast was considered by removing records for structures located in areas of North Carolina west of the corrosive zone boundary line (discussed in Chapter 1) based on latitude and longitude. This brought the dataset down to 1,333 total structures with 265 in the highly corrosive zone, 192 in the corrosive zone, and 876 that are located west of the corrosive boundary lines. All structures that contained a condition rating of N, which is used to indicate a culvert or nonapplicable situation (such as an overhead sign), for either the substructure or superstructure were removed to limit the structures to bridges only. It should be noted that bridges were identified with a condition rating of N for an unknown reason, however, there were very few cases of this. Due to the large number of structures remaining in the dataset, all structures that were coded with a condition rating of N were removed.

Due to the field work portion of this thesis (discussed in Chapter 3) being focused primarily on substructure elements (due to accessibility as well as the substructure typically being located within the splash zone), it was of interest for this study to also focus on substructure elements, particularly structures that have piers submerged in the water. To implement this filter, the underwater inspection column was transferred from the NBI database (coded as UNDWATER_LAST_DATE_093B in NBI database) to the

Excel spreadsheet described above. By adding this column, structures with no underwater elements such as piers were coded with a blank and were easily filtered out of the database.

The current corrosive sites design policy (discussed in Chapter 1) was enacted in 2003. One of the outcomes of this analysis was to determine if there are noticeable differences or trends between bridges constructed before the policy was put in place and bridges constructed after. To ensure there was an equivalent representation of bridges constructed before the policy was enacted and bridges constructed after the policy was enacted, a range of 20 years was chosen. This range was broken up by 10 years before and 10 years after 2003, or 1993-2002 and 2003-2012. These ranges are further referred to as pre-policy and post-policy, respectively. This also ensured that all the structures were constructed using relatively similar methods. Since the pre-policy structures considered here could have structures with condition rating data from 1993 to 2018 (23 years) and the post-policy structures could have structures with, at the maximum, condition rating data from 2003 to 2018 (15 years), there was an uneven representation. To account for this, the pre-policy condition rating data was limited to the years 1993 to 2008 (15 years). This process of limiting the number of years of condition rating data considered is called censoring and is used to describe when an event is not completely observed (Goyal et al. 2016). In this dataset, censoring occurs at the tail end of the dataset. As the additional years of condition rating data are not accounted for in this analysis, the deterioration models created are overly conservative (i.e. the deterioration models will demonstrate a more rapid deterioration than what is actually occurring). With

the previously described filters applied, the final breakdown of structures included in the analysis is shown below in Table 5.1.

Table 5.1. Breakdown of Structures Included for Deterioration Modeling.

Location	Number of Structures Included	
	Pre-Policy 1993 - 2002	Post-Policy 2003 - 2012
Highly Corrosive Zone (Zone 1)	26	28
Corrosive Zone (Zone 2)	21	18
Outside Corrosive Zone (Zone 3)	68	67
Total	115	113

Additionally, a map of the structures described in Table 5.1 above is shown in Figure 5.2 along with a map displaying the current location of the corrosive sites boundary lines (see Figure 5.1 below). In Figure 5.2, the structures denoted by a red pinpoint are in the highly corrosive zone, the structures denoted by a yellow pinpoint are in the corrosive zone and the structures denoted by a green pinpoint are not in either zone.

Figure 5.1. Corrosive Sites Boundary Lines.

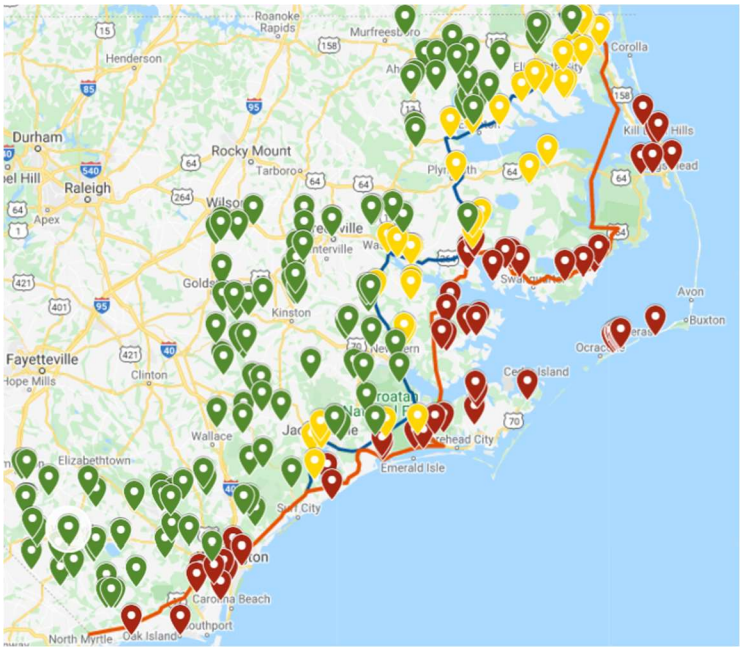

Figure 5.2. Map of Bridges for Analysis.

The structures falling outside of either zone were included in this analysis so that a comparison of performance could be made between structures that were being constructed with specific guidelines to deter the onset of corrosion (highly corrosive zone and corrosive zone) and those that are not (outside corrosive zone). As shorthand notation in this chapter, these zones will sometimes be referred to as zone 1, zone 2, and zone 3 (or simply 1, 2, and 3) which corresponds to the highly corrosive zone, corrosive zone, and outside corrosive zone, respectively.

5.1.2 Deterioration Modeling

To perform the deterioration modeling, the time spent in each condition rating for each structure was determined from the historical NBI data. Due to the large number of structures involved in this analysis it was necessary to write a code for use in MATLAB to complete this stage. Additionally, it was of interest to perform this analysis for both the

substructure and superstructure. The datasets were first organized in an Excel spreadsheet to include the structure number, latitude and longitude, year built, and the condition rating reported for each year from 1993 to 2012. The Excel spreadsheet for each of these were used as the input files for MATLAB. A sample line of the input described above is shown in Table 5.2 below.

Table 5.2. Sample MATLAB Input Table for SN 130098 Superstructure.

Structure Number	Latitude	Longitude	Year Built	Superstructure Condition Rating																			
				1993	1994	1995	1996	1997	1998	1999	2000	2001	2002	2003	2004	2005	2006	2007	2008	2009	2010	2011	2012
130098	35.6333	-77.009	1994	0	0	0	0	0	0	0	9	9	9	8	8	8	8	8	8	8	6	8	8

The code for MATLAB was designed to proceed from earliest year to most recent year, ignoring zeroes which indicate that there was no condition rating recorded that year, and then tally the number of years a structure spent in each condition rating. The code would repeat this step for a structure given that the condition rating was either constant or decreasing. If the condition rating increased at any point during a structure's lifecycle, the code would not record that increase and proceed to the next structure. This was to eliminate any structures that received maintenance actions that significantly improved the structural element, causing the condition rating to increase. Eliminating any increase in condition rating ensures that the data demonstrates the natural deterioration of a structure with no intervention. The code created for this analysis can be found in Appendix C. A sample line of the output described above is shown in Table 5.3 below.

Table 5.3. Sample MATLAB Output Table for SN 130098 Superstructure.

Structure Number	Time Spent in Condition Rating (years)								
	1	2	3	4	5	6	7	8	9
130098	0	0	0	0	0	1	0	7	3

Note that in Tables 5.2 and 5.3 above, the same structure was used. In Table 5.2, it is shown that the condition rating decreases from an 8 to a 6 in 2010 and then increases back to an 8 in 2011 and remains an 8 in 2012. The output from MATLAB (Table 5.3) demonstrates that the code only recorded the condition rating data until 2010 and does not include the two years spent in condition rating 8 in 2011 and 2012. While this decrease to a 6 appears to be an outlier or error in the database due to it being a single year decrease and the inspection scheduling in North Carolina being on a two year cycle, the code was designed to eliminate any potential coding mistakes. This is a conservative approach to this type of analysis at it typically demonstrates a more rapid deterioration than what is actually occurring.

5.1.3 Methodology of Minitab Analysis

In addition to the creation of deterioration models, an analysis using a statistical software program, Minitab, was performed on both the substructure and superstructure condition rating data. This analysis was intended to aid in the determination of whether differences between pre-policy and post-policy condition ratings shown on the deterioration model graphs are statistically significant. The test chosen for this analysis was a two-sample t-test. A two-sample t-test is ideal when comparing the means of two similar samples (pre-policy and post-policy condition rating data) that have received

different treatments with the intention of determining whether the difference is significant (Devore 2010).

To perform this analysis, the pre-policy and post-policy condition rating data was copied directly from the deterioration modeling Excel spreadsheet (in the format shown in Table 5.3 above) and pasted into Minitab. The data included in this analysis was condition ratings 6 through 9 for both the substructure and superstructure. Once the data was in Minitab, the analysis was performed by choosing two-sample t-test and selecting the two datasets to be analyzed (pre-policy versus post-policy condition rating data in this case). The output from this analysis includes the n-value, mean, standard deviation, standard error mean, 95% confidence interval, t-value, p-value, and the degrees of freedom.

A sample Minitab output is shown in Figure 5.3 below. This figure shows the output for average time spent in condition rating 8 for substructures in the highly corrosive zone. The naming convention follows the shorthand notations shown in Table 5.4 below and makes use of the following format: Zone/Element/Policy/Condition Rating. For example, z1/sub/pre/8 corresponds to the following group of structures: highly corrosive zone/substructures/constructed pre-policy/condition rating 8.

Two-Sample T-Test and CI: z1/sub/pre/8, z1/sub/post/8

```
Two-sample T for z1/sub/pre/8 vs z1/sub/post/8

                N  Mean  StDev  SE Mean
z1/sub/pre/8   19  5.05   2.04     0.47
z1/sub/post/8  19  2.95   1.54     0.35


Difference = μ (z1/sub/pre/8) - μ (z1/sub/post/8)
Estimate for difference:  2.105
95% CI for difference:  (0.911, 3.300)
T-Test of difference = 0 (vs ≠): T-Value = 3.59  P-Value = 0.001  DF = 33
```

Figure 5.3. Sample Output from Minitab Analysis.

Table 5.4. Shorthand Notation used in Minitab Analysis.

Label	Shorthand Notation	Longhand Notation
Zone	z1	Highly Corrosive Zone
	z2	Corrosive Zone
Element	sub	Substructure
	super	Superstructure
Policy	pre	Pre-Policy
	post	Post-Policy
Condition Rating	-	Condition Ratings 6 - 9

It should be noted that when there was not enough datapoints input or if all the datapoints input in a single column were identical, the software would return one of the following two error messages:

1. * ERROR * All values in column are identical.
2. * ERROR * Not enough data in column.

This was the case for 5 out of the 16 analyses performed in this study. The most important results from the Minitab output (see Figure 5.3) in determining whether the difference between the two datasets is statistically significant were the t-value and the p-value. These parameters are discussed below.

The t-value is a measure of the difference between the means of two datasets. A smaller t-value indicates a small or insignificant difference between the means while a larger t-value indicates a more significant difference between the datasets, although this does not directly indicate whether this difference is statistically significant. Additionally, the sign of the t-value (positive versus negative) is an indication of which dataset possesses a larger mean (Devore 2010). For this analysis, the pre-policy data was always input first, and the post-policy data was input second. Given the order of this input, a positive t-value indicates that the mean of the pre-policy data is larger than that of the post-policy data while a negative t-value indicates that the mean of the post-policy data is larger than that of the pre-policy data.

The p-value is a probability and, for the purpose of this analysis, is used to determine whether the null hypothesis can be rejected. For this study, the null hypothesis is that the pre-policy mean time spent in a condition rating is larger than the post-policy mean time. The p-value is commonly compared against a minimum significance level (typically referred to as alpha) which is chosen based on the type of investigation. Some of the typical values chosen are 0.01, 0.05, and 0.1 which correspond to a 1%, 5%, and 10% probability, respectively. The most common value chosen is 0.05, which is what was used as the minimum significance level for this analysis (Devore 2010).

5.2 Deterioration Modeling Results

The deterioration model graphs are each organized with the cumulative time to deterioration in years on the x-axis and the condition rating from 1 to 9 on the y-axis. Due to the pre-policy and post-policy results being plotted together in certain figures below, the pre-policy data is shown with a dashed line while the post-policy data is shown with a

solid line. This is repeated in the legend of each graph. The legends refer to the data in shorthand as follows:

- Pre Pre-Policy (Constructed between 1993 – 2002)
- Post Post-Policy (Constructed between 2003 – 2012)
- 1 Zone 1 (Highly Corrosive Zone)
- 2 Zone 2 (Corrosive Zone)
- 3 Zone 3 (Outside Corrosive Zone)

On Figures 5.6 and 5.10 below, error bars are included for each condition rating showing a range of years based on a confidence interval of 75%. These intervals were determined for each condition rating individually using the following steps:

1. Calculate the average time spent in a condition rating;
2. Calculate the standard deviation (std.dev) of the time spent in a condition rating;
3. Determine the number of recordings (n);
4. Calculate the standard error (std.err) using the formula below:

$$Standard\ Error = \frac{std.dev}{\sqrt{n}}$$

5. Use the built-in Excel function T.INV.2T(probability, deg_freedom) where probability is set to 0.25 (for a 75% confidence interval) and deg_freedom is equal to n minus one;
6. Calculate the 75% confidence interval in Excel by using the formula below:

$$75\%\ Confidence\ Interval = std.err \times T.INV.2T(0.25, n-1)$$

The confidence intervals were not created for every figure presented in this section, however, a table (Table 5.5) presenting the n-value for each element (substructure versus superstructure), age (pre-policy versus post-policy), and condition

rating (9 through 5) is shown below. In the table, CR refers to condition rating and the shorthand notation introduced on the previous page was used. This table is intended for use as an aid in understanding the level of certainty of each condition rating on the deterioration models. The width of confidence intervals are influenced by the magnitude of the n-value; a larger n-value results in a more confident statement whereas a smaller n-value results in a less confident statement (i.e. a small range of potential values versus a large range of potential values, respectively).

Table 5.5. N-Value for Structures in each Condition Rating.

Element	Policy / Zone	N-Value				
		CR 9	CR 8	CR 7	CR 6	CR 5
Substructure	Pre / 1	4	19	20	8	0
	Post / 1	3	19	26	1	2
	Pre / 2	4	16	13	1	0
	Post / 2	3	11	18	2	0
	Pre / 3	11	59	33	9	0
	Post / 3	14	40	67	6	2
Superstructure	Pre / 1	6	20	13	5	0
	Post / 1	3	19	25	5	1
	Pre / 2	5	16	8	1	0
	Post / 2	3	11	18	0	0
	Pre / 3	14	57	20	4	0
	Post / 3	13	40	64	2	1

Additionally, Figures 5.7 and 5.11 below show the deterioration curves for the eight structures visited during the field investigations (see Chapter 3). These deterioration curves were created following the same process as described above, however, they were not created using the MATLAB code since there were so few datapoints. They are plotted

alongside the post-policy deterioration models for the highly corrosive zone and corrosive zone (zones 1 and 2, respectively).

The deterioration models presented below were created for both the substructure and superstructure using the MATLAB output tables previously described. From these output tables, the average time spent in each condition rating was calculated and graphed for the following scenarios:

- Figure 5.4: Deterioration Model Comparing Pre-Policy Substructures.
- Figure 5.5: Deterioration Model Comparing Post-Policy Substructures.
- Figure 5.6: Deterioration Model Comparing Pre- and Post-Policy Substructures.
- Figure 5.7: Deterioration Model Comparing Substructures from Field Investigations.
- Figure 5.8: Deterioration Model Comparing Pre-Policy Superstructures.
- Figure 5.9: Deterioration Model Comparing Post-Policy Superstructures.
- Figure 5.10: Deterioration Model Comparing Pre- and Post-Policy Superstructures.
- Figure 5.11: Deterioration Model Comparing Superstructures from Field Investigations.

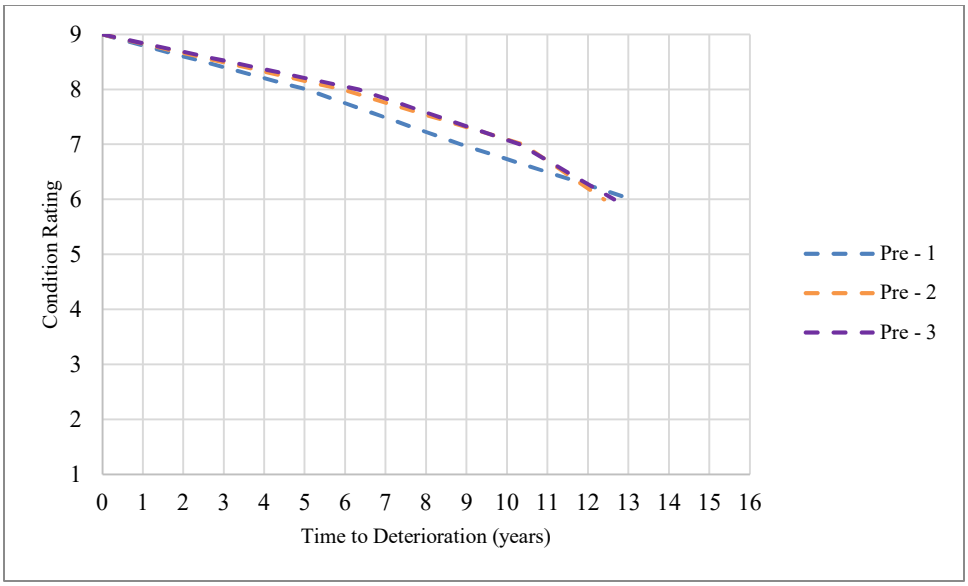

Figure 5.4. Deterioration Model Comparing Pre-Policy Substructures.
(Zone 1: n = 28. Zone 2: n = 21. Zone 3: n = 68)

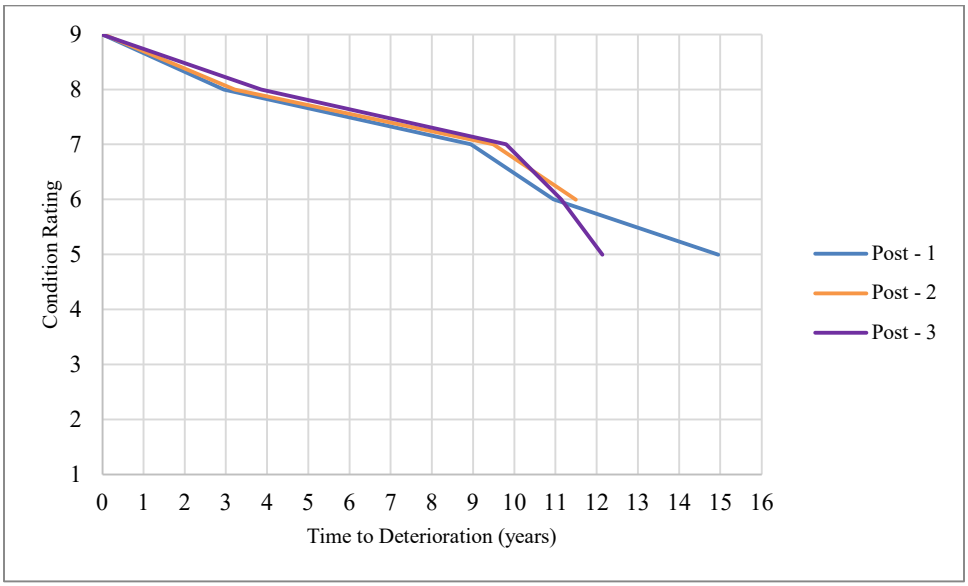

Figure 5.5. Deterioration Model Comparing Post-Policy Substructures.
(Zone 1: n = 26. Zone 2: n = 18. Zone 3: n = 67)

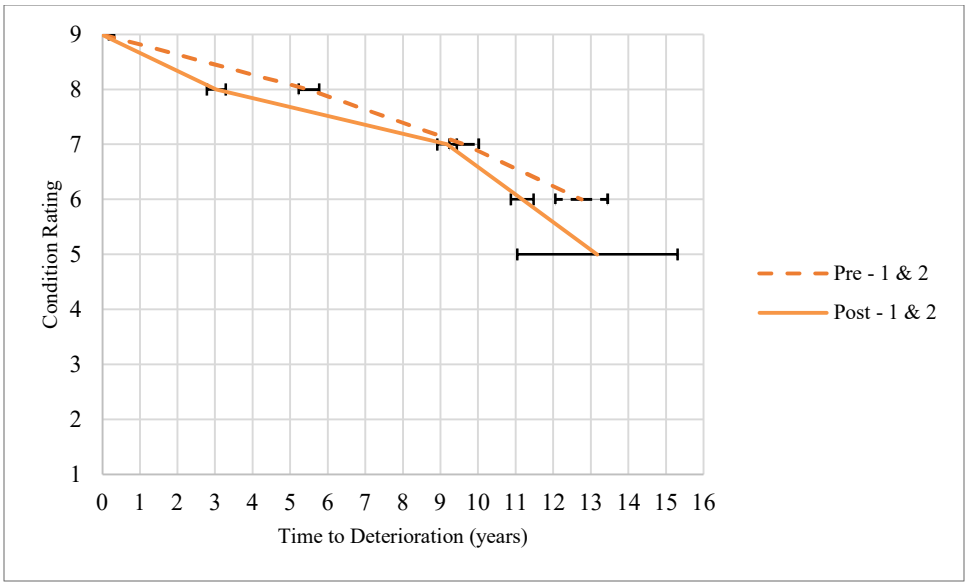

Figure 5.6. Deterioration Model Comparing Pre- and Post-Policy Substructures.
(Pre-Policy: n = 49. Post-Policy: n = 44)

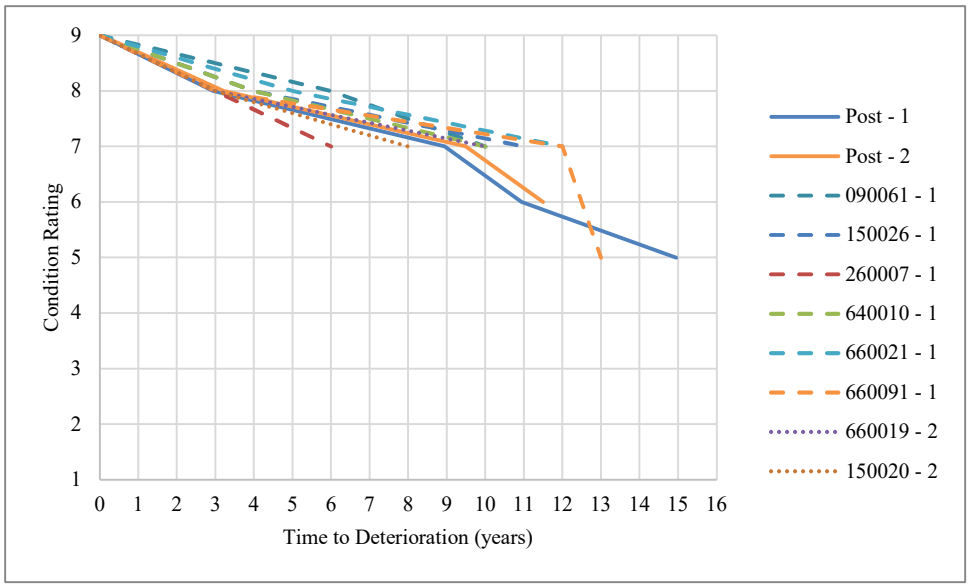

Figure 5.7. Deterioration Model Comparing Substructures from Field Investigations.
(Zone 1: n = 26. Zone 2: n = 18)

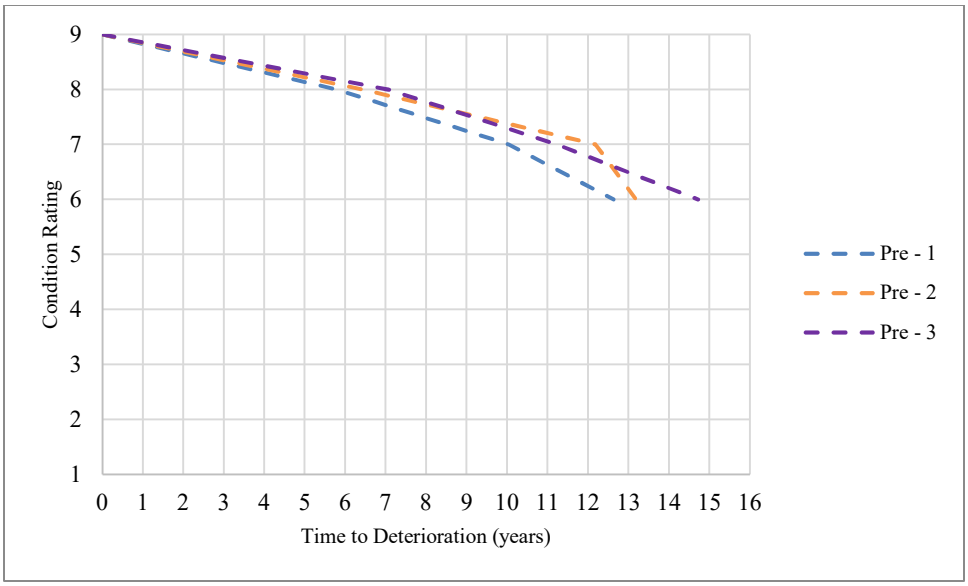

Figure 5.8. Deterioration Model Comparing Pre-Policy Superstructures. (Zone 1: n = 28. Zone 2: n = 21. Zone 3: n = 68)

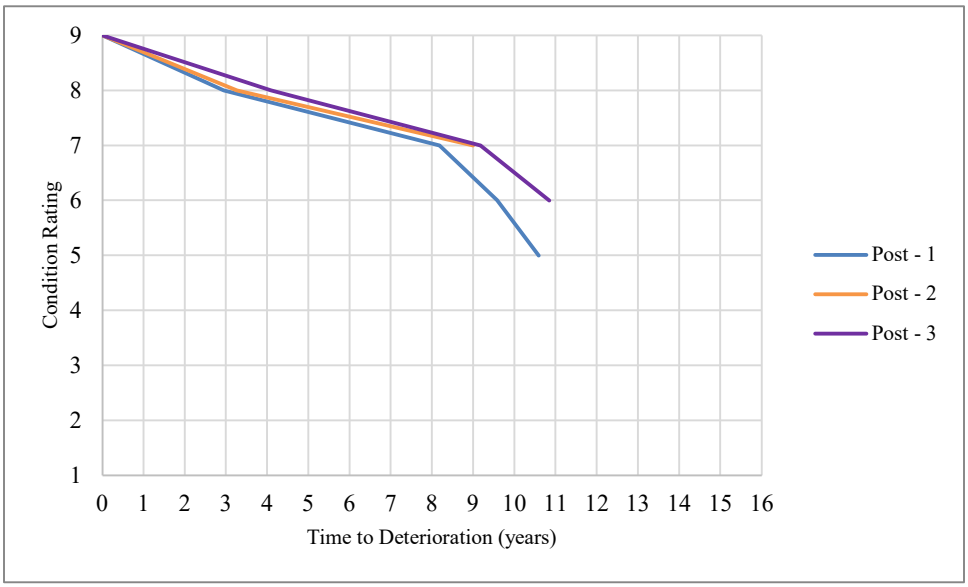

Figure 5.9. Deterioration Model Comparing Post-Policy Superstructures. (Zone 1: n = 26. Zone 2: n = 18. Zone 3: n = 67)

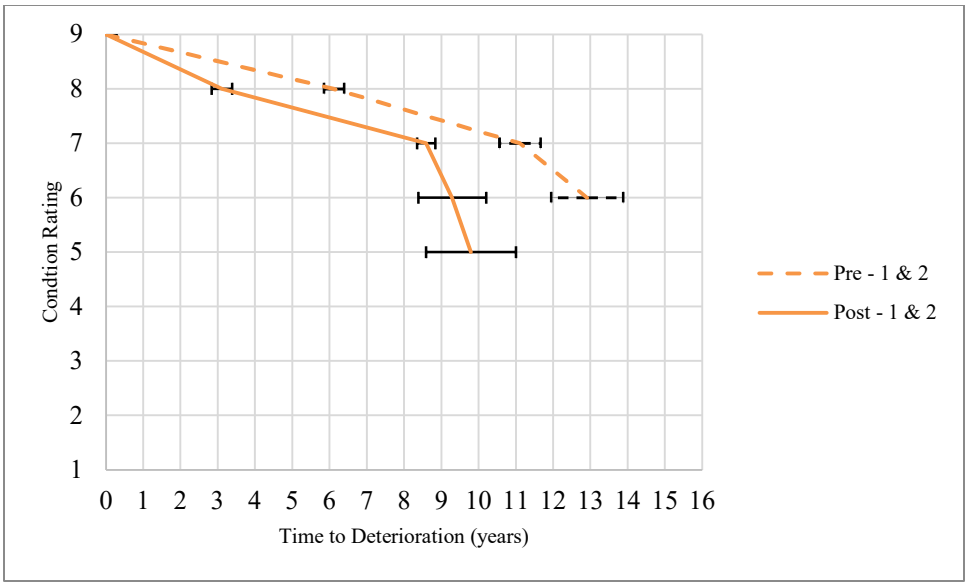

Figure 5.10. Deterioration Model Comparing Pre- and Post-Policy Superstructures. (Pre-Policy: n = 49. Post-Policy: n = 44)

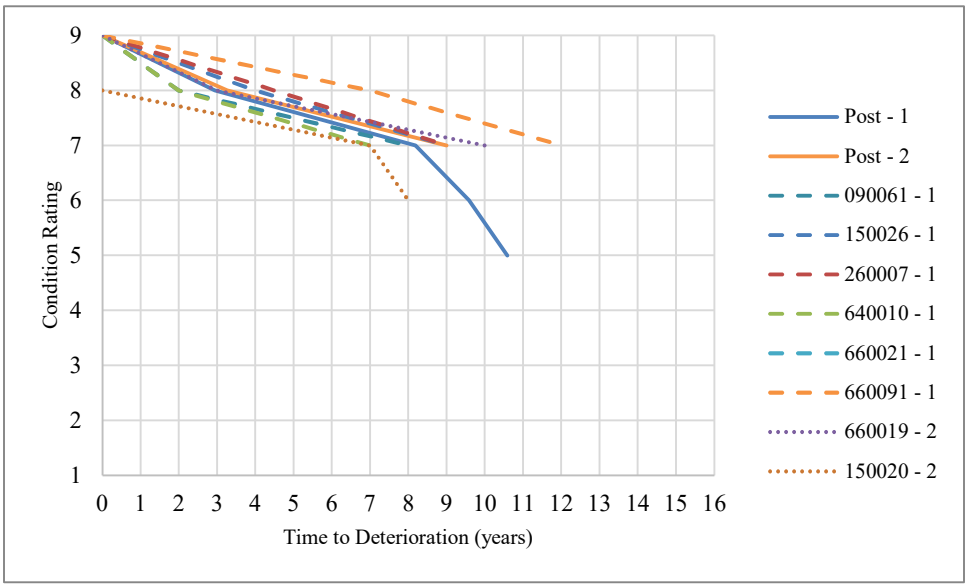

Figure 5.11. Deterioration Model Comparing Superstructures from Field Investigations. (Zone 1: n = 26. Zone 2: n = 18)

5.3 Statistical Correlation Results

The results presented below are summary tables created using the output from the Minitab two-sample t-test analysis. Tables 5.6 through 5.9 show the lower and upper limits of the 95% confidence intervals, t-values, p-values, degrees of freedom, interpretation of results, justification of results, and a note on what the interpretation implies for each condition rating. Tables 5.10 and 5.11 show the n-value, mean, and standard deviation of the time spent in each condition rating. This analysis was completed for substructures in the highly corrosive zone, substructures in the corrosive zone, superstructures in the highly corrosive zone, and superstructures in the corrosive zone, and are presented in this order.

Table 5.6. Two-Sample T-Test Results for Substructures in the Highly Corrosive Zone.

Parameter	Condition Rating			
	9	8	7	6
95% CI Lower Limit	-	0.911	-3.821	-
95% CI Upper Limit	-	3.300	-0.579	-
t-Value	-	3.59	-2.77	-
p-Value	-	0.001	0.009	-
Degrees of Freedom	-	33	30	-
Interpretation	-	Significant	Significant	-
Justification	-	p-value < 0.05	p-value < 0.05	-
Notes	Error: All values are identical.	Pre-policy performs better.	Post-policy performs better.	Error: Not enough data.

Table 5.7. Two-Sample T-Test Results for Substructures in the Corrosive Zone.

Parameter	Condition Rating			
	9	8	7	6
95% CI Lower Limit	-2.128	1.175	-4.020	-
95% CI Upper Limit	2.962	4.337	0.380	-
t-Value	0.45	3.63	-1.71	-
p-Value	0.673	0.002	0.101	-
DF	4	21	23	-
Interpretation	Not Significant	Significant	Not Significant	-
Justification	p-value > 0.05	p-value < 0.05	p-value > 0.05	-
Notes	-	Pre-policy performs better.	-	Error: Not enough data.

Table 5.8. Two-Sample T-Test Results for Superstructures in the Highly Corrosive Zone.

Parameter	Condition Rating			
	9	8	7	6
95% CI Lower Limit	-	1.359	-2.950	-0.830
95% CI Upper Limit	-	4.346	0.931	5.370
t-Value	-	3.88	-1.10	1.79
p-Value	-	0.000	0.287	0.124
DF	-	34	16	6
Interpretation	-	Significant	Not Significant	Not Significant
Justification	-	p-value < 0.05	p-value > 0.05	p-value > 0.05
Notes	Error: All values are identical.	Pre-policy performs better.	-	-

Table 5.9. Two-Sample T-Test Results for Superstructures in the Corrosive Zone.

Parameter	Condition Rating			
	9	8	7	6
95% CI Lower Limit	-1.551	1.657	-2.830	-
95% CI Upper Limit	3.284	4.673	2.890	-
t-Value	0.92	4.35	0.02	-
p-Value	0.399	0.000	0.983	-
DF	5	22	12	-
Interpretation	Not Significant	Significant	Not Significant	-
Justification	p-value > 0.05	p-value < 0.05	p-value > 0.05	-
Notes	-	Pre-policy performs better.	-	Error: Not enough data.

Table 5.10. Summary of Substructure Statistical Results.

Zone	Parameter	CR 9		CR 8		CR 7		CR 6	
		Pre	Post	Pre	Post	Pre	Post	Pre	Post
Highly Corrosive Zone	n-Value	-	-	19	19	20	26	-	-
	Mean	-	-	5.05	2.95	3.80	6.00	-	-
	Standard Deviation	-	-	2.04	1.54	3.11	1.96	-	-
Corrosive Zone	n-Value	4	3	16	11	13	18	-	-
	Mean	2.75	2.33	5.94	3.18	4.46	6.28	-	-
	Standard Deviation	1.26	1.15	2.69	1.17	3.07	2.7	-	-

Table 5.11. Summary of Superstructure Statistical Results.

Zone	Parameter	CR 9		CR 8		CR 7		CR 6	
		Pre	Post	Pre	Post	Pre	Post	Pre	Post
Highly Corrosive Zone	n-Value	-	-	20	19	13	25	6	5
	Mean	-	-	5.80	2.95	4.23	5.24	3.67	1.40
	Standard Deviation	-	-	2.67	1.87	3.03	1.81	2.94	0.894
Corrosive Zone	n-Value	5	3	16	11	8	18	-	-
	Mean	3.20	2.33	6.44	3.27	5.75	5.72	-	-
	Standard Deviation	1.48	1.15	2.53	1.16	3.15	2.95	-	-

5.4 Combined Field Investigation and Deterioration Modeling Results

The table and figures presented below compare the results from the field investigations (Chapter 3) to the results from the deterioration modeling (presented in Section 5.2). The table (Table 5.12) presents the condition rating (as of 2018), deterioration rate (measured in number of condition ratings declined per year), low, median, and high readings for the corrosion rate and surface resistivity, as well as the n-value and standard deviation (abbreviated as Std.Dev.). The n-value in this case refers to the number of readings that the corrosion rate and resistivity results are based on. The results are organized by zone, structure, and structural component (substructure versus superstructure). The figures present the same set of corrosion rate and surface resistivity readings that were used to create the summary table (Table 5.12), however, they are presented in a box-and-whisker plot format to provide a visualization of the variation associated with each group of readings (corrosion rate and surface resistivity readings on the substructure and superstructure).

Table 5.12. Summary Results from Field Investigations and Deterioration Modeling.

Zone	Structure Number	Year Built	Structural Component	Condition Rating (as of 2018)	Deterioration Rate (Condition Ratings/Year)	n-Value	Corrosion Rate (µm/year)				Surface Resistivity (kohm-cm)			
							Low	Median	High	Std.Dev.	Low	Median	High	Std.Dev.
Highly Corrorisve	660091	2005	Substructure	5	0.31	12	0	10	54	19.2	92.7	128.9	459.6	98.6
			Superstructure	7	0.15	27	0	7.7	31	7.4	38.5	62.9	187.8	40.9
	090061	2005	Substructure	7	0.15	36	0.59	33	274	84.4	6.7	49	403	81.6
			Superstructure	7	0.15	24	3.8	11.5	29	5.7	26	52.5	93	16.5
	660021	2005	Substructure	7	0.15	20	0.23	3.05	10	2.3	112	230	646	162.8
			Superstructure	7	0.15	28	0	2.35	9.7	2.0	45	102.5	411	71.1
	640010	2006	Substructure	7	0.17	74	0.03	4.2	99	21.6	13	113	801	142.9
			Superstructure	7	0.17	32	1.1	11.5	40	8.9	7.2	28.5	195	35.3
	150026	2006	Substructure	7	0.17	16	0.13	2.55	52	14.1	134	388	775	183.6
			Superstructure	7	0.17	20	1.4	4.5	13	3.0	123	233.5	312	55.5
	260007	2007	Substructure	7	0.18	27	0.72	18	67	16.5	42	112	315	70.6
			Superstructure	7	0.18	7	0.34	6.6	11	3.6	137	155	180	16.2
Corrosive	150020	2008	Substructure	7	0.20	24	0.43	4.65	20	5.3	106	430	866	233.4
			Superstructure	6	0.30	27	12	22	52	9.4	21	30	48.3	5.8
	660019	2008	Substructure	7	0.20	24	0.82	10	136	33.3	49	104.5	190	40.6
			Superstructure	7	0.20	20	4	8.8	21	4.2	26	38	52	7.5

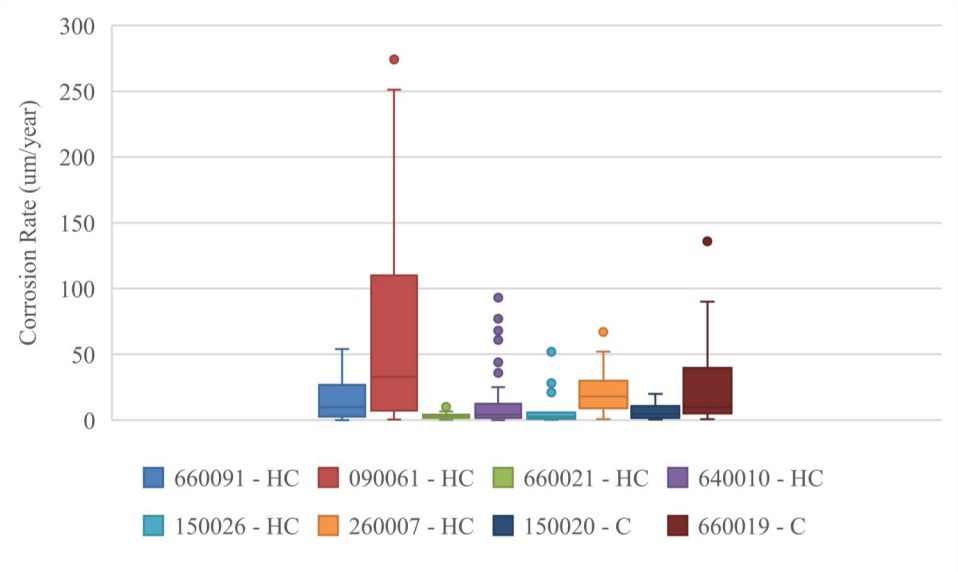

Figure 5.12. Box-and-Whisker Plot of Substructure Corrosion Rate Readings.

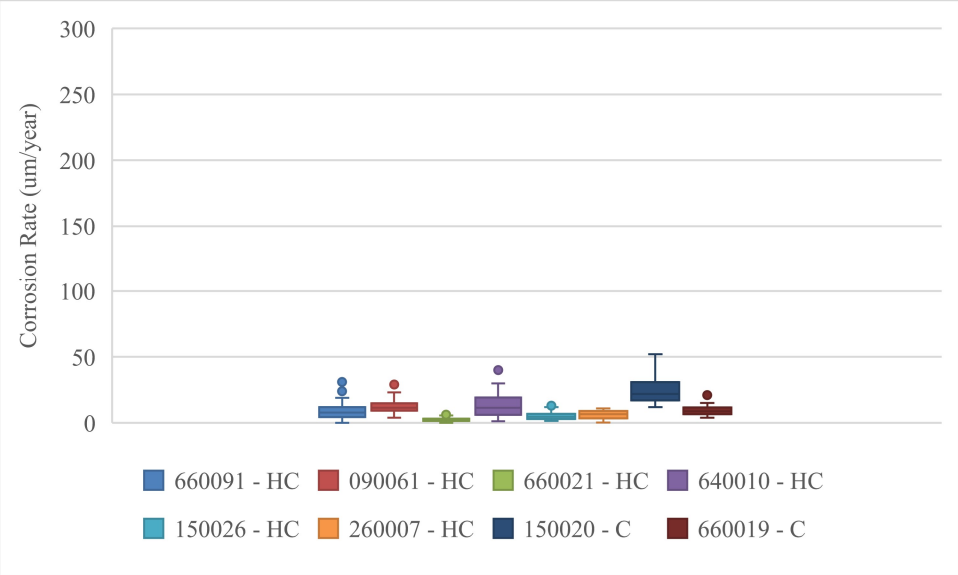

Figure 5.13. Box-and-Whisker Plot of Superstructure Corrosion Rate Readings.

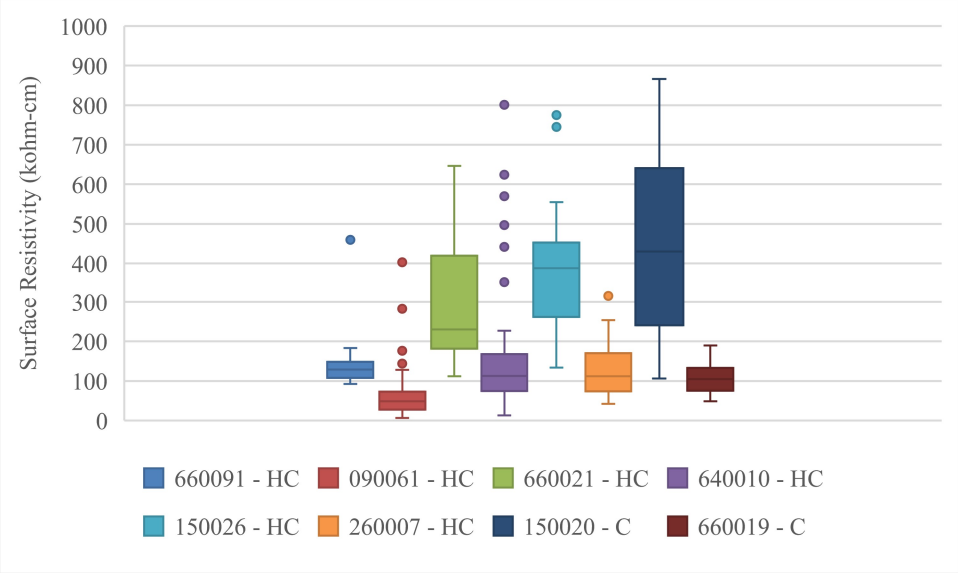

Figure 5.14. Box-and-Whisker Plot of Substructure Surface Resistivity Readings.

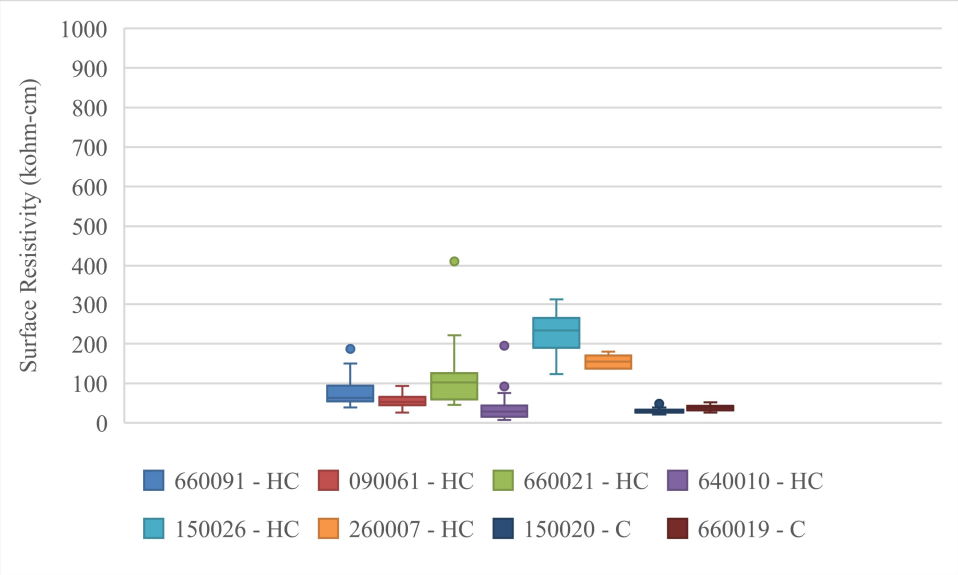

Figure 5.15. Box-and-Whisker Plot of Superstructure Surface Resistivity Readings.

5.5 Statistical Correlation Discussion

The following subsections present a discussion of the Minitab results in the order of the two-sample t-test results followed by the basic statistical analysis results.

5.5.1 Discussion of Two-Sample T-Test Results

The Minitab analysis showed that pre-policy structures typically spent more time in condition rating 8 than post-policy structures. This was true for substructures and superstructures in both corrosive zones (highly corrosive and corrosive). It was shown that post-policy substructures in the highly corrosive zone spent more time in condition rating 7 than pre-policy substructures. These observations were the only differences that the two-sample t-test determined to be significant.

The analysis determined that the difference in average time spent in condition rating 9 for both substructures and superstructures in the corrosive zone were not significant. This was also the case for substructures and superstructures in the corrosive

zone and superstructures in the highly corrosive zone; the differences seen in condition rating 7 were not significant. Additionally, superstructures in the highly corrosive zone in condition rating 6 showed were determined to have no significant differences between pre-policy and post-policy.

While there were four cases (condition rating 8 for all four scenarios) that showed a statistically significant difference in performance with the pre-policy structures performing better, there were six cases that were determined to have no statistically significant differences between them and one case where the post-policy structures were performing better. The remaining five cases returned one of the error messages defined in Section 5.1.3 (either not enough datapoints or all values in a single column were identical).

5.5.2 Discussion of Basic Statistical Analysis Results

The summary of substructure results (Table 5.10) shows the pre-policy structures having a higher mean and higher standard deviation for condition ratings (CR) 9 and 8 in the highly corrosive zone and the corrosive zone than the post-policy structures. The higher means indicate that the pre-policy substructures are typically spending more time in CR 9 and 8 than post-policy substructures. However, the higher standard deviation indicates that the post-policy substructures are performing more consistently (due to less variation) in CR 9 and 8. For CR 7, the post-policy substructures have a higher mean and a lower standard deviation, indicating that they are performing more consistently than pre-policy substructures and are spending more time in this particular condition rating.

The summary of superstructure results (Table 5.11) shows similar trends to those discussed above for the substructure. The post-policy superstructures are showing a lower

standard deviation in both corrosive zones for condition ratings 9 through 6. The pre-policy superstructures are showing a higher mean for all conditions considered except for condition rating 7 in the highly corrosive zone. These trends indicate that while the pre-policy superstructures are typically spending more time in each condition rating than post-policy superstructures, the post-policy structures are performing more consistently throughout all condition ratings.

5.6 Deterioration Models Discussion

The following subsections present a discussion of the results in order of substructure, superstructure, and an overall discussion making comparisons between the substructure and superstructure.

5.6.1 Substructure Deterioration Models Discussion

Prior to the enactment of the current NCDOT corrosion policy, substructures appear to be performing approximately the same regardless of the proximity to the coast, with substructures in the highly corrosive zone deteriorating at a slightly quicker rate than in the corrosive zone and outside corrosive zone (see Figure 5.4). This implies that prior to the enactment of the corrosion policy, the substructures were performing roughly equally whether they were in a corrosive environment or not (i.e. with no defined corrosive boundary or difference in specifications).

Following the enactment of the NCDOT corrosion policy, substructures located within the highly corrosive zone and the corrosive zone appear to be performing equally, if not slightly better, to those located west of both corrosive boundary lines until condition rating 6, at which point the highly corrosive zone appears to outperform substructure in the outside corrosive zone (see Figure 5.5). This is an indication that the

current corrosion policy is having the intended effects and is extending the maintenance-free service lives of the substructure elements. This is shown in Figure 5.5 because the deterioration models both follow nearly the same trajectory from condition rating 9 to condition rating 6, at which point the structures located in the highly corrosive zone and corrosive zone appear to be performing better (i.e. taking a longer time to deteriorate from condition rating 7 to condition rating 5) than structures located west of the corrosive boundary lines.

The deterioration curves in Figure 5.6 show that substructures constructed pre-policy are performing better than substructures constructed post-policy, however, this may be due to the shorter period of time structures built post-policy spend in condition rating 9. It was determined in the statistical analysis (discussed in Section 5.5) that the difference of time spent in condition rating 9 between pre-policy and post-policy substructures constructed in the corrosive zone was not significant. Post-policy substructures appear to spend more time in condition rating 8 than pre-policy substructures by 2.1 years on average. This was confirmed by the statistical analysis.

The eight structures visited for the field investigation portion of this thesis appear to typically be performing at or above average (Figure 5.7). There were two (SN 150020 in the corrosive zone and SN 260007 in the highly corrosive zone) of the eight structures' deterioration curves that showed a quicker deterioration than the deterioration model for the corrosive zone they are located in. This is an indication that the structures visited represent a variety of performance with some structures performing above average and some performing below. SN 090061 and SN 660091 showed conflicting results to what was observed in the field and are discussed below.

The deterioration curve of SN 090061 on Figure 5.7 suggests that the substructure was performing better than the deterioration model for substructures in the highly corrosive zone, however, this was not reflected in the field testing of corrosion rate and surface resistivity (see Table 5.12). The corrosion rate readings obtained on the substructure were the highest observed from all eight structures. The median corrosion rate was 33 μm/year and the maximum reading was 274 μm/year. The surface resistivity readings were fairly low (median surface resistivity was 49 kohm-cm) compared to the other substructures investigated, although the maximum readings were typical of other structures (see Table 5.12). It should be noted that the high corrosion rate readings and low surface resistivity readings were measured within or near the splash zone. Above the splash zone, the corrosion rate and surface resistivity readings were typical of the other structures investigated.

SN 660091 in the highly corrosive zone appeared to be performing very well until condition rating 7, at which point it dropped rapidly (within 1 year) to condition rating 5. The corrosion rate readings on the substructure were typical of the eight structures visited (the maximum was 54 μm/year and the median was 10 μm/year), however, the surface resistivity readings were very high (the minimum was 92.7 kohm-cm and the median was 128.9 kohm-cm) on the substructure (see Table 5.12). This is an indication that the reason for the rapid decline in condition rating was likely due to non-corrosion related damages or an error in coding.

5.6.2 Superstructure Deterioration Models Discussion

The superstructures in the corrosive zone before the enactment of the current corrosion policy appear to be performing equally until condition rating 7, where

structures located within the corrosive zone reach condition rating 6 before structures located west of the corrosive boundary lines by about 2 years on average (see Figure 5.8). Superstructures in the highly corrosive zone start declining at a quicker rate than in the corrosive zone or outside corrosive zone after condition rating 8. The same trend is observed for the superstructures after the enactment of the corrosion policy. The superstructures in both corrosive zones appear to be performing equally to those in the outside corrosive zone until condition rating 7, where the condition rating of superstructures located within the highly corrosive zone begins to decline at a quicker rate than structures located in the corrosive zone and outside corrosive zone (see Figure 5.9).

The superstructures constructed post-policy appear to be deteriorating at a quicker rate than the superstructures constructed pre-policy (see Figure 5.10). Similar to the trend shown for the substructures, post-policy superstructures appear to be spending slightly more time in condition rating 8 than pre-policy superstructures by 0.5 years on average. The statistical analysis showed a significant difference of time spent in condition rating 8 (post-policy outperforming pre-policy), with the differences of time spent in condition ratings 7 and 6 being insignificant. This implies that the differences seen on the deterioration models are mostly statistically insignificant (except for condition rating 8) and structures built post-policy are performing approximately equal to structures constructed pre-policy.

The eight structures visited for the field investigation portion of this thesis appear to be performing close to the average of all structures considered for this study, although there appears to be more superstructures performing below average (see Figure 5.11) than

there were substructures. There were three structures (SN 640010 in the highly corrosive zone, SN 150020 in the corrosive zone, and SN 090061 highly corrosive zone) that fell below the superstructure deterioration model of the highly corrosive zone and the corrosive zone. This is an indication that the structures visited represent a variety of performance with some structures performing above average and some performing below.

5.6.3 Substructure versus Superstructure Discussion

It appears that the structures constructed pre-policy are typically performing slightly better (i.e. longer maintenance-free service lives) than structures constructed post-policy based on the deterioration models presented above. Looking at post-policy substructures only, it appears that the substructures located in the highly corrosive zone and corrosive zone are performing approximately equal to or better than substructures located west of the corrosive boundary lines. However, looking at post-policy superstructures only, it appears that the superstructures located in either the highly corrosive zone or corrosive zone are performing approximately equal to superstructures located west of the corrosive boundary line only until condition rating 7. After condition rating 7, the condition rating of superstructures located within the highly corrosive zone begins to decline rapidly compared to superstructures located in the corrosive zone and the outside corrosive zone.

Comparing Figure 5.5 (Deterioration Model Comparing Post-Policy Substructures) and Figure 5.9 (Deterioration Model Comparing Post-Policy Superstructures), it appears that the substructures and superstructures are performing equally until condition rating 7 where the superstructures begin to deteriorate quickly

while the substructures maintain approximately the same trajectory. This could be due to the differing requirements for substructures versus superstructures that are defined in the current NCDOT corrosion policy. The policy was described in detail in Chapter 1, however, some of the differences are reiterated below.

For structures located within the highly corrosive zone, all elements (substructure and superstructure) must follow the corrosion-related design and construction measures laid out in the NCDOT SMU Design Manual (see Figure 1.3 in Chapter 1). For structures located within the corrosive zone, only elements that are located within 15 feet of the mean high tide line must follow the corrosion-related design and construction measures laid out in the NCDOT SMU Design Manual. Since the substructure is more likely to be located within 15 feet of the mean high tide line than the superstructure, it is likely that there are many structures located within the corrosive zone that the substructures are receiving additional treatment while the superstructures are not. This could be the cause of the differing deterioration curves shown between the substructure and superstructure.

5.6.4 Combined Field Investigation and Deterioration Modeling Discussion

The low and median corrosion rate values appeared to be fairly consistent across all eight structures, regardless of which zone the structure was located in (highly corrosive versus corrosive). However, the high values at certain structures (090061, 640010, and 660019) were significantly higher than what was typically recorded. The surface resistivity readings showed a high amount of variability across the eight structures, although the readings were typically high.

The plots shown in Figures 5.12 through 5.15 demonstrate that the variability of measurements at each structure was typically much higher on the substructure than on the

superstructure. This could be due to the inclusion of the cast-in-place concrete readings from the interior caps in the substructure category while the superstructure consists only of precast concrete. This is what would be expected as precast concrete typically has less variability due to being constructed off site and in a more controlled environment.

The deterioration rates were consistent across all eight structures, however, there did not appear to be a relationship between the recorded corrosion rate or surface resistivity readings and the magnitude of the deterioration rates. The structures that were showing a more rapid deterioration rate were not necessarily showing higher than typical corrosion rates or lower than typical surface resistivities. However, the deterioration rates demonstrated that the substructure and superstructure are typically deteriorating at the same rate with the exception of SN 660091 and SN 150020. This was not reflected in the field investigation results, which appears to show the trend of higher corrosion rates on the substructure based on median values (5 out of 8 structures) and high values (7 out of 8 structures). The low values of corrosion rate readings did not appear to follow this trend. Additionally, the trend of higher values on the substructure was observed for the surface resistivity readings (6 out of 8 structures based on low values, 6 out of 8 structures based on median values, and 8 out of 8 structures based on high values).

CHAPTER 6: CONCLUSIONS AND RECOMMENDATIONS

This chapter contains conclusions drawn from each portion of this thesis (field investigations, defect mapping, and deterioration modeling) followed by conclusions drawn from considering all three portions. Finally, future work to further confirm or deny the conclusions discussed in this Chapter are recommended.

6.1 Field Investigation Conclusions

The field investigation of eight structures near the North Carolina coastline, with six in the highly corrosive zone and two in the corrosive zone, resulted in the following findings for structures constructed under the current NCDOT corrosion policy:

- The only significant visual signs of corrosion identified included a corroded prestressed strand exposed by a large honeycomb on the underside of a cored slab (SN 660091) and efflorescence located near the splash zone on all eight structures.
- High values of corrosion rates were rare and only found on a few elements that regularly experience frequent wetting.
- Low values of surface resistivity were rare and only found on a few elements that regularly experience frequent wetting. This indicates that these low values were most likely related to the differential moisture content of the element.
- As a structural element's height above the splash zone increased, the corrosion rates decreased rapidly and the surface resistivities increased rapidly.

Based on the brief summary of results above, as well as the detailed discussion of results found in Chapter 3, it was concluded that the structures investigated at the North Carolina coast are performing well and are not typically experiencing high levels of active corrosion after 10 to 15 years of service. The only exception to this was structure 090061, which showed corrosion rates categorized as severe according to Table 2.8 or very high according to the ranges suggested by Bertolini et al. (2013) (see Section 2.5.4.3). These were the highest values measured at any of the structures, however, they were only found on elements within the splash zone. Above the splash zone, the corrosion rates quickly decreased to low or negligible levels. Additionally, the surface resistivities measured on these structural elements were typically high indicating that they should be capable of delaying the ingress of chlorides, thereby increasing the time required for corrosion to initiate.

The investigated structures were strategically chosen such that they were representative (by means of typical construction and varying locations north and south along the NC coast) therefore it was assumed that other structures with similar construction, proximity to the coastline, and exposure to chloride-rich waters are performing similarly. It should be clarified that this conclusion is not implying that all structures located in the corrosive boundaries are performing well. However, it was assumed that structures meeting the criteria mentioned above (similar construction, proximity, and exposure) are also performing well.

6.2 Defect Mapping Conclusions

The defect mapping investigation resulted in the following findings for structures when constructed under the current NCDOT corrosion policy:

- Delaminations and Spalling
    - The percentage of structures affected decreased from pre-policy to post-policy in the highly corrosive zone and corrosive zone.
    - A lower percentage of structures in the highly corrosive zone were affected by delaminations and spalling than structures in the outside corrosive zone.
    - The average condition state of this defect decreased in all zones. This indicates that even though delaminations and spalling are still occurring, they are typically less severe post-policy than they were pre-policy.
    - The average condition state was lower (less severe) for structures constructed post-policy in the highly corrosive zone and corrosive zone than in the outside corrosive zone.
- Efflorescence and Rust Staining
    - The percentage of structures affected increased in both corrosive zones from pre-policy to post-policy.
    - Structures located in the highly corrosive zone had a lower percentage of structures affected than in the outside corrosive zone (post-policy).
    - The average condition state of this defect increased in all zones. This indicates that this defect was typically more severe on post-policy structures than pre-policy structures.

    - The average condition state was slightly higher (more severe) for structures located in the highly corrosive zone and corrosive zone than in the outside corrosive zone (post-policy).
- Cracking (RC and Other)
    - The percentage of structures affected by this defect increased in both corrosive zones (post-policy).
    - Structures located in the corrosive zone had a lower percentage of structures affected than in the outside corrosive zone (post-policy).
    - The average condition state of this defect decreased in all zones. This indicates that even though reinforced concrete cracking was still occurring post-policy, they are typically less severe post-policy than they were pre-policy.
    - The average condition state was slightly higher (more severe) for structures located in the highly corrosive zone and slightly lower (less severe) for structures located in the corrosive zone than structures located in the outside corrosive zone.

Based on the summary of results described above and the detailed results and discussion in Chapter 4, it was concluded that structures located in the highly corrosive zone and corrosive zone are performing very similarly to structures located west of the corrosive boundary lines (also referred to as outside corrosive zone in this thesis). In most cases it was observed that structures in either corrosive zone were performing roughly equally to those located west of the boundaries. In some cases, it was observed that structures located in the corrosive zones were performing better than those located west

of these zones. This is a good indication that the corrosion policy is working well under the current specifications as structures located in aggressive, chloride-rich environments are performing equally to structures located in milder environments (relative to corrosion). From this analysis, it could not be definitively determined whether structures were performing better or worse when comparing pre-policy structures to post-policy structures.

6.3 Deterioration Modeling Conclusions

The deterioration modeling investigation resulted in the following findings for structures when constructed under the current NCDOT corrosion policy:

- Substructures located in both corrosive zones appear to be performing equally to or slightly better than substructures located in the outside corrosive zone.
- Superstructures located in both corrosive zones appear to be performing equally to superstructures located in the outside corrosive zone until condition rating 7. After condition rating 7, the highly corrosive zone begins to decline at a quicker rate than the corrosive zone and outside corrosive zone.
- The deterioration model comparing pre-policy and post-policy substructures shows the pre-policy substructures performing slightly better. However, based on low n-value, the statistical analysis could not support the significance of this observed trend.
- The deterioration model comparing pre-policy and post-policy superstructures shows the pre-policy superstructures performing considerably better. However, based on low n-value, the statistical analysis could not support the significance of this observed trend.

- The comparison of structures visited during the field investigations to the deterioration models showed that the structures investigated represented a wide variety of performance (i.e. some structures were performing better than the deterioration model suggested and some were performing worse).
- The comparison of corrosion rate and surface resistivity readings did not show any strong correlations to structures that were experiencing higher deterioration rates.

From the deterioration models alone, it appeared that the substructures and superstructures perform equally until condition rating 7, at which point the superstructures begin to deteriorate at a quicker rate. However, the comparison of deterioration rates from the modeling and the corrosion rate and surface resistivity data from the field investigations show the substructure typically having higher corrosion rates than the superstructure. The source of this difference in performance could be attributed to the variation in specifications based on which corrosive boundary the structure is located in and the element height above the mean high tide line. As discussed in Chapter 5, only elements located in the corrosive zone and within 15 feet of the mean high tide line are required to follow the corrosion-related specifications. Given that the superstructure is always located at an elevation higher than the substructure, it is more likely that the substructure will receive additional treatment than the superstructure. In this case, the substructure would be more equipped to delay the onset of corrosion and outperform the superstructure.

Based on the summary of results above and the detailed discussion in Chapter 5, it was concluded that structures located in either the highly corrosive zone or corrosive

zone are performing equal to or slightly better than those located west of the corrosive zones and not receiving additional treatment. From these analyses, it could not be definitively concluded whether structures constructed post-policy were performing better or worse than those constructed pre-policy.

6.4 Overall Conclusions

One of the desired outcomes of this thesis was to determine whether there was an increase in performance following the enactment of the current corrosion policy in 2003. The defect mapping investigation (Chapter 4) showed a significant decrease in percentage of structures in the highly corrosive zone and corrosive zone with delaminations from pre-policy to post-policy structures, however, this trend was not observed for efflorescence/rust staining or cracking (RC and other). The deterioration modeling investigation (Chapter 5) appeared to show a decrease in performance from pre-policy to post-policy structures, although the statistical analysis could not support the significance of this observed trend (based on low n-value). As neither of these studies were able to produce sufficient evidence to support or deny this claim, it could not be concluded definitively whether there was a significant difference in performance between pre-policy and post-policy structures. To make a definitive conclusion on this claim, future work involving the review of inspection and maintenance reports would be required. More information on this work is discussed in Section 6.5 below.

The general trend seen in the conclusions for each portion of this thesis was that structures located within the corrosive boundaries are performing roughly equally to and in certain circumstances (such as structures further from the coast, elements located relatively high above brackish water, and elements that are not submerged) better than

those located west of the corrosive boundaries. This is an indication that the NCDOT corrosion policy in its current form is sufficient to roughly equalize the performance of structures located in aggressive, chloride-rich environments to that of structures in less aggressive environments.

Given the research and results collected across the three investigations, it was concluded that the corrosion policy as currently written is conservative and it seems under certain circumstances (such as location further from the coast, elements high above brackish water, and unsubmerged elements), the policy is likely overly conservative. Additionally, as there were multiple investigations from different sources (field investigation, NCDOT database, and NBI database) suggesting the same result, the following was concluded: the current location of the corrosive boundary lines and specifications for each zone are adequate to delay the onset of corrosion. From this, it was recommended that no changes be made to the current location of the corrosive boundary lines or to the current specifications.

6.5 Recommendations for Future Work

A study of location-based defects based on water salinity was desired to be included in the defect mapping investigation of this thesis (found in Chapter 4), however, a detailed salinity map of the North Carolina coastline could not be found. The benefit of this analysis would be in mirroring other states' definition of corrosive boundaries based on water salinity at the intended site of the structure (such as Florida – see Table 2.1.a for more information). This could be included in the NCDOT corrosion policy as an additional criterion when determining the level of corrosion prevention measures required.

The deterioration modeling investigation (Chapter 5) showed the trend of substructures outperforming the superstructures. While there was not enough evidence collected to support this claim in this thesis, it may be of interest to the NCDOT to investigate this theory further. If it were proven definitively that there is a difference in performance between substructure and superstructure, it could lead to an improvement in the NCDOT corrosion policy that would impose more stringent requirements on superstructure elements. This study could be completed by performing a similar analysis to the deterioration models created in this thesis, however, with an approach that included the actual element height above the mean high tide line. The mean high tide line data was not collected at the time of this study but is likely available through the NCDOT maintenance records. This study would aid in determining whether 15 feet was an adequate height to specify in the policy.

A continuation of the deterioration modeling investigation (Chapter 5) is suggested as it could lead to more refined results and conclusions. This continuation would involve individually selecting structures constructed post-policy that have already reached the lower condition ratings (5 or 6) for the substructure or superstructure. Once these structures have been identified, an in-depth study of the historic maintenance and inspection records could be performed with the intent to identify whether the structures reaching low condition ratings are specifically a result of corrosion. This step was not performed in the deterioration modeling study for this thesis therefore the results are not specific to corrosion-related deterioration. It could be discovered that some of the structures causing the post-policy structures to appear to deteriorate faster than pre-policy structures are deteriorating due to non-corrosion related causes which could include a

significantly higher average daily traffic than designed for or damage caused by natural disasters. This study would also aid in concluding whether post-policy structures are performing better than, equal to, or worse than pre-policy structures.

REFERENCES

ACI (2001). *Protection of Metals in Concrete Against Corrosion*, American Concrete Institute.

ACI (2008). *Guide to Durable Concrete*, American Concrete Institute.

ACI (2019). *Guide to Protection of Reinforcing Steel in Concrete against Corrosion*, American Concrete Institute.

ALDOT (2017). "Structural Design Manual." A. B. Bureau, ed.Alabama.

Andrade, C. (2002). "Concepts on the Chloride Diffusion Coefficient." RILEM, ed.

Arnold, C. J. (1976). "Galvanized Steel Reinforced Concrete Bridge Decks: Progress Report." *Report N. FHWA-MI-78-R1033*, Federal Highway Administration, Washington, D.C.

ASTM (2003). "ASTM G1-03: Standard Practice for Preparing, Cleaning, and Evaluating Corrosion Test Specimens." ASTM International, West Conshohocken, PA.

ASTM (2013). "ASTM C1585." *Standard Test Method for Measurement of Rate of Absorption of Water by Hydraulic-Cement Concretes*, ASTM International, West Conshohocken, PA.

ASTM (2019). "ASTM C618." *Standard Specification for Coal Fly Ash and Raw or Calcined Natural Pozzolan for Use in Concrete*, ASTM International, West Conshohocken, PA.

Basheer, L., Kropp, J., and Cleland, D. J. (2001). "Assessment of the Durability of Concrete from its Permeation Properties: A Review." *Construction and Building Materials*, 15(2-3), 93-103.

Bertolini, L., Elsner, B., Pedeferri, P., Redaelli, E., and Polder, R. (2013). *Corrosion of Steel in Concrete: Prevention, Diagnosis, Repair*, Wiley-VCH.

Biggers, R. B. (2019). "Development of a Surface Resistivity Specficiation for Durable Concrete." University of North Carolina at Charlotte, Charlotte, NC.

Caltrans (2003). "Bridge Design Specifications." C. D. o. Transportation, ed.California.

Cavalline, T. L., Tempest, B. Q., Biggers, R. B., Lukavsky, A. J., McEntyre, M. S., and Newsome, R. A. (2020). "Durable and Sustainable Concrete Through Performance Engineered Concrete Mixtures." North Carolina Department of Transportation.

Cook, A. R., and Radtke, S. F. (1977). "Recent Research on Galvanized Steel for Reinforcement of Concrete." *ASTM STP 629*, D. E. Tonini, and S. W. Dean, eds., ASTM International, West Conshohocken, PA.

Cornet, I., and Bresler, B. (1996). "Corrosion of Steel and Galvanized Steel in Concrete." *Materials Protection*, 5(4), 69-72.

Cox, R. N., Cigna, R., Vennesland, O., and Valente, T. (1997). "Corrosion and protection of metals in contact with concrete."Brussels.

DelDOT (2017). "Bridge Design Manual." D. D. o. Transportation, ed.Delaware.

Devore, J. L. (2010). *Probability and Statistics for Engineering and the Sciences*.

Fahim, A., Ghods, P., Isgor, O. B., and Thomas, M. D. A. (2018). "A critical examination of corrosion rate measurement techniques applied to reinforcing steel in concrete." *Materials and Corrosion*, 69, 1784-1799.

FDOT (2019). "Structures Design Guidelines." F. D. o. Transportation, ed.Florida.

Feliu, S., Andrade, C., González, J. A., and Alonso, C. (1996). "A new method for in-situ measurement of electrical resistivity of reinforced concrete." *Materials and Structures*, 29(6), 362-365.

GDOT (2018). "Bridge and Structures Design Manual." G. D. o. Transportation, ed.Georgia.

Giatec (2019). *iCOR User Manual*, Giatec Scientific Inc.

Goyal, R., Whelan, M.J., and Cavalline, T.L. (2016). "Characterising the effect of external factors on deterioration rates of bridge components using multivariate proportional hazards regression." *Structure and Infrastructure Engineering, 13(7), 894-905.*

Griffin, D. F. (1969). "Effectiveness of Zinc Coating on Reinforcing Steel in Concrete Exposed to a Marine Environment." U. D. o. t. Navy, ed., Defense Technical Information Center, Naval Civil Engineering Lab Port Hueneme CA.

LADOTD (2005). "Bridge Design Manual." L. D. o. T. a. Development, ed.Louisiana.

Lataste, J. F. (2010). "Electrical resistivity for the evaluation of reinforced concrete structures." *Non-destructive evaluation of reinforced concrete structures*, C. Maierhofer, H.-W. Reinhardt, and G. Dobmann, eds., Woodhead Publishing Limited.

Li, K. (2016). *Durability Design of Concrete Structures: Phenomena, Modeling, and Practice*, John Wiley & Sons.

Lukavsky, A. J. (2019). "Impact of Concrete Mixture Design Parameters on Early Age Characteristics and Long Term Performance of Bridges and Pavements." University of North Carolina at Charlotte, Charlotte, NC.

MassDOT (2013). "LRFD Bridge Manual." M. D. o. Transportation, ed.Massachusetts.

McCarter, W. J., Starrs, G., and Chrisp, T. M. (2000). "Electrical Conductivity, Diffusion, and Permeability of Portland Cement-Based Mortars." *Cement and Concrete Research*, 30.

MDOT (2010). "Bridge Design Manual." M. D. o. Transportation, ed.Mississippi.

MEDOT (2003). "Bridge Design Guide." M. D. o. Transportation, ed.Maine.

NCDOT (2017). "Structure Safety Report (090061)." B. Croom, ed., North Carolina Department of Transportation, Division of Highways, Structure Management Unit.

NCDOT (2017). "Structure Safety Report (150026)." P. D. Ipock, ed., North Carolina Department of Transportation, Division of Highways, Structure Management Unit.

NCDOT (2018). "Structure Safety Inspection (660021)." B. Croom, ed., North Carolina Department of Transportation, Division of Highways, Structure Management Unit.

NCDOT (2018). "Structure Safety Report (260007)." G. L. Harrington, ed., North Carolina Department of Transportation, Division of Highways, Structure Management Unit.

NCDOT (2018). "Structure Safety Report (660019)." B. Croom, ed., North Carolina Department of Transportation, Division of Highways, Structure Management Unit.

NCDOT (2018). "Structures Management Unit Manual." N. C. D. o. Transportation, ed.North Carolina.

Newsome, R. (2020). "Evaluating Corrosive Site Performance of Coastal Bridges." University of North Carolina at Charlotte, Charlotte, NC.

NJDOT (2016). "Design Manual for Bridges & Structures." N. J. D. o. Transportation, ed.New Jersey.

NYDOT (2017). "Bridge Manual." N. Y. D. o. Transportation, ed.New York.

ODOT (2018). "Bridge Design Manual." O. D. o. Transportation, ed.Oregon.

Poe, J. H. (2019). "Corrosion Testing Equipment Comparison." MSCE, University of North Carolina at Charlotte.

Polder, R., Andrade, C., Elsener, B., Vennesland, O., Gulikers, J., Weidert, R., and Raupach, M. (2000). "RILEM TC 154-EMC: Electrochemical Techniques for Measuring Metallic Corrosion." *Materials and Structures*, 33, 603-611.

Presuel-Moreno, F., Suares, A., and Liu, Y. (2010). "Characterization of New and Old Concrete Structures Using Surface Resistivity Measurements." Florida Atlantic University.

Pruckner, F., and Gjorv, O. E. (2001). "Electrical Resistivity for Evaluation of Concrete Corrosivity." *Concrete under Severe Conditions*, Banthia, Sakai, and Gjorv, eds.The University of British Columbia, Vancouver, Canada.

Ramezanianpour, A. A., Pilvar, A., Mahdikhani, M., and Moodi, F. (2011). "Practical Evaluation of Relationship between Concrete Resistivity, Water Penetration, Rapid Chloride Penetration and Compressive Strength." *Construction and Building Materials*, 25, 2472-2479.

RIDOT (2007). "LRFD Bridge Design Manual." R. I. D. o. Transportation, ed.Rhode Island.

Rochelle, R. D. (2000). "Corrosion Modeling and Design Specifications for a 100 Year Service Life along North Carolina's Outer Banks." *Symposium proceedings : PCI/FHWA/FIB International Symposium on High Performance Concrete, September 25-27, 2000, Orlando, Florida : the economical solution for durable bridges and transportation structures*, Precast/Prestressed Concrete Institute.

Ryan, T. W., Mann, J. E., Chill, Z. M., and Ott, B. T. (2012). "Bridge Inspector's Reference Manual (BIRM)." Federal Highway Administration.

Saleem, M., Shemeem, M., Hussain, S. E., and Maslehuddin, M. (1996). "Effect of Moisture, Chloride and Sulfate Contamination on the Electrical Resistivity of Portland Cement Concrete." *Construction and Building Materials*, 10.

SCDOT (2006). "Bridge Design Manual." S. C. D. o. Transportation, ed.South Carolina.

Shi, C., Stegemann, J. A., and Caldwell, R. J. (1998). "Effect of Supplementary Cementing Materials on the Specific Conductivity of Pore Solution and Its Implications on the Rapid Chloride Permeability Test (AASHTO T277 and ASTM C1202) Results." *ACI Materials Journal*, 95(4), 389-394.

Sopler, B. (1973). "Corrosion of Reinforcement in Concrete - Part Series D." *Report No. FCB 73-4*, Norwegian Institute of Technology, University of Trondheim.

TXDOT (2018). "Bridge Design Manual - LRFD." T. D. o. Transportation, ed.Texas.

VDOT (2011). "Instructional and Informational Memoranda." V. D. o. Transportation, ed.Virginia.

Zhao, Y., and Jin, W. (2016). *Steel Corrosion-Induced Concrete Cracking*.

APPENDIX A: NARRATIVE OF FIELD INVESTIGATIONS

The following sections and subsections contain detailed narratives along with pictures of the eight structures investigated over the course of this thesis. The sections are organized by each field visit with the subsections each being a description of the structures investigated during that field visit.

A1.1 Field Visit #1 – August 5, 2019

During the first field visit on August 5, 2019, two structures were investigated in the Jacksonville area of North Carolina. The structures investigated include Structure Number (SN) 150020 (SR1124 at East Prong Broad Creek) and SN 660091 (SR1509 at Parrot Swamp), whose locations can be seen in the map below (Figure A1.1). SN 150020 is located in the corrosive zone and SN 660091 is located in the highly corrosive zone.

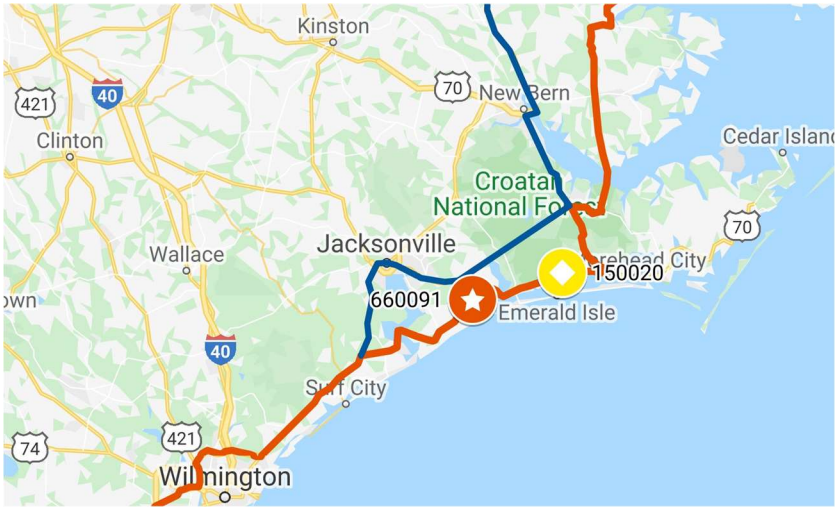

Figure A1.1. Locations of SN 150020 and 660091.

A1.1.1 Structure 150020 (SR1124 at East Prong Broad Creek)

The inspection of SN 150020 included a full visual observation with picture documentation of any potential signs of corrosion or degradation, drilling for powder samples at three locations, and use of the Giatec iCOR at eight locations.

The iCOR test grids were chosen to test a variety of elements at varying heights and locations. The piers that were tested with the iCOR were tested just above the surface in an area that appeared to experience submersion during high tides or storms. The face of the interior bent was selected to obtain data at an elevation that most likely would not experience any submersion. Test grids were set up on the underside of multiple different cored slabs. Two grids were set up on the top side of the cored slabs but were limited in location to the shoulder due to live traffic.

Powder samples were collected from two piers and the face of the interior bent. The location of these samples was chosen to be close to a test grid where the iCOR was also used to compare results at a similar location. Pictures from this inspection can be found below (Figures A1.12 through A1.7).

Figure A1.2. Research Team Using Pachometer To Locate Rebar.

Figure A1.3. Collection of Powder Samples from West-Most Pier.

Figure A1.4. Measuring Corrosion Rate and Surface Resistivity (iCOR) At Center Pier.

Figure A1.5. Location of iCOR Test Grid and Powder Sample Collection at Center Pier.

Figure A1.6. Location of iCOR Test Grid and Powder Sample Site on Face of Interior Bent.

Figure A1.7. Location of iCOR Test Grid on Top Surface of Cored Slabs and Barrier Rail.

A1.1.2 Structure 660091 (SR1509 at Parrot Swamp)

The inspection of SN 660091 was performed in a similar manner to that of SN 150020, which included a full visual observation with picture documentation of any potential signs of corrosion or degradation, drilling for powder samples at two locations, and use of the Giatec iCOR at five locations.

The iCOR test grids were selected to test all of the accessible elements. For this bridge, only the underside of the cored slabs and the end bents were accessible. As this structure was a single span, there were no elements near the surface of the water that would be expected to regularly experience submersion. The iCOR was used at both ends

of one end bent and the underside of three cored slabs. Only one end bent was tested due to the symmetry of the structure. No test grids were set up on the top surface of the bridge due to live traffic and the iCOR's inability to test through an asphalt overlay.

Powder samples were collected from both sides of one end bent. The location of these samples was chosen to be close to a test grid where the iCOR was also used in order to compare results at a similar location. Pictures from this inspection can be found below (Figures A1.8 through A1.14).

Figure A1.8. Efflorescence on Side Face of Cored Slab at Southwestern Side of End Bent 1.

Figure A1.9. Deep Section of Honeycombing on Underside of Cored Slab.

Figure A1.10. Efflorescence on Underside of Cored Slab.

Figure A1.11. Close-Up of Honeycombing (Shown in Figure A1.9); Note Exposed Rebar.

Figure A1.12. Using iCOR On Underside of Cored Slabs.

Figure A1.13. Location Of iCOR Test Grid and Powder Sample Collection; East Side of End Bent.

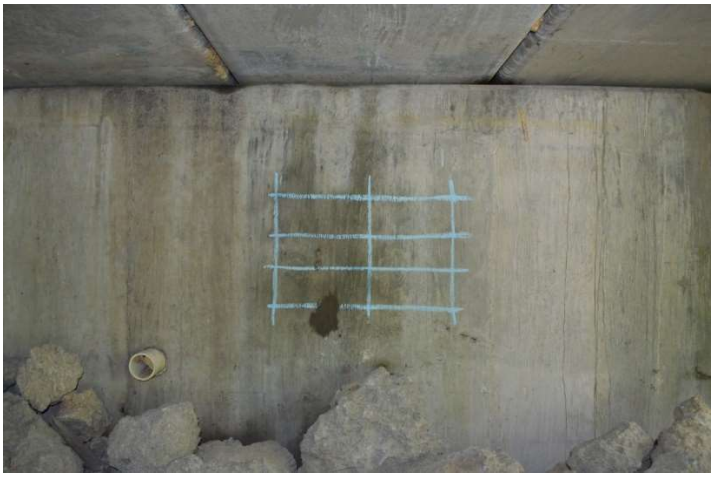

Figure A1.14. Location of iCOR Test Grid and Powder Sample Collection; West Side of End Bent.

A1.2 Field Visit #2 – November 1 - 3, 2019

To enhance the data set from the first field visit similar testing practices were performed. This included taking corrosion rate and surface resistivity measurements with the Giatec iCOR and powder samples for chloride concentration analysis. Additional powder samples were collected to determine the current calcium nitrite concentration of the concrete.

The experience of the first field visit allowed for improvements in the corrosion rate mapping methodology to be made. The first visit involved testing multiple small grids on different elements of the bridges. To maximize the data output and analyze the condition of the bridge on a larger scale rather than focusing on localized areas, the testing grids were created with significantly larger spacing.

Over the dates of November 1 through 3, 2019, a second field visit was made to investigate three additional bridges for corrosion impacts. The structures investigated include Structure Number (SN) 660019 (NC210 at Stones Creek), SN 090061 (NC133 at Town Creek), and SN 640010 (SR1411 at Bradley Creek), whose locations can be seen in

the map below (Figure A1.15). SN 660019 is located in the corrosive zone while SN 640010 and SN 090061 are located in the highly corrosive zone.

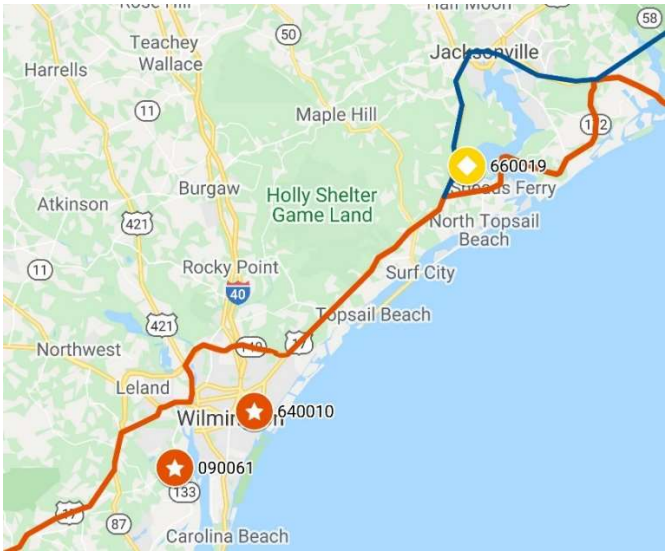

Figure A1.15. Locations of SN 660019, 090061, and 640010.

A1.2.1 Structure 660019 (NC210 at Stones Creek)

The inspection of SN 660019 included a full visual observation with picture documentation of any potential signs of corrosion or degradation, drilling for powder samples at two locations, and use of the Giatec iCOR at seven locations.

The iCOR test grids were selected to test elements that regularly experience tidal submersion and exposure and elements that do not. The two piers that were tested with the iCOR were tested just above the surface in an area that appeared to experience submersion during high tides or storms. The underside of the cored slabs was selected to obtain data at an elevation that most likely would not experience any submersion. For this, every third cored slab was tested across the transverse direction of the bridge. No test grids were set up on the top surface of the bridge due to live traffic and the small width of the shoulder.

Powder samples were collected from two piers. The location of these samples was chosen to be close to the water level as well as a test grid where the iCOR was used to compare results at a similar location. Pictures from this inspection can be found below (Figures A1.16 through A1.20).

Figure A1.16. Research Team Utilizing Boat to Perform iCOR Testing of Piers.

Figure A1.17. Research Team Filling Powder Sample Holes After Collection.

Figure A1.18. Location 1 Of iCOR Testing Grid and Powder Sampling Location.

Figure A1.19. Location 2 Of iCOR Testing Grid and Powder Sampling Location.

Figure A1.20. Research Team Using iCOR To Test Underside of Cored Slabs.

A1.2.2 Structure 090061 (NC133 at Town Creek)

The inspection of SN 090061 included a full visual observation with picture documentation of any potential signs of corrosion or degradation, drilling for powder samples at two locations, and use of the Giatec iCOR at five locations.

The iCOR test grids were selected to test elements that regularly experience tidal submersion and exposure and elements that do not. The two piers that were tested with the iCOR were tested just above the surface in an area that appeared to experience submersion during high tides or storms. The underside of the cored slabs was selected to obtain data at an elevation that most likely would not experience any submersion. For this, an edge cored slab was tested on both the bottom and side face and the underside of a central cored slab was tested. The number of cored slabs tested was limited by access. No test grids were set up on the top surface of the bridge due to the iCOR's inability to test through an asphalt overlay.

Powder samples were collected from two piers. The location of these samples was chosen to be close to a test grid where the iCOR was also used to compare results at a similar location. No interior bent caps or end bents were sampled due to issues with

accessibility. The end bents were not exposed, and the interior bent caps were too high above the water level. Pictures from this inspection can be found below (Figures A1.21 through A1.25).

Figure A1.21. Growth Along Underside of Cored Slabs.

Figure A1.22. Research Team Using Pachometer To Identify Steel Location in Piers.

Figure A1.23. Testing Grid Location on Piers with Powder Sample Locations Identified.

Figure A1.24. Large Driftwood Leaning Against Guardrail and Cored Slab.

Figure A1.25. Interior Bent Caps and Piers; Notice The Identical Staining on All Piers Showing High Tide Location.

A1.2.3 Structure 640010 (SR1411 at Bradley Creek)

The inspection of SN 640010 included a full visual observation with picture documentation of any potential signs of corrosion or degradation, drilling for powder samples at four locations, and use of the Giatec iCOR at eight locations.

The iCOR test grids were selected to test elements that regularly experience tidal submersion and exposure and elements that do not. The piers that were tested with the iCOR were tested just above the surface in an area that appeared to experience submersion during high tides or storms. The lowest level of testing was limited at certain piers due to buildup, which can be seen in Figure A1.26 below. The underside of the cored slabs and the interior bent caps were selected to obtain data at an elevation that most likely would not experience any submersion. No test grids were set up on the top surface of the bridge due to the iCOR's inability to test through an asphalt overlay.

Powder samples were collected from two piers and two interior bent caps. The location of these samples was chosen to be close to a test grid where the iCOR was also used to compare results at a similar location. However, one of the sampling locations was not tested with the iCOR. Pictures from this inspection can be found below (Figures A1.26 through A1.29).

Figure A1.26. Research Team Using Drill to Collect Powder Samples from Pier.

Figure A1.27. Testing Grid For iCOR And Powder Sample Locations 1 And 2.

Figure A1.28. Testing Grid For iCOR And Powder Sample Locations 3 And 4.

Figure A1.29. Testing Grid For iCOR; Notice the Significant Shell Buildup on The Piers.

A1.3 Field Visit #3 – February 20 - 23, 2020

To further enhance the data set from the first and second field visits similar testing practices were performed. This included taking corrosion rate and surface resistivity measurements with the Giatec iCOR and collecting powder samples for chloride concentration and calcium nitrite concentration analysis.

Over the dates of February 20 through 23, 2020, a third field visit was made to investigate three additional bridges for corrosion impacts. To clarify the accuracy of the powder sample results collected during the first field visit, an additional two powder samples were collected at SN 150020. The structures investigated include SN 150026

(SR1154 at Newport Creek), SN 260007 (NC615 Marsh Causeway at Creek off Back Bay), and SN 660021 (SR1503 at Bear Creek), whose locations can be seen in the map below (Figure A1.30). SN 150020 is located in the corrosive zone while SN 150026, SN 260007, and SN 660021 are located in the highly corrosive zone.

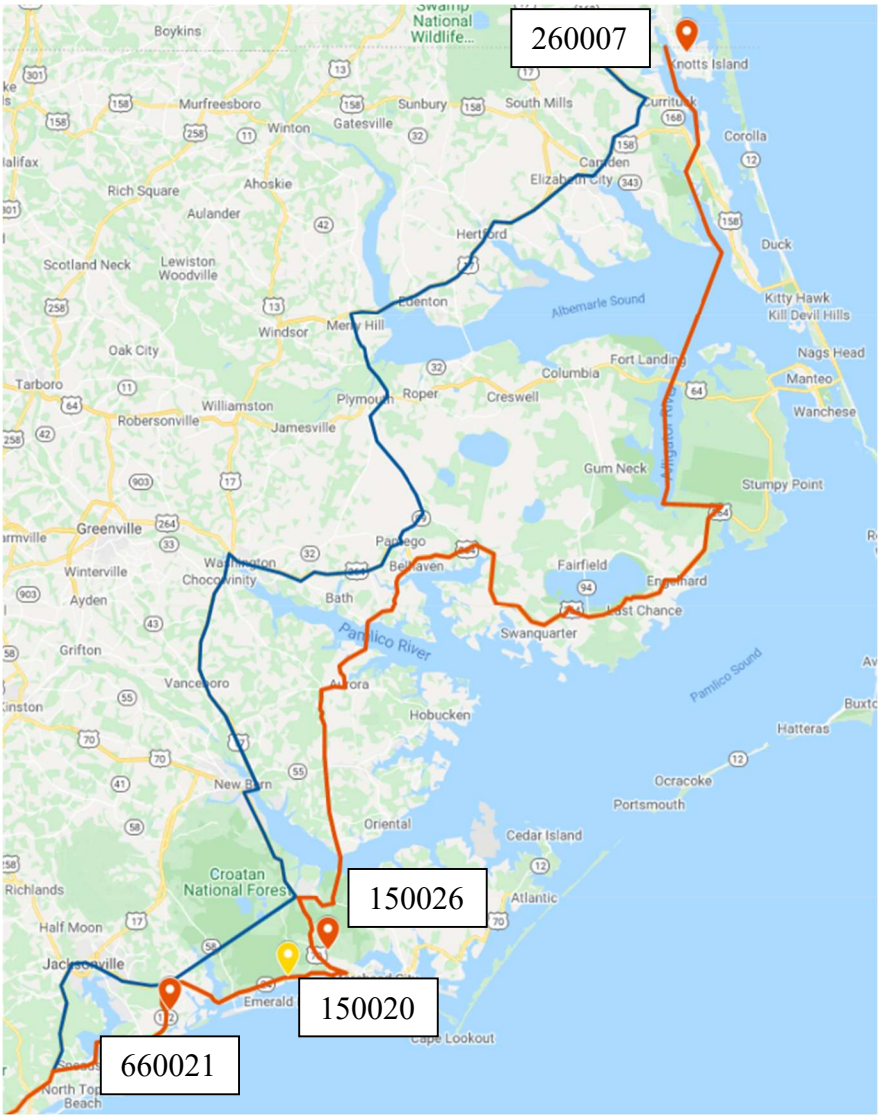

Figure A1.30. Locations of SN 660021, 150020, 150026, and 260007.

A1.3.1 Structure 150020 (SR1124 at East Prong Broad Creek)

Due to SN 150020 having already been investigated during field visit one, the only work performed included drilling two locations for powder samples and additional use of the Giatec iCOR. The locations were intended to be on the same piers that were tested during field visit one at the same elevation, however, due to the soaking of one of the piers from rain the next pier over was chosen to collect a powder sample.

Only one new iCOR test grid was selected for this visit. The new pier that was chosen to collect powder samples from was testing using the iCOR to obtain corrosion rate and surface resistivity data at a similar location to compare results. Since this structure was thoroughly inspected during the first field visit, no additional pictures were taken during this visit.

A1.3.2 Structure 150026 (SR1154 at Newport Creek)

The inspection of SN 150026 included a full visual observation with picture documentation of any potential signs of corrosion or degradation, drilling for powder samples at three locations, and use of the Giatec iCOR at three locations.

The iCOR test grids were selected primarily based on accessibility. The locations tested included the side face of the interior bent, the face of a wing wall, and the underside of multiple cored slabs. The cap appeared to be at an elevation that regularly experienced minor submersion during high tides or storms. The underside of the cored slabs was selected to obtain data at an elevation that most likely would not experience any submersion but may experience splashing. For this, five cored slabs were tested across the transverse direction of the bridge. No test grids were set up on the top surface of the bridge due to live traffic and the presence of an asphalt surface.

Powder samples were collected at two locations on the side face of the interior cap and the face of a wing wall. The location of these samples was chosen to be close to a test grid where the iCOR was also used in order to compare results at a similar location. Pictures from this inspection can be found below (Figures A1.31 through A1.34).

Figure A1.31. Lower Right: Using Pachometer To Locate Steel in Wing Wall; Left of Center: Performing iCOR Testing on Face of Cap from Boat.

Figure A1.32. Using iCOR On Underside of Cored Slabs.

Figure A1.33. Side Face of Cored Slabs. Note the Staining on Right Side of Image.

Figure A1.34. Location of Powder Samples And iCOR Grid on Side Face of Interior Cap.

A1.3.3 Structure 260007 (NC615 Marsh Causeway at Creek off Back Bay)

The inspection of SN 260007 included a full visual observation with picture documentation of any potential signs of corrosion or degradation, drilling for powder samples at two locations, and use of the Giatec iCOR at five locations.

The iCOR test grids were selected primarily based on accessibility. The locations tested included the side face, interior face, and underneath an interior bent, the underside of multiple cored slabs, and a location along the sidewalk on the top surface of the cored slabs. The cap did not appear to be at an elevation that would experience submersion and no visual signs of a water line were apparent, however, it may experience wetting due to splashing. The underside of the cored slabs was selected to obtain data at an elevation that most likely would not experience any submersion. For this, seven cored slabs were tested across the transverse direction of the bridge. A single test grid was set up on the sidewalk on the top surface of the cored slabs. The data at that location is incomplete due to the battery on the companion tablet dying during testing.

Powder samples were collected at two locations on the interior face of the interior bent. The location of these samples was chosen to be close to a test grid where the iCOR was also used in order to compare results at a similar location. Pictures from this inspection can be found below (Figures A1.35 through A1.38).

Figure A1.35. Center: Using iCOR On Side Face of Interior Bent; Left of Center: Drilling for Powder Samples on Interior Face of Interior Bent.

Figure A1.36. Location of Powder Samples on Interior Face of Interior Bent.

Figure A1.37. Location Of iCOR Testing Grid on Side Face of Bent Cap.

Figure A1.38. Interior Cap with Piers. Note the Significant Barnacle Buildup at The High Tide Line.

A1.3.4 Structure 660021 (SR1503 at Bear Creek)

The inspection of SN 660021 included a full visual observation with picture documentation of any potential signs of corrosion or degradation, drilling for powder samples at two locations, and use of the Giatec iCOR at four locations.

The iCOR test grids were selected in order to test elements that regularly experience tidal submersion and exposure and elements that do not. The piers that were tested with the iCOR were tested just above the surface in an area that appeared to experience submersion during high tides or storms. The lowest level of testing was

limited due to testing during high tide. The underside of the cored slabs and the interior bent cap was selected to obtain data at an elevation that most likely would not experience any submersion. No test grids were set up on the top surface of the bridge due to the iCOR's inability to test through an asphalt overlay.

Powder samples were collected from two piers. The location of these samples was chosen to be close to a test grid where the iCOR was also used in order to compare results at a similar location. No interior bent caps or end bents were sampled due to issues with accessibility. The end bents were not exposed, and the interior bent caps were too high above the water level. Pictures from this inspection can be found below (Figures A1.39 through A1.42).

Figure A1.39. Interior Cap with Piers; Note the Drainage Patterns on Right Side of Cap.

Figure A1.40. Underside of Exterior Cored Slab; Note the Significant Efflorescence.

Figure A1.41. Location of Multiple iCOR Test Grids and Powder Sample Sites.

Figure A1.42. Exterior Face of Concrete Barrier Wall; Note the Cracking and Staining.

APPENDIX B: RAW RESULTS FROM FIELD INVESTIGATIONS

The following sections contain the raw corrosion rate and surface resistivity data obtained during field visits one through three. Each section is dedicated to a single structure and contains the readings from the Giatec iCOR along with a sketch or reference picture detailing the location of the grid where measurements were taken. The structures presented, in order, include Structure Numbers (SN) 150020, 660091, 090061, 640010, 660019, 150026, 260007, and 660021.

B1.1 Structure 150020 Results

Table B1.1. Readings from face of pier (see Figure B1.1).

Reference Location	Corrosion Rate (µm/year)	Concrete Resistivity (kohm.cm)	Temperature (°F)	Humidity	R^2
1	0.45	477	77	88%	0.94
2	1.4	367	75	87%	0.98
3	1.4	332	75	87%	0.87
4	11	183	77	89%	0.79
5	6.4	109	77	89%	0.89
6	2.1	136	77	88%	0.70

Figure B1.1. Reference locations for Table B1.1.

Table B1.2. Readings from face of pier (see Figure B1.2).

Reference Location	Corrosion Rate (µm/year)	Concrete Resistivity (kohm.cm)	Temperature (°F)	Humidity	R^2
1	0.62	851	45	80%	1
2	4	681	43	85%	0.94
3	0.46	786	43	81%	0.97
4	11	498	45	80%	0.97
5	9.2	866	43	82%	0.97
6	9.4	739	43	81%	0.93
7	6.9	470	43	81%	0.96
8	3.5	549	43	82%	1
9	2.3	666	43	82%	0.98
10	1.4	407	43	82%	0.9
11	4.7	453	43	84%	0.99
12	2.1	565	43	85%	0.91

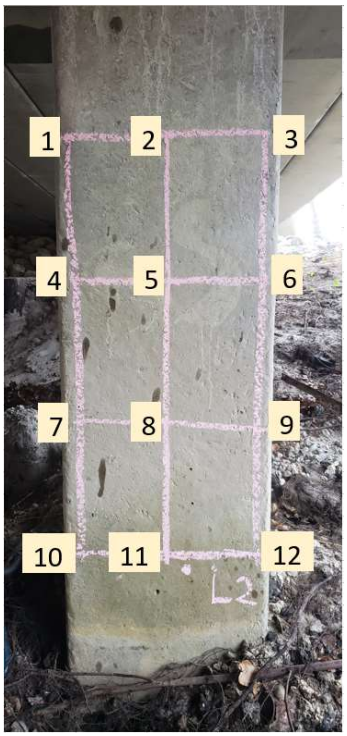

Figure B1.2. Reference locations for Table B1.2.

Table B1.3. Readings from face of pier (see Figure B1.3).

Reference Location	Corrosion Rate (µm/year)	Concrete Resistivity (kohm.cm)	Temperature (°F)	Humidity	R^2
1	0.45	477.3	77	88%	0.94
2	1.4	367.2	75	87%	0.98
3	1.4	332.3	75	87%	0.87
4	11	183.3	77	89%	0.79
5	6.4	108.5	77	89%	0.89
6	2.1	136.2	77	88%	0.70

Figure B1.3. Reference locations for Table B1.3.

Table B1.4. Readings from face of cap (see Figure B1.4).

Reference Location	Corrosion Rate (µm/year)	Concrete Resistivity (kohm.cm)	Temperature (°F)	Humidity	R^2
1	0.29	508	79	88%	0.99
2	31	152	77	89%	0.9
3	0.17	459	79	87%	0.97
4	1.1	378	79	88%	0.79
5	20	105	77	89%	0.78
6	17	178	79	87%	0.92

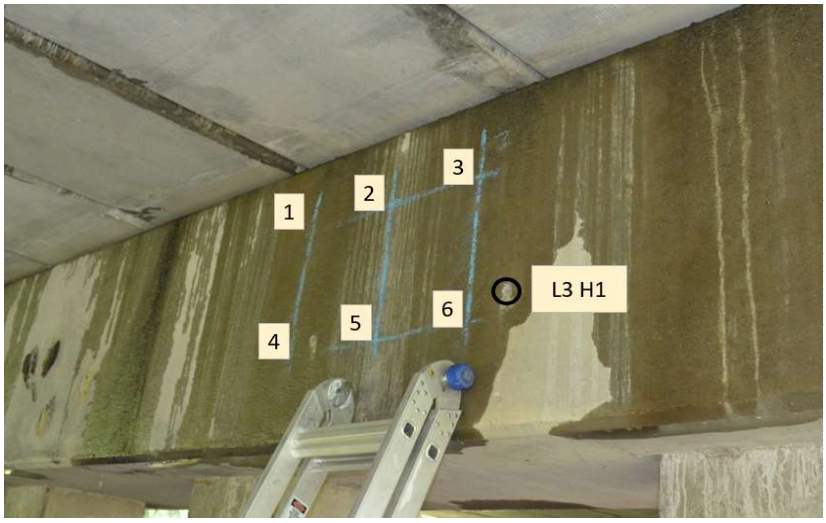

Figure B1.4. Reference locations for Table B1.4.

Table B1.5. Readings from top shoulder of deck near expansion joint (see Figure B1.5).

Reference Location	Corrosion Rate (µm/year)	Concrete Resistivity (kohm.cm)	Temperature (°F)	Humidity	R^2
1	36	49	31	56%	0.84
2	51	25.1	31	63%	0.98
3	153	23.9	31	59%	0.88
4	110	10.5	31	60%	0.96
5	1.7	292.4	31	61%	0.99
6	109	37.8	31	62%	0.33
7	33	25.3	31	59%	0.99
8	1	284	31	63%	0.99
9	28	34.3	31	64%	0.99
10	6.7	193.6	31	60%	0.92

Figure B1.5. Reference locations for Table B1.5.

Table B1.6. Readings from top shoulder of deck (see Figure B1.6).

Reference Location	Corrosion Rate (µm/year)	Concrete Resistivity (kohm.cm)	Temperature (°F)	Humidity	R^2
1	87	56.1	88	53%	0.83
2	3.5	118.4	88	53%	0.99
3	14	178.5	88	53%	0.98
4	19	51.2	88	53%	0.9
5	1.6	133.6	88	54%	1
6	41	26.2	86	56%	0.99
7	13	92	88	56%	0.98
8	124	42	88	55%	0.96
9	36	8.4	88	56%	1
10	6.3	112.2	88	54%	1

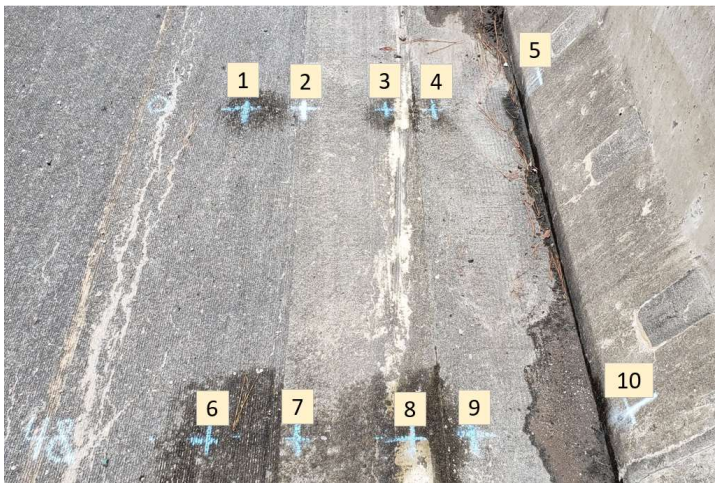

Figure B1.6. Reference locations for Table B1.6.

B1.2 Structure 660091 Results

Table B1.7. Results from face of end bent (see Figure B1.7).

Reference Location	Corrosion Rate (µm/year)	Concrete Resistivity (kohm.cm)	Temperature (°F)	Humidity	R^2
1	1.6	130	79	92%	0.98
2	39	136	79	92%	0.99
3	31	106	79	92%	0.86
4	35	116	79	92%	0.88
5	15	92	79	92%	1
6	12	71	79	92%	0.94

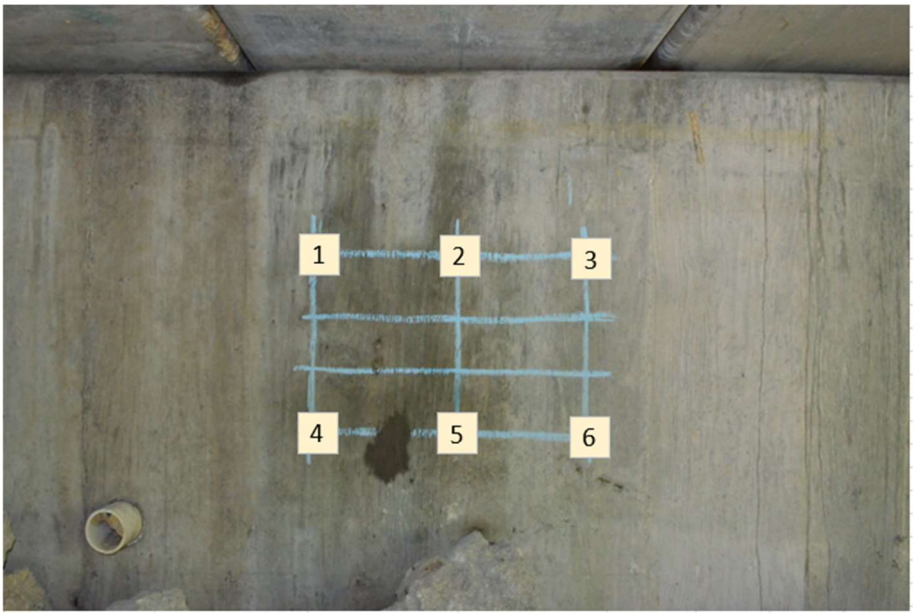

Figure B1.7. Reference locations for Table B1.7.

Table B1.8. Results from face of end bent (see Figure B1.8).

Reference Location	Corrosion Rate (µm/year)	Concrete Resistivity (kohm.cm)	Temperature (°F)	Humidity	R^2
1	24	796	79	91%	0.96
2	31	1061	81	84%	0.98
3	23	1482	79	84%	0.88
4	2.4	1498	79	91%	0.97
5	45	1235	79	90%	0.67
6	46	1476	79	89%	0.69

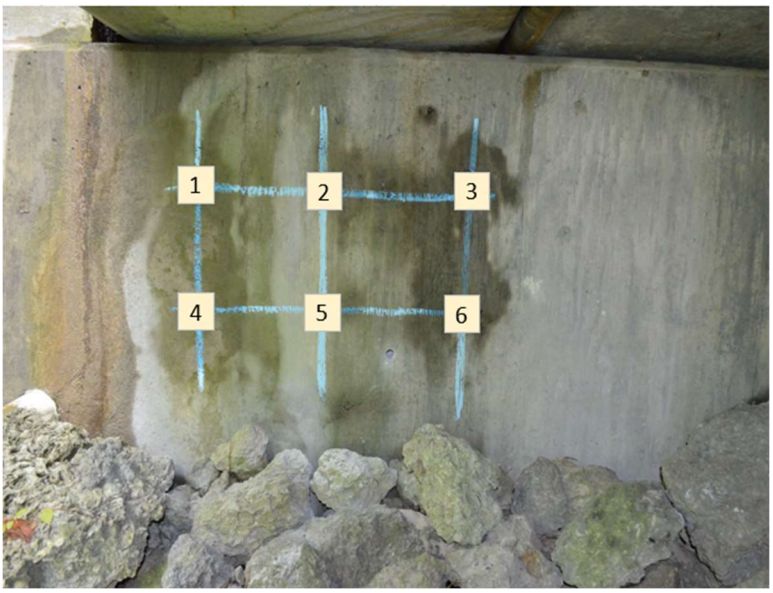

Figure B1.8. Reference locations for Table B1.8.

B1.3 Structure 090061 Results

Table B1.9. Results from side face of cored slab (see Figure B1.9).

Reference Location	Corrosion Rate (µm/year)	Concrete Resistivity (kohm.cm)	Temperature (°F)	Humidity	R^2
1	19	145	64	59%	1
2	29	80	64	59%	0.93
3	7.4	268	64	60%	1
4	5.9	173	64	58%	1
5	9.2	118	64	59%	1
6	9.2	143	64	60%	1
7	16	110	64	61%	1
8	11	155	64	61%	1
9	41	19	63	62%	0.99
10	74	7.2	63	61%	0.99
11	22	30	63	61%	1
12	30	20	63	61%	1
13	22	10	63	62%	0.99
14	9	70	63	63%	1
15	8.5	6.8	63	63%	0.99
16	8.9	66	63	60%	1

Figure B1.9. Reference locations for Table B1.9.

Table B1.10. Results from underside of cored slab #1 (see Figure B1.10).

Reference Location	Corrosion Rate (µm/year)	Concrete Resistivity (kohm.cm)	Temperature (°F)	Humidity	R^2
1	6.9	49	63	61%	1
2	8.2	56	63	61%	1
3	9.8	61	63	62%	1
4	13	34	61	61%	1
5	9.2	57	61	61%	0.99
6	14	34	61	62%	1
7	9.7	52	61	63%	1
8	12	51	61	62%	0.99
9	10	53	61	64%	1
10	12	57	61	64%	1
11	23	27	61	64%	1
12	29	26	61	65%	0.99

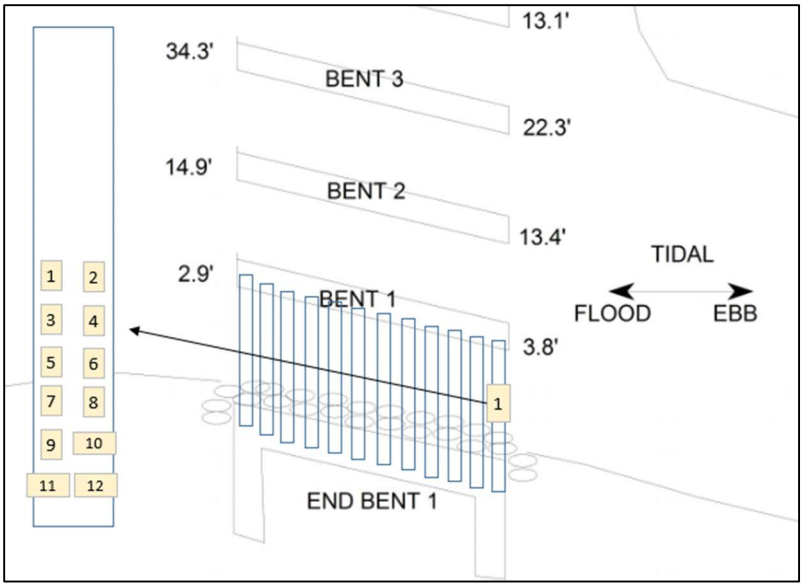

Figure B1.10. Reference locations for Table B1.10 (sketch from 2017 NCDOT inspection report of SN 090061 (NCDOT 2017)).

Table B1.11. Results from underside of cored slab #7 (see Figure B1.11).

Reference Location	Corrosion Rate (µm/year)	Concrete Resistivity (kohm.cm)	Temperature (°F)	Humidity	R^2
1	3.8	43	61	65%	1
2	20	41	61	65%	0.98
3	11	48	61	64%	1
4	12	49	59	64%	1
5	7.6	50	59	65%	1
6	15	64	59	66%	0.99
7	9.4	93	59	66%	1
8	18	74	59	66%	0.98
9	10	66	59	66%	0.99
10	13	82	59	66%	1
11	15	73	59	67%	1
12	5.1	67	59	66%	0.98

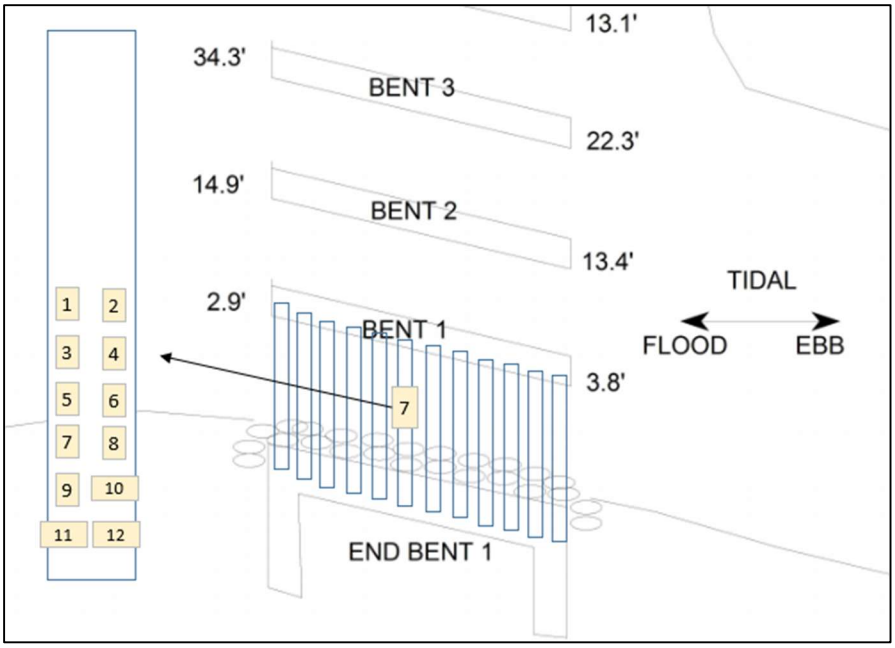

Figure B1.11. Reference locations for Table B1.11 (sketch from 2017 NCDOT inspection report of SN 090061 (NCDOT 2017)).

Table B1.12. Results from face of pier #1 (see Figure B1.12).

Reference Location	Corrosion Rate (µm/year)	Concrete Resistivity (kohm.cm)	Temperature (°F)	Humidity	R^2
1	8.8	73	59	69%	0.93
2	8.7	144	59	66%	0.98
3	4	283	57	68%	1
4	88	30	59	68%	0.97
5	104	40	59	69%	0.96
6	1.4	176	59	69%	1
7	47	44	59	68%	0.99
8	13	59	59	67%	0.99
9	0.59	403	59	69%	0.98
10	37	11	57	71%	0.99
11	65	29	57	70%	0.99
12	61	73	57	70%	0.99
13	251	6.7	57	73%	0.98
14	209	14	57	72%	0.98
15	4.2	49	57	72%	0.99
16	203	6.8	57	73%	0.99
17	238	14	57	70%	0.99
18	16	49	57	70%	1

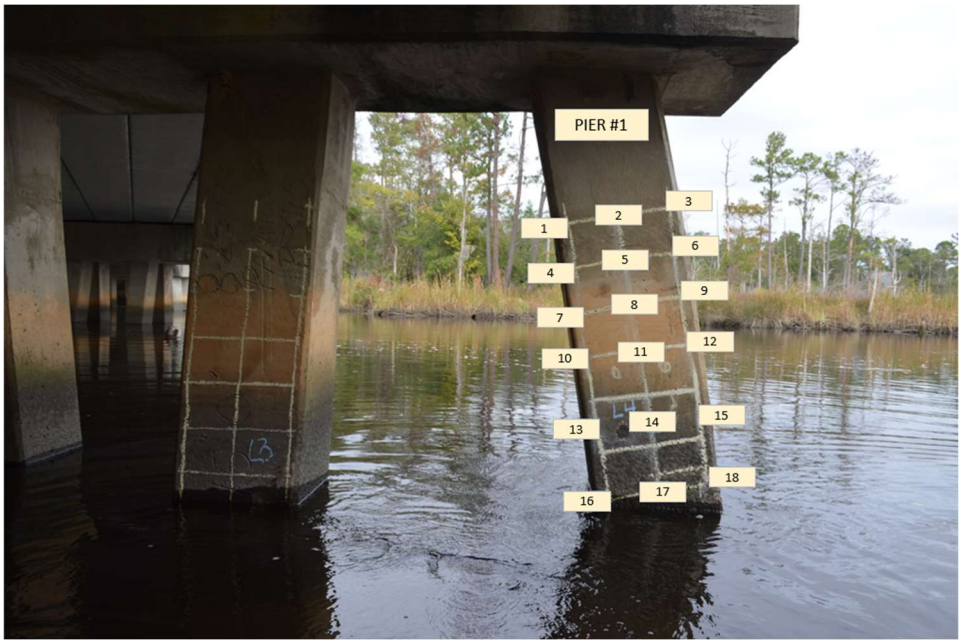

Figure B1.12. Reference locations for Table B1.12.

Table B1.13. Results from face of pier #2 (see Figure B1.13).

Reference Location	Corrosion Rate (µm/year)	Concrete Resistivity (kohm.cm)	Temperature (°F)	Humidity	R^2
1	5.1	70	59	69%	0.96
2	0.6	185	59	69%	0.92
3	3.6	128	59	68%	1
4	7.2	52	59	68%	0.98
5	16	51	59	69%	1
6	4.5	35	59	67%	1
7	61	58	59	68%	0.93
8	15	73	59	67%	0.99
9	7.4	103	59	71%	1
10	130	9.9	57	70%	1
11	139	40	57	69%	1
12	31	72	57	70%	0.99
13	274	7.2	57	71%	0.99
14	35	27	57	71%	1
15	112	31	57	72%	1
16	233	7.8	57	72%	1
17	53	41	57	69%	0.99
18	15	55	57	70%	0.99

Figure B1.13. Reference locations for Table B1.13.

B1.4 Structure 640010 Results

Table B1.14. Results from face of interior bent (see Figure B1.14).

Reference Location	Corrosion Rate (µm/year)	Concrete Resistivity (kohm.cm)	Temperature (°F)	Humidity	R^2
1	2.7	159	54	52%	1
2	2.5	161	54	53%	1
3	3.8	162	54	55%	0.99
4	1.6	182	54	54%	1
5	3	62	54	49%	0.96
6	1.8	364	54	49%	0.99
7	0.88	352	55	51%	1
8	1.9	497	55	49%	0.99

Figure B1.14. Reference locations for Table B1.14.

Table B1.15. Results from face of pier on interior bent (see Figure B1.15).

Reference Location	Corrosion Rate (µm/year)	Concrete Resistivity (kohm.cm)	Temperature (°F)	Humidity	R^2
1	8.7	72	57	48%	1
2	6	65	57	51%	1
3	4.3	13	57	53%	1
4	9.2	189	55	49%	1
5	7	50	55	47%	1
6	5.4	57	55	51%	1
7	1.7	160	55	49%	0.99
8	17	88	55	50%	1
9	7.6	124	55	49%	1

Figure B1.15. Reference locations for Table B1.15.

Table B1.16. Results from face of interior bent (see Figure B1.16).

Reference Location	Corrosion Rate (µm/year)	Concrete Resistivity (kohm.cm)	Temperature (°F)	Humidity	R^2
1	0.83	173	57	53%	1
2	3.3	127	57	50%	1
3	2.9	186	57	50%	1
4	7	172	55	50%	1
5	3	350	55	56%	0.99
6	0.46	442	55	52%	1
7	0.37	801	55	53%	1
8	0.76	624	55	54%	1
9	0.92	461	55	54%	1
10	1.5	570	55	55%	0.99

Figure B1.16. Reference locations for Table B1.16.

Table B1.17. Results from face of pier on interior bent (see Figure B1.17).

Reference Location	Corrosion Rate (µm/year)	Concrete Resistivity (kohm.cm)	Temperature (°F)	Humidity	R^2
1	19	172	55	52%	1
2	4.1	144	59	49%	0.98
3	6.5	130	55	53%	1
4	77	91	59	50%	0.97
5	14	136	55	55%	1
6	67	134	57	50%	0.96
7	36	107	55	54%	0.99
8	44	111	55	57%	0.96
9	15	131	55	53%	0.97

Figure B1.17. Reference locations for Table B1.17.

Table B1.18. Results from face of interior bent (see Figure B1.18).

Reference Location	Corrosion Rate (µm/year)	Concrete Resistivity (kohm.cm)	Temperature (°F)	Humidity	R^2
1	7.4	103	73	39%	0.99
3	1.7	227	66	42%	0.99
4	5.5	101	72	38%	0.99
5	2.3	71	68	41%	0.88
6	2.3	117	70	41%	0.99
7	4.3	80	70	38%	1
8	4.4	113	68	46%	0.96
9	0.91	111	70	39%	1
10	0.82	167	68	42%	1
12	3.5	130	66	41%	1
13	4.5	107	66	43%	1
14	0.03	151	68	43%	0.99
16	37	84	68	45%	0.99
17	8.7	63	66	40%	1
18	22	71	66	45%	1
19	11	29	66	41%	0.99
20	6.7	73	68	43%	1
21	12	80	66	44%	1
22	25	37	68	42%	1
23	1.8	134	66	41%	0.99
24	2.8	128	68	39%	0.99
25	0.11	187	66	43%	1
26	1.4	113	68	42%	0.99
27	3.8	98	66	43%	1
28	2.1	114	68	41%	0.97
29	3.2	83	66	42%	1
30	5.3	75	68	42%	1

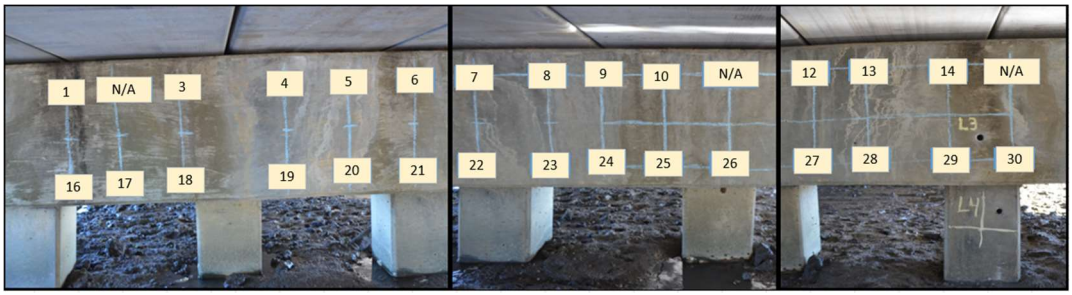

Figure B1.18. Reference locations for Table B1.18.

B1.5 Structure 660019 Results

Table B1.19. Results from face of pier #1 (see Figure B1.19).

Reference Location	Corrosion Rate (µm/year)	Concrete Resistivity (kohm.cm)	Temperature (°F)	Humidity	R^2
1	8.1	133	66	63%	1
2	8.4	99	66	63%	1
3	2.7	130	66	62%	1
4	5	187	66	63%	1
5	4.6	161	66	63%	1
6	10	190	66	63%	0.95
7	40	102	66	65%	0.99
8	36	95	66	64%	0.99
9	49	133	66	63%	0.98
10	90	49	66	65%	0.99
11	73	52	66	63%	0.94
12	47	56	66	61%	0.99

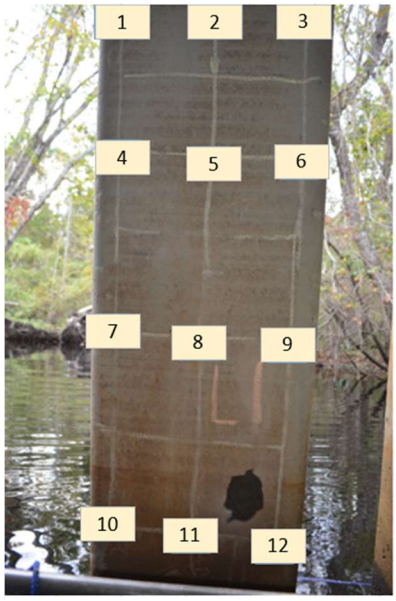

Figure B1.19. Reference locations for Table B1.19.

Table B1.20. Results from face of pier #2 (see Figure B1.20).

Reference Location	Corrosion Rate (µm/year)	Concrete Resistivity (kohm.cm)	Temperature (°F)	Humidity	R^2
1	2.9	104	66	62%	1
2	5.2	57	66	60%	1
3	0.82	129	66	64%	1
4	8.2	115	68	59%	1
5	13	78	68	60%	0.99
6	3.6	147	68	60%	1
7	19	104	68	60%	1
8	17	105	68	60%	0.99
9	5	138	68	61%	1
10	10	105	68	62%	1
11	39	51	68	62%	1
12	136	75	66	64%	0.95

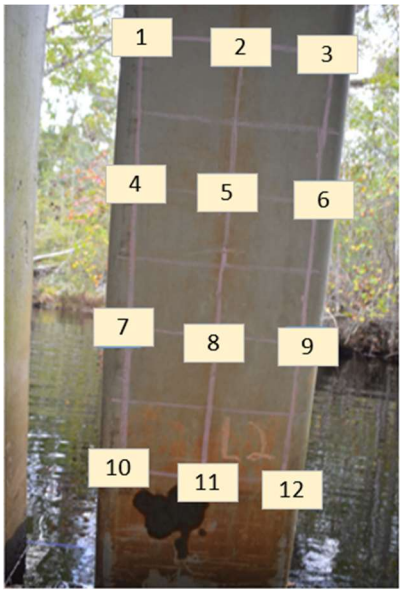

Figure B1.20. Reference locations for Table B1.20.

Table B1.21. Results from underside of cored slabs (see Figure B1.21).

Reference Location	Corrosion Rate (µm/year)	Concrete Resistivity (kohm.cm)	Temperature (°F)	Humidity	R^2
1	15	42	66	61%	1
	11	32	66	60%	1
2	21	51	66	61%	1
	11	52	66	61%	1
3	6.3	37	66	62%	1
	4	46	66	62%	1
4	6.6	27	66	61%	1
	10	38	66	61%	1
5	6.6	32	66	63%	1
	7.2	37	66	63%	1
6	6.6	42	66	63%	1
	8	38	66	63%	0.99
7	5.9	31	66	66%	1
	5.8	41	66	63%	1
8	7.5	46	64	63%	1
	12	43	64	63%	0.99
9	11	38	64	62%	0.99
	9.6	29	64	62%	1
10	14	31	64	62%	1
	15	26	64	63%	1

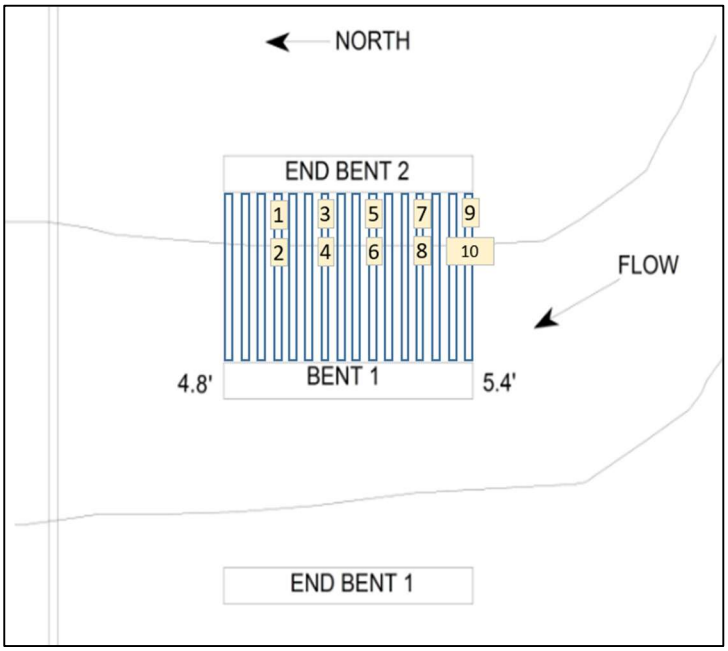

Figure B1.21. Reference locations for Table B1.21 (sketch from 2018 NCDOT inspection report of SN 660019 (NCDOT 2018)).

B1.6 Structure 150026 Results

Table B1.22. Readings from face of wing wall (see Figure B1.22).

Reference Location	Corrosion Rate (µm/year)	Concrete Resistivity (kohm.cm)	Temperature (°F)	Humidity	R^2
1	52	134	39	71%	0.93
2	5.9	148	39	78%	0.92
3	3.8	328	39	77%	0.99
4	1.2	404	39	74%	1

Figure B1.22. Reference locations for Table B1.22.

Table B1.23. Readings from face of interior cap (see Figure B1.23).

Reference Location	Corrosion Rate (µm/year)	Concrete Resistivity (kohm.cm)	Temperature (°F)	Humidity	R^2
1	1.2	745	39	73%	0.99
2	1.4	402	39	73%	0.99
3	0.98	400	39	71%	0.99
4	0.57	555	39	70%	0.99
5	0.59	775	39	85%	1
6	5.3	397	39	83%	0.99
7	2.6	379	39	82%	0.99
8	0.13	469	39	79%	1
9	2.5	309	39	73%	1
10	21	246	39	68%	0.96
11	28	199	39	69%	0.94
12	4.1	316	39	72%	0.96

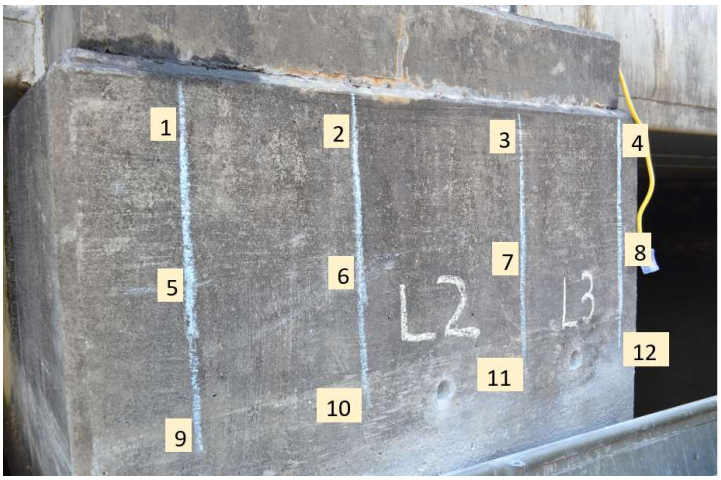

Figure B1.23. Reference locations for Table B1.23.

Table B1.24. Readings from underside of cored slabs (see Figure B1.24).

Reference Location	Corrosion Rate (µm/year)	Concrete Resistivity (kohm.cm)	Temperature (°F)	Humidity	R^2
1	4.4	293	39	65%	1
	6.7	133	39	68%	1
2	6.8	206	39	69%	1
	12	123	39	68%	0.97
3	6.8	188	39	68%	1
	4.7	246	39	68%	0.97
4	2.2	304	39	69%	1
	3	277	39	69%	0.99
5	4.8	234	39	69%	1
	3	221	39	69%	1
6	3.8	272	39	64%	1
	4.6	239	39	67%	0.99
7	2.9	245	39	70%	0.99
	6.3	239	39	71%	0.99
8	1.9	312	39	71%	0.97
	3.3	233	39	71%	0.98
9	1.4	196	39	70%	0.91
	6.8	143	39	71%	0.99
10	4	216	39	71%	0.97
	13	150	39	70%	0.95

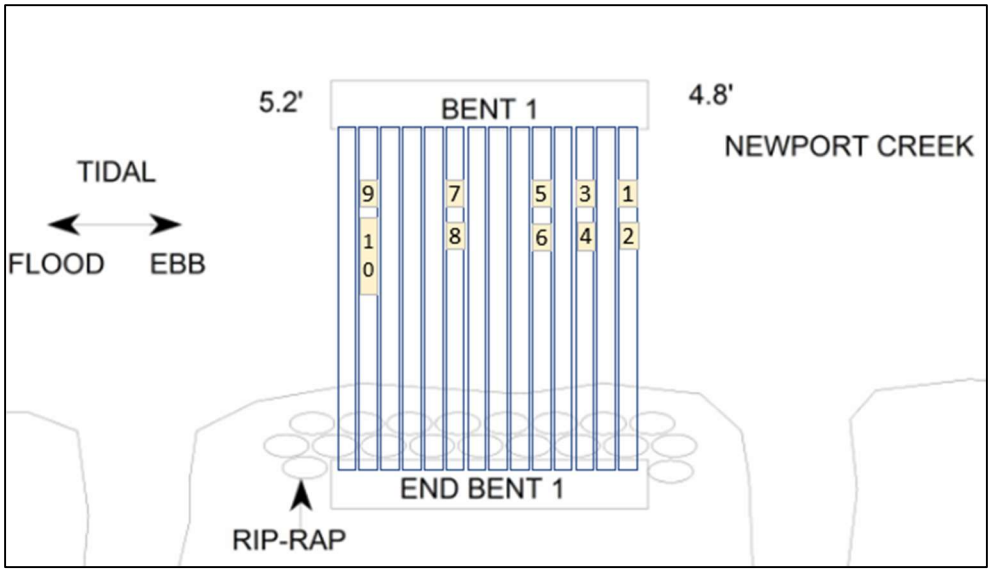

Figure B1.24. Reference locations for Table B1.24 (sketch from 2017 NCDOT inspection report of SN 150026 (NCDOT 2017)).

B1.7 Structure 260007 Results

Table B1.25. Readings from side face of cap (see Figure B1.25).

Reference Location	Corrosion Rate (µm/year)	Concrete Resistivity (kohm.cm)	Temperature (°F)	Humidity	R^2
1	40	64	59	48%	0.96
2	22	81	46	80%	0.93
3	67	55	46	80%	0.96
4	10	74	55	38%	0.88
5	20	42	55	42%	0.99
6	13	56	57	55%	0.97
7	27	48	55	38%	0.99
8	9.1	157	57	40%	0.99
9	9.2	89	57	44%	0.99

Figure B1.25. Reference locations for Table B1.25.

Table B1.26. Readings from interior face of cap (see Figure B1.26).

Reference Location	Corrosion Rate (µm/year)	Concrete Resistivity (kohm.cm)	Temperature (°F)	Humidity	R^2
1	19	125	54	34%	0.99
2	17	76	55	37%	0.99
3	9.2	88	57	32%	1
4	31	112	54	37%	0.99
5	40	95	55	37%	0.98
6	52	108	54	34%	0.99
7	46	67	52	37%	0.99
8	0.72	315	52	37%	0.97
9	18	170	52	36%	0.95
10	22	170	52	43%	0.97
11	4.6	210	50	40%	0.98
12	7	254	50	40%	1

Figure B1.26. Reference locations for Table B1.26.

Table B1.27. Readings from top of sidewalk (see Figure B1.27).

Reference Location	Corrosion Rate (µm/year)	Concrete Resistivity (kohm.cm)	Temperature (°F)	Humidity	R^2
1	3.1	874	55	37%	0.98
4	0.27	899	54	41%	1
5	6.9	452	57	43%	0.97
7	0.63	734	54	45%	1
8	1.1	180	57	40%	1
10	2.2	189	55	38%	1
11	3.7	355	55	39%	0.98
12	2.5	638	57	39%	1

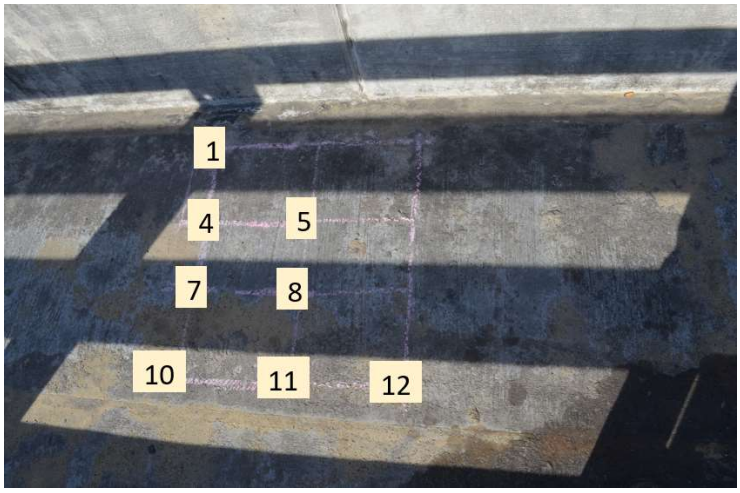

Figure B1.27. Reference locations for Table B1.27.

Table B1.28. Readings from underside of cap (see Figure B1.28).

Reference Location	Corrosion Rate (µm/year)	Concrete Resistivity (kohm.cm)	Temperature (°F)	Humidity	R^2
1	25	120	54	36%	0.99
2	11	194	55	33%	0.99
3	1.5	180	55	35%	0.98
4	30	161	59	30%	0.99
5	8.7	245	55	35%	0.98
6	3.8	158	61	30%	1

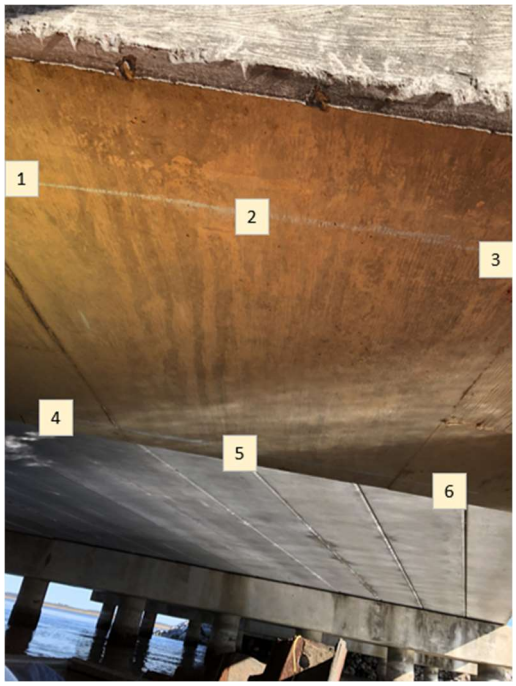

Figure B1.28. Reference locations for Table B1.28.

Table B1.29. Readings from underside of cored slabs (see Figure B1.29).

Reference Location	Corrosion Rate (µm/year)	Concrete Resistivity (kohm.cm)	Temperature (°F)	Humidity	R^2
1	6.6	147	54	38%	1
2	7.9	137	55	38%	0.90
3	3.3	180	55	35%	0.99
4	0.34	155	57	33%	0.99
5	9.1	170	59	34%	0.99
6	11	137	59	36%	0.98
7	6.2	159	61	41%	0.95

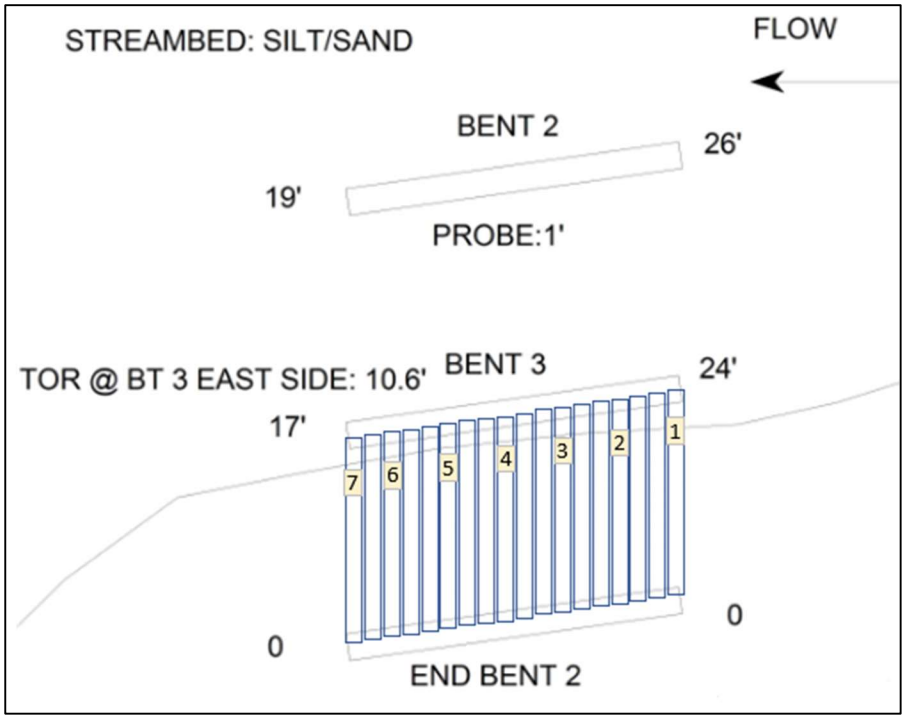

Figure B1.29. Reference locations for Table B1.29 (sketch from 2018 NCDOT inspection report of SN 260007 (NCDOT 2018)).

B1.8 Structure 660021 Results

Table B1.30. Readings from face of pier #1 (see Figure B1.30).

Reference Location	Corrosion Rate (µm/year)	Concrete Resistivity (kohm.cm)	Temperature (°F)	Humidity	R^2
1	4.2	119	34	77%	1
2	5.4	112	34	77%	0.97
3	4.6	208	34	77%	0.99
4	1.1	204	34	76%	0.99
5	4.1	234	34	77%	0.96
6	6.5	200	34	78%	0.89

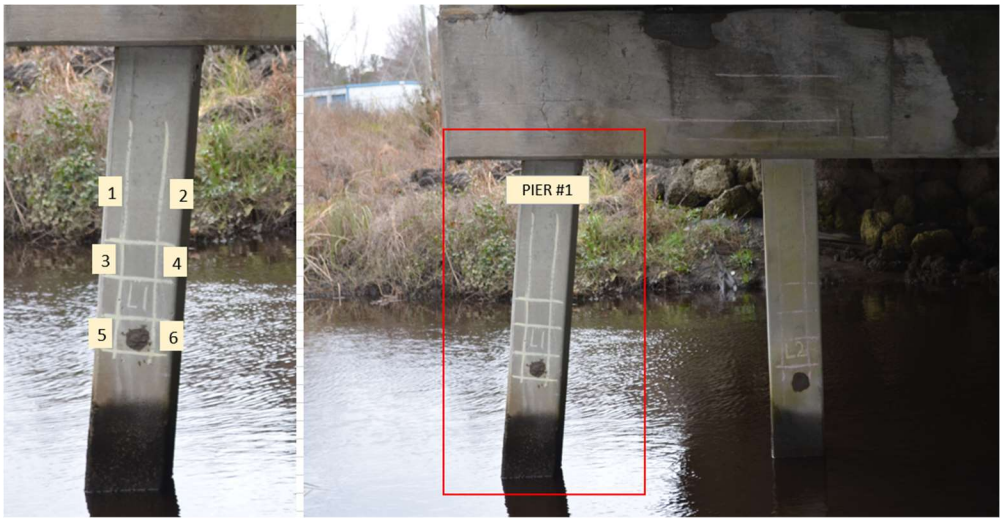

Figure B1.30. Reference locations for Table B1.30.

Table B1.31. Readings from face of pier #2 (see Figure B1.31).

Reference Location	Corrosion Rate (µm/year)	Concrete Resistivity (kohm.cm)	Temperature (°F)	Humidity	R^2
1	0.23	257	34	76%	0.97
2	2.9	226	34	76%	0.97
3	3.2	178	34	76%	1
4	3	191	34	76%	0.98
5	2.6	177	34	77%	0.99
6	10	158	34	77%	0.98

Figure B1.31. Reference locations for Table B1.31.

Table B1.32. Readings from face of cap (see Figure B1.32).

Reference Location	Corrosion Rate (µm/year)	Concrete Resistivity (kohm.cm)	Temperature (°F)	Humidity	R^2
1	2.3	515	34	77%	0.97
2	1.4	640	34	78%	0.97
3	3.3	237	34	78%	0.98
4	0.69	310	34	78%	1
5	0.47	646	34	75%	0.94
6	3.1	368	34	77%	1
7	2.8	436	34	76%	0.99
8	4.1	461	34	77%	0.98

Figure B1.32. Reference locations for Table B1.32.

Table B1.33. Readings from underside of cored slabs (see Figure B1.33).

Reference Location	Corrosion Rate (µm/year)	Concrete Resistivity (kohm.cm)	Temperature (°F)	Humidity	R^2
1	2.4	45	34	74%	1
	3.7	56	34	74%	1
2	2.5	54	34	73%	1
	4.7	69	34	73%	1
3	3.3	100	34	73%	0.99
	5.7	83	34	73%	1
4	9.7	115	34	73%	0.98
	1.4	153	34	73%	1
5	1.9	101	34	74%	0.99
	2.7	96	34	73%	1
6	2.7	122	34	74%	0.99
	3.1	143	34	73%	1
7	1.8	121	34	75%	1
	-0.21	145	34	75%	1
8	1.7	50	36	74%	1
	1.3	56	36	74%	0.98
9	2.9	47	34	73%	1
	2.2	50	34	73%	1
10	1.9	96	34	72%	0.99
	3	127	34	72%	1
11	0.69	221	34	73%	0.93
	6.3	108	34	72%	0.97
12	4.1	105	34	74%	1
	0.38	80	34	74%	1
13	2.3	104	34	73%	1
	1.9	107	34	73%	1
14	0.74	130	34	75%	0.99
	0.38	411	34	76%	1

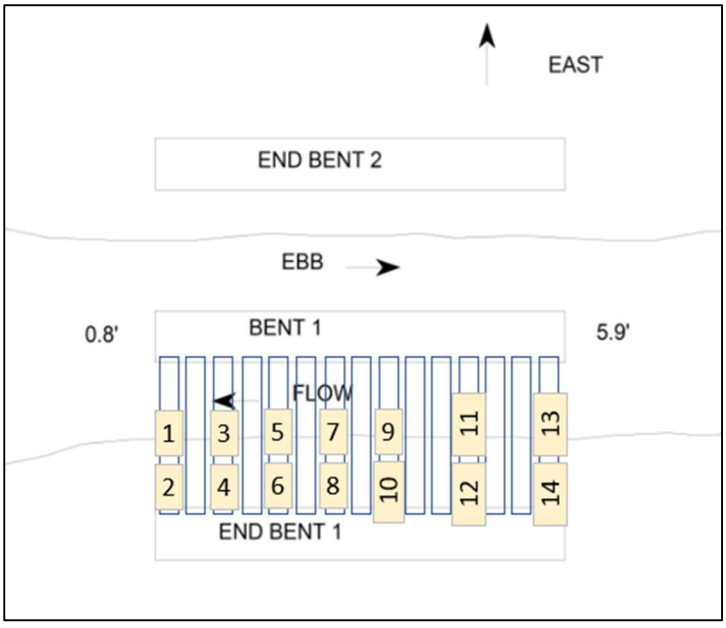

Figure B1.33. Reference locations for Table B1.33 (sketch from 2018 NCDOT inspection report of SN 660021 (NCDOT 2018)).

APPENDIX C: MATLAB CODE FOR DETERIORATION MODELING

```
1.  while m<514
2.  n=5
3.  m=m+1
4.  CR=input{m,n}
5.          if CR==0
6.                  while CR==0
7.                  CR=input{m,n}
8.                          if n==20
9.                          break
10.                         end
11.                 n=n+1
12.                 end
13.         output{m,CR+1}F=output{m,CR+1}+1
14.         end
15.         if CR==input{m,n}
16.                 while CR==input{m,n}
17.                 CR=input{m,n}
18.                 output{m,CR+1}=output{m,CR+1}+1
19.                         if n==20
20.                         break
21.                         end
22.                 n=n+1
23.                 end
24.         end
25.         while CR>input{m,n}
26.         CR=input{m,n}
27.                 while CR==input{m,n}
28.                 output{m,CR+1}=output{m,CR+1}+1
29.                         if n==20
30.                         break
31.                         end
32.                 n=n+1
33.                 end
34.         end
35. end
```